Aus der Neurologie-Klinik

Universitätsklinikum des Saarlandes, Homburg/Saar

Direktor: Prof. Dr. med. K. Faßbender

Investigation of CSF outflow in mice by in vivo, dynamic magnetic resonance imaging

vorgelegt von: Jonas Uwe Krämer

geboren am 27.01.1998 in Völklingen

Table of content

Abbreviations

BBB	Blood brain barrier
CLN	Cervical lymph nodes
CNS	Central nervous system
CSF	Cerebrospinal fluid
DCLN	Deep cervical lymph nodes
ICP	Intracranial pressure
MRI	Magnetic resonance imaging
NIR	Near-infrared
PNS	Perineural space
PSS	Perisagittal superior sinus
SAS	Subarachnoid space
SEM	Standard error of the mean

List of figures

1. <u>Abstract</u>

The cerebrospinal fluid describes a clear fluid circulating in the subarachnoid space (SAS) of the central nervous system (CNS). It is localized between the semi-permeable pia mater and the tight barrier of the arachnoid mater.

The amount of around 150 mL of cerebrospinal fluid (CSF) circulates up to four times per day in the human central nervous system cumulating to a production of 500 mL of cerebrospinal fluid per day by the human central nervous system (PARDRIDGE, 2016). The production is mainly localized in the choroid plexus in the ventricles while the ependymal cells lining the cerebrospinal fluid system seem to have only a minor role in this process (CSERR, BUNDGAARD, 1984).

On the one hand, the central nervous system swims in the cerebrospinal fluid. As a consequence, the cerebrospinal fluid works as a buffer a against mechanical impact on the brain. Moreover, its metabolic and nutritional functions are essential for the function of our central nervous system. The cerebrospinal fluid eliminates toxic metabolites and foreign substances which harm the susceptible chemical homeostasis created by the blood-cerebrospinal fluid barrier. Therefore, an immunological function with a steady process of clearance prevents neurological infections and a toxic chemical milieu.

A disrupted cerebrospinal fluid system creates a high variability of diseases, from which the disfunction in controlling the amount of cerebrospinal fluid is the most public one. Most common medical issues are the hydrocephalus or the idiopathic intracranial hypertension. In addition to that, many neurodegenerative and neuroinflammatory diseases emenate mainly from a lack of elimination of toxic metabolites. For example, the genesis of a disease like Alzheimer´s dementia is explained by the accumulation of toxic metabolites, called ß-amyloid-plaques. It keeps under strong scientific debate if this has its source in a dysfunctional cerebrospinal fluid outflow. Unfortunately, there isn´t any consensus on how the elimination of these metabolites works and which anatomical structures are part of this process. However, it is essential to know the process of central nervous system outflow to explain how the central nervous system is cleared by toxic metabolites to finally understand and heal neurodegenerative diseases like Alzheimer´s dementia.

The importance of cerebrospinal fluid for the function of the central nervous system leads to an early scientific effort to get a better understanding. In the 18th century, the first description of arachnoid villi resulted in the theory of a cerebrospinal fluid outflow through the arachnoid villi. This hypothessis delivered a possible connection between the subarachnoid space and the venous system. However, in the 19th century, the cervical lymph nodes (CLN) were detected as a cerebrospinal fluid drainage localization and new descriptions of cerebrospinal fluid drainage along cranial nerves were established as a new idea of cerebrospinal fluid outflow. These findings are the basis for the current understanding. The cerebrospinal fluid outflow to the lymphatic system appears as the major pathway supported by a high density of publications in the last years.

Major nervous dysfunctions like Alzheimer´s disease are correlated with increased age. The impaired elimination of toxic metabolites due to an inefficient circulation of cerebrospinal fluid, as part of the aging process, dominates current debates. Therefore, it is necessary to observe not only the characteristics of a heterogeneous group of animals or humans. Moreover, it is necessary to take a look at physiological processes that change with aging to understand the age correlation of many neuronal diseases. In this experiment, observations in two groups of mice at different ages demonstrated a significantly decreased cerebrospinal fluid outflow for elder mice. New pathways of the cerebrospinal fluid outflow were shown that change due to age, confirming descriptions of other groups. By using 9,4 T Magnetic resonance imaging (MRI) and low rate infusion in the lateral ventricle, dynamic imaging under physiological, in vivo conditions was established. On the one hand, Magnetic resonance imaging allows an overview of the whole skull in combination with a high resolution of anatomical structures and tissues. As a consequence, the visualized anatomical structure with tracer increase can be identified. The bulk of the contrast agent drained rapidly to the subarachnoid space of the basal cisterns while only a minor increase was detectable at the dorsal aspect of the skull. The cerebrospinal fluid outflow follows predominantly the ventral cranium through the cribriform plate to the collected by the lymphatic vessels in the nasopharyngeal area. Therefore, a major part of the cerebrospinal fluid flows through the ventral aspect of the skull while the dorsal skull has a minor function contrary to recently published observations (ILIFF et al., 2012; LOUVEAU et al., 2015; OLIVER et al., 2020).

2. <u>Introduction</u>

2.1. <u>Anatomical Pathway of cerebrospinal fluid outflow</u>

The observations of CSF outflow were initiated in the 18th century. In the beginning, the basic observations were limited to the anatomical structures that are part of the intracranial CSF circulation. As shown in Figure 1, the blue arrow illustrates the first descriptions and further investigations of the arachnoid villi and a potential CSF outflow through the arachnoid barrier. In the 19th century, CLN were claimed as an endpoint of CSF pathways along with the cranial nerves, as shown by the yellow arrow in Figure 1. Moreover, CSF routes through the ventral aspect of the skull like the nasal cavity were described for the first time. These studies proved several times the drainage of CSF to the CLN which is commonly accepted today. However, the pathway from the SAS to CLN remained discussed as recent publications focus on the role of lymphatic vessels in the CSF circulation, demonstrated by the green arrow. Today, there is a strong debate about the CSF outflow pathway from the SAS to the CLN.

Timeline of CSF outflow research:

Blue arrow:

Pacchioni 1721

Key and Retzius 1875

Clark 1920

Alksne and Lovines 1972

- Description of arachnoid villi
- Tracer accumulation in the arachnoid villi and venous system
- Endothelial barrier at the top of the arachnoid villi
- Electron microscopic description of the arachnoid barrier and theory of an active transport meachnsim

Yellow arrow:

Schwalbe 1869

Key and Retzius 1876

Mortensen and Sullivan 1933

Czerniawska 1970

- CSF outflow along cranial nerves and accumulation in the nasal cavity
- Tracer outflow along the pharynx to the DCLN
- Retrograde flow from the nasal cavity to the SAS

Green arrow:

Wustmann 1933

Bradburry and Cole 1980

Louveau 2015

Aspelund 2015

Ma et al. 2017

Ahn et al. 2019

Ma et al. 2019

- Tracer accumulation in lymphatic system
- First in vivo imaging detects tracer in optical and olfactory perineurium
- First quantification of the lymphatic's role for the CSF outflow
- Described lymphatics around the dural sinus leading to the CLN
- NRI demonstrated CSF outflow in the lymphatic system before entering blood system
- MRI demonstrates nerval route and drainage along PVS
- Lymphatic vessels penetrate CP, draining directly in the SAS
- Interruption of arachnoid barrier at the exit points of cranial nerves
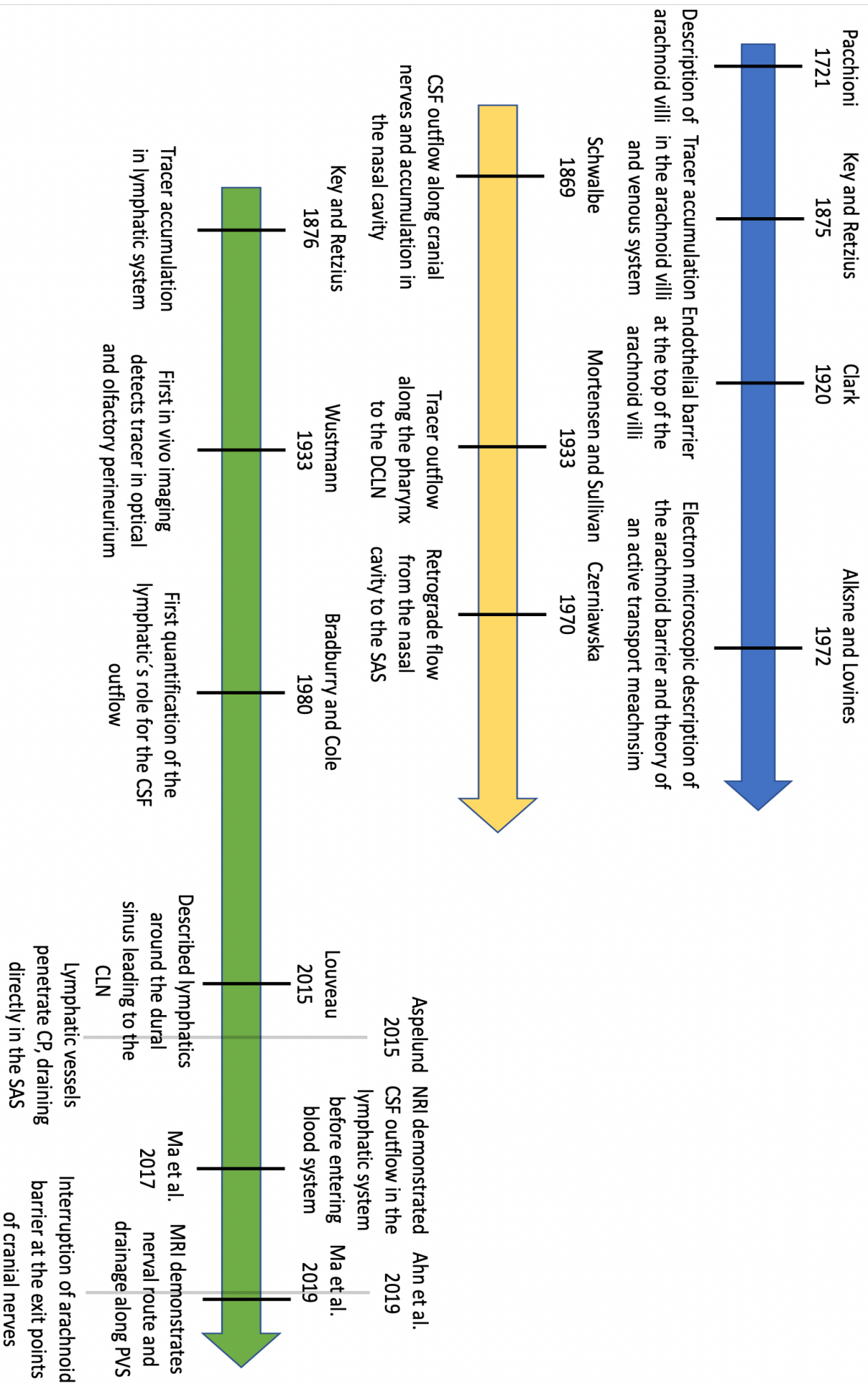
8

Figure 1: Chronological summary of key explorations of cerebrospinal fluid outflow

The blue arrow indicates the focus on the arachnoid pathway as the major CSF outflow passage. At the beginning of the 18th century, Pacchioni described as the first person the presence of arachnoid villi which resulted in the publication of many more studies which confirmed or opposed the CSF outflow through the arachnoid villi. The role of the cranial nerves as a part of the CSF outflow is illustrated by the yellow arrow. It was established over a century later, as Schwalbe could detect a CSF outflow along the cranial nerves outside the skull. Many years later, the CSF could be detected in the CLN, which was interpreted as an outflow along with cranial nerves to the CLN. The importance of the lymphatic system, illustrated by the green arrow, was established by studies over the last years and is the main idea for the CSF outflow currently. Especially the recently published studies by Ma et al. indicate a CSF outflow along the cranial nerves to the lymphatic system. They concluded, that the CSF outflow is mainly drained to the lymphatic system and from there, the tracers reach the blood system.

2.1.1. <u>Arachnoid villi</u>

Over 300 years ago, the arachnoid villi were firstly described by the Italian Pacchioni. He published observations in humans showing arachnoid structures penetrating the dura mater (WOOLLAM, 1957). This structural connection between the CSF system in the SAS and the venous system in the subdural space would create a stable pathway for a potential CSF outflow. Confirmation for this theory came from the experiments of Key and Retzius in 1875. In their work, they injected Berlin blue dye in the SAS and reported an accumulation of their tracer in the arachnoid villi and drainage through them to the venous system (KEY, 1875). At the top of the arachnoid formations, a layer of cells has a direct connection to the venous system (LE GROS CLARK, 1920). The work of Key and Retzius was criticized for using high injection pressure around 60 mmHg which could have led to a rupture of the arachnoid membrane (HOFFMANN, THIEL, 1956).

Therefore, several decades later, Weed published a concept of CSF outflow using the arachnoid villi. He inserted a cannula in the intrathecal space of the upper lumbar spinal cord and infused an isotonic solution. Weed took care that the infusion pressure was at maximum slightly about the physiological intracranial pressure (ICP) around 9-13 mmHg to prevent pressure damage at the arachnoid membrane. After the infusion, the animals were killed and the brain and the meninges were formalin-fixed. In his findings, he observed an accumulation of tracer through the whole CSF shortly after injection. Several hours later, only a few granulations were found in the sinus while the arachnoid villi along the perisagittal superior sinus (PSS) were filled with the tracer. Afterward, he observed the arachnoid villi in serial cuttings by using light microscopy, which made him the first person who examined the microscopic structure of the arachnoid villi. He described a lack of valves or stomata in the arachnoid villi which would require an active transport mechanism for CSF outflow (WEED, 1914a, b, c).

Furthermore, the electron microscopy showed that the arachnoid did not penetrate the dura through the endothelial layer which is why the presence of tight junctions was suggested (ALKSNE, LOVINGS, 1972). Even after establishing a higher ICP, creating distension of the arachnoid projection, they stayed in contact with the dura by this endothelial layer. As a result, the authors were sure that there must be

an active process like micropinocytosis to transport molecules outside the brain, although these findings were not fit with the knowledge of a fast bulk flow for the molecules (DAVSON et al., 1970). As a compromise, a possible system of vacuoles in the covering cells of the SAS was proposed to transport molecules from the CSF to the venous system like in the canal of Schlemm (WEED, 1914c). This mechanism would allow a dynamic flow that supports the bulk flow theory.

A point of criticism against Weed´s hypothesis was the post-mortem examination of the structures. It was mentioned that after the ex vivo fixation, diffusion of the dye particles was supported. Reproductions of his work showed an accumulation in bones and ligaments around the CSF and the neck tissue (ERLICH et al., 1989; SPERANSKY AD, 1943).
Dandy separated the hemispheres from the dura mater and could not observe an accumulation of CSF or edema in the brain parenchyma. This disagrees with the hypothesis, that the pathway through the arachnoid villi is a potential major CSF route because the connection between the arachnoid villi and the venous system was not intact anymore (DANDY, 1929).

Finally, we have to admit that the complete role of the arachnoid villi is not understood yet. The condition of active transport through the arachnoid barrier disagrees with the knowledge of a rapid CSF outflow. Therefore, the CSF pathway through the arachnoid barrier in the venous system is disqualified as a major passage. However, it can be discussed whether the arachnoid barrier opens under high ICP and works as a backup mechanism to prevent higher, unphysiological ICP. The common opinion declares the arachnoid layer as a strong barrier that allows no passive flow through it. Therefore, no anatomical mechanism is known that would explain the drainage through this barrier. Moreover, no in vivo study was produced that could show a CSF drainage directly from the SAS to the blood.

2.1.2. <u>Cranial nerves</u>

The outflow along cranial nerves had been detected by Schwalbe in 1869. He was the first person, that showed an accumulation in the nasal cavity and the orbit after tracer injection. Therefore, he suggested that the CSF follows the cranial nerves on their route outside the skull which as he described an accumulation within the sheath of the optic nerve (SCHWALBE, 1869). These sheaths seemed to be a projection of the SAS outside the skull. Extracranially, the arachnoid membrane was penetrated, and the CNS drained into the lymphatic system. Mortensen and Sullivan demonstrated tracers accumulation in the lymphatic vessels of the nasal cavity and transport along with lymphatics in the pharynx to the deep cervical lymph nodes (DCLN)(MORTENSEN, 1933).

Several hypotheses had been established to explain the drainage of CSF from the perineural space (PNS) of the olfactory nerve to the lymphatics.

The first idea assumed that the perineural cells are loosely connected to the nerve which would make an easy flow in the interstitial space possible. As a consequence, the perineurium would have no barrier function and a free CSF circulation to the interstitial space and the lymphatic vessels would be a potential pathway (MARTINEZ et al., 1973). Fitting with this theory, Czerniawska described a retrograde passage that transported tracers from the nasal cavity in the SAS and potentially to the brain (CZERNIAWSKA, 1970). This could be a plausible explanation for the virus penetration in the CNS.

The second proposal characterized the perineurium as a tight barrier as the meninges which would require an active transport of CSF to the lymphatics. This concept disagrees with the concept of rapid bulk outflow (JACKSON et al., 1979).

The last proposed solution is penetration of lymphatic vessels penetrate through the cribriform plate and direct access to the SAS (ANTILA et al., 2017; ASPELUND et al., 2015). Experiments indicated that the arachnoid barrier does not exist anymore above the cribriform plate and does not follow along with the cranial nerve outside the skull (WELLER et al., 2018). As a result, the lymphatics would be able to drain passively CSF from the SAS.

The optic nerve is extracranially surrounded by the meningeal layers contrary to the olfactory nerve. The meningeal layer reaches until entering the sclera, which is a significant structural difference from the discontinuous arachnoid of the olfactory nerve. However, intraorbital tracer drainage through intercellular channels in the arachnoid indicate that the arachnoid barrier at the end of the SAS is not intact anymore (SHEN et al., 1985).

The connective tissue of the orbit contains lymphatic vessels which access the mandibular lymph nodes. The CSF outflow along with the optic nerve seems to provide an important outflow route as the orbit-draining lymphatics showed tracer accumulation 10 min after intraventricular injection (MA et al., 2019b). However, no study was able to quantify the role of the optic nerve route in comparison to the olfactory nerve. The strong accumulation in the mandibular lymph nodes could be explained by lymphatic drainage from the nasal and orbital region.

Concerning the neuronal outflow route, the jugular foramen has a prominent role as the exit point of three cranial nerves. Among these, the glossopharyngeal, vagus, and accessory cranial nerves. It has been demonstrated that tracer is transported through the jugular foramen connected to the lymphatic vessels draining to the DCLN (MA et al., 2017).

2.1.3. <u>Lymphatic vessels</u>

The lymphatic vessels in the dura reawakened scientific focus in 2015, after the redescription of their presence by two CNS studies (ASPELUND et al., 2015; LOUVEAU et al., 2015). Their findings indicate a strong presence of dural lymphatics at the base of the skull and the venous sinuses like the PSS and transverse sinuses (ASPELUND et al., 2015). These lymphatics seem to be enabled to transport immune cells and fluid from the CSF to the DCLN as they offer a direct connection. Moreover, the concept of the CNS without the presence of lymphatics was falsified.

Using 2-photon imaging, the group of Kipnis detected endothelial and different immune cells by immunohistochemistry. Their method visualized a high presence of immune cells in the abluminal space around the sinuses (LOUVEAU et al., 2015). Further investigations of the perisinusoidal vessels detected markers for the expression of lymphatic endothelial cells at these vessels. As a consequence, it was shown that these vessels are lymphatics running parallel along with the sinuses offering a distinct lumen. Investigations with an electron microscope showed that the lymphatic vessels around the sinuses have similar characteristics to the periphery ones, even though they recognized unique characteristics concerning distribution and organization. After intraventricular tracer injection, observations with multiphoton microscopy showed a tracer accumulation in the dural lymphatic vessels around the SSS. Therefore, they resumed the presence of connections between the SAS and the dural lymphatics at several locations like the transverse sinus. However, no anatomical confirmation exists to prove this connection. Moreover, other studies were unable to detect tracer drainage to the dorsal lymphatic vessels (AHN et al., 2019; MA et al., 2017).

The first in vivo imaging study using X-ray observed tracer outflow after injection in the SAS (MORTENSEN, 1933; WUSTMANN, 1933). The contrast agent drained through the PNS of the olfactory nerve to the nasal cavity. From there, the pathway continued over lymphatic vessels to the SLN and DCLN. Besides the nasal cavity, tracer accumulation was detected in the perineurium of the optic nerve and the papillae where it flowed along the facial veins to the SLN. Moreover, a smaller part of the tracer was near the larger blood vessels and another cranial nerve which are leaving at the base of the skull (WUSTMANN, 1933).

In the 1950th the first approach had been made to quantify the role of the lymphatics as a major pathway for the CSF outflow. However, this work was a throwback for the supporters of the lymphatic pathway. After injecting Evans blue into the SAS of cats and rabbits, the concentration of dye was estimated by cannulations over several times up to 24 hours at the circulating blood and the cervical and thoracic duct lymph. The different chronological increase of contrast led to the hypothesis, that lymphatics play a minor role in the elimination of the blood system (COURTICE, SIMMONDS, 1951). However, the cannulization was a point of criticism, because it was argued, their calculation in only one lymphatic

trunk draining to the DCL is not representative (FOLDY et al., 1959). Therefore, they repeated the work but measured the concentration of dye in cannulated lymph comparing these values with blood from the jugular vein and femoral artery. They could demonstrate that the accumulation firstly appeared in the lymphatic system and later in the blood system.

The work of Bradburry calculated the tracer clearance to cervical lymphatic vessels after tracer injection in the SAS for rabbits and cats. However, for rabbits, only 30% of the injected dye was detectable within the cervical lymphatics while in cats the participation of the lymphatic system was even lower around only around 13%. However, up to 50% of the injected tracer was undetectable adding the measured tracer amount in CNS, blood system, and lymphatics (BRADBURY, COLE, 1980). The discrepancies indicate that the tracer has to accumulate in other regions which had not been calculated by the study. A direct flow from the SAS to the cervical lymphatics would have not shown such a big amount of undetectable tracer. Potential routes through other lymphatic pathways that play a role between the SAS and the blood system were missed.

Several years later, the blocking of the cribriform plate with cyanoacrylate glue reduced the tracer accumulation in the DCLN from 14,8% to 1,9% which indicates a major role for the nasal region in the CSF outflow (BRADBURY, WESTROP, 1983). Andres et al visualized dural lymphatic vessels surrounding the PSS close to the blood vessels of the dura mater. These lymphatics leave the skull by following the sinus transversus and meningeal artery or at the cribriform plate (ANDRES et al., 1987). Recent works used the technical progress and new methods of imaging. Ma et al used near-infrared (NIR) imaging while injecting a 40kDa macromolecular tracer in the CSF. They could demonstrate a strong outflow of tracer along with the cranial nerves and an immediate accumulation in the extracranial lymphatic vessels. The NRI allowed them to follow the tracer under dynamic physiological conditions and showed an increase of contrast in the SLN and DCLN before reaching the blood system (MA et al., 2017). Besides the outflow was less efficient in older mice than in young ones (MA et al., 2017) while anesthetized and glioblastoma-bearing animals showed a lack of outflow too (MA et al., 2019c). Intraventricular injection confirmed the outflow along with the cranial nerves (MA et al., 2019a).

Another MRI-based study claimed that the CSF outflow would be dominated by the meningeal lymphatic vessels leaving the basal skull (AHN et al., 2019). The CSF seemed to drain through the exit points like petrosquamous fissure, jugular, and stylomastoid foramen. It could be demonstrated by immunostaining that the arachnoid barrier is not intact when the nerves penetrate the meningeal layers at the exit points. As a consequence, the tracer could perfectly drain from the SAS into the lymphatic vessels. However, the group did not show the perineural routes of the optic and olfactory nerve. Therefore, this work seems to be incomplete even if drainage to the DCLN was demonstrated.

To summarize, lymphatic vessels were described at several locations in the meningeal layers. However, the existence of a intact barrier of arachnoid objects the concept of CSF outflow from the SAS to the dural lymphatics (BRADBURY, 1979; KRISCH et al., 1983). As the arachnoid barrier establishes a

separation between the CNS and the dura, it seems that the lymphatics in the dura exist for the collection of extravasated fluid. This idea is confirmed by intravenous tracer injection that was collected by these dural lymphatic vessels (ABSINTA et al., 2017). The intact arachnoid barrier around the whole brain is especially prominent at the base of the skull. However, it shows interruptions at exit points of cranial nerves (BRØCHNER et al., 2015). The penetration of the cranial nerves through skull and meningeal layers offers a potential connection between the SAS and lymphatic vessels. It is still unknown, in which dimension the drainage through these vessels participates in the CSF outflow process in general.

2.2. <u>Clinical relevance</u>

The CSF as a clearance pathway for molecules and toxic metabolites offers an essential function to remain the fragile chemical and molecular balance of a optimal environment for the brain. Besides the elimination of foreign molecules and metabolites, immunological and nutritional function are discussed. A dysfunctional CSF outflow could be part of the etiology of several neurodegenerative and neuroinflammatory diseases and is associated with hydrocephalus, pseudotumor cerebri and more.

Glioblastoma is one of the most dangerous neurological tumors. Even after medical progress in surgery and chemotherapy, the survival duration is fewer than 15 months even (MA et al., 2019c). The origin of glioblastoma are degenerated astrocytes in the CNS. The strong vascularization and following damage on the blood-brain barrier (BBB) result in peritumoral edema and higher ICP (MACK et al., 2017). Fitting with the theory of a CSF bulk outflow, it is plausible that the CSF outflow is accelerated under increased ICP (BOULTON et al., 1998; HEISEY et al., 1962). However, under pathological conditions of an active-spreading glioblastoma with intracranial edema, this was never observed. On the one hand, the increased amount of fluid could accelerate the CSF flow, while others claim that the tumor could block CSF outflow. A decelerated CSF flow would explain the clinical observations of persistent intracranial edema. Moreover, the rare presence of extracranial metastasis (LUN et al., 2011) and the limited immunological response against the tumor (PRINS, LIAU, 2004) indicate an impaired CSF flow under the glioblastoma condition. Therefore, a better understanding of the malfunction of physiological processes under glioblastoma conditions could support a better supply and drainage of intrathecal drugs or glioblastoma antigen presentation and containment of edema.

It was observed that glioma breading mice showed a reduced tracer accumulation along the cranial nerves at the front of the skull and a massive reduction of contrast in the CLN. Using a combination of MRI and NRI imaging, bolus injection in the cisterna magna of glioma mice showed massively reduced tracer accumulation in the CLN and along the PNS compared to physiological conditions. Measurements in the DCLN and SCLN indicted a significantly reduced tracer accumulation in these structures, too. Tracer transportation time to the saphenous vein was massively increased following NIR-imaging. Post-

mortem analyses detected tracer intensity at the optical nerve was reduced significantly in glioblastoma mice. In addition to that, the lymphatic vessels leading from the orbital region to the SLN did not show detectable tracer accumulation at all or very slightly increased contrast (MA et al., 2019c).

Generally, the outflow was delayed compared to non-glioblastoma mice and most of the tracer remained in the cisterna magna. While the contrast in the control group showed a steady decrease in the cisterna magna, the glioblastoma group indicated a nearly constant level of contrast. Quantification of contrast at the dorsal brain surface and the basal skull showed a massive decreased outflow compared to the control group. Instead of the physiological routes, which show a very limited CSF drainage to the spinal cord, the tracer of the glioblastoma mice drained to the SAS of the spinal. Furthermore, dye drainage to the lymphatics in glioblastoma mice was only detectable, when the contrast was visible in the sacral spinal cord. The tracer was detectable in the iliac and caudal mesenteric lymph nodes indicating a CSF passage from the spinal cord to the lymph nodes and the blood system. Therefore, the spinal regions seem to work as a compensative outflow route for the CSF.

Concerning the outflow to the blood system, the study did not find any evidence for a direct CSF flow to the blood system. Delayed detection of tracer in the blood system after a contrast increase in the lymphatic system indicated a CSF flow through the lymphatics in the blood system. However, the glioblastoma group showed a delayed increase in the blood system, although the highly vascularized tumor impairs the BBB (JAIN et al., 2007). Therefore, under glioblastoma conditions, especially with an increased size of the tumor, a direct leakage of CSF to the blood system could be possible. However, the study could not confirm any direct passage to the blood system at all, but the pathological condition. While other types of cancer are characterized by lymphangiogenesis, the intracranial and intraparenchymal glioblastoma grows within a tissue without lymphatic structures (JENNY et al., 2006). As a consequence, the physiological anti-tumor immunological response is reduced. Moreover, the impaired CSF circulation could support inflammatory processes as clearance of toxic metabolites and pro-inflammatory cytokines is blocked. Furthermore, the tumor-antigen presentation is minimalized, because the antigen transportation by CSF to the CLN is reduced. Therefore, the proliferation of T-cells and restricts immunological response is limited (MA et al., 2019c).

As a result, glioblastoma impacts CSF circulation in a way that intensifies the creation of the intracranial edema as the physiological CSF passages are blocked. However, the spinal cord seems to compensate at least a part of the CSF outflow, as the spine was described as another CSF outflow pathway under increased ICP (EISENBERG et al., 1974; FAULHAUER, DONAUER, 1985; WELCH, 1977). The changed CSF circulation could affect the efficiency of intrathecal drug application and restricts an adequate antigen presentation in the CLN which is required for a sufficient immunological response.

Alzheimer´s disease is the most common neurological disorder and will affect public health more and more in the next decades due to demographical developments. Interestingly, the mechanism of this disease is not finally understood as many questions remain unsolved. Due to the high relevance for the

health system, scientific research in this field is accelerating. In general, Alzheimer´s dementia is explained by the intraparenchymal accumulation of senile plaques build-up by amyloid-ß and intracellular neurofibrillary tangles. It is generally accepted that the increasing levels of amyloid-ß result in a dysfunctional synaptic work that increases tau accumulation and neurofibrillary tangles formation (HARDY, SELKOE, 2002; KARRAN et al., 2011). These processes cause neurodegeneration through neuroinflammation with astrogliosis and microgliosis (ROGERS et al., 2002) visible by the decreasing cognitive capacity. As described by Ma et al, the reduced CSF outflow in aged mice could benefit this neuroinflammatory process. The synaptic activity produces ß-amyloid as a waste product which is formed by several steps including ß- and γ-secretases and amyloid protein precursor. The different ß-amyloids are responsible for the senile plaques resulting in Alzheimer´s diseases and the intraluminal blocking of cerebral and leptomeningeal arteries responsible for cerebral amyloid angiopathy (ATTEMS et al., 2011).

However, physiological changes like a decreased CSF outflow due to increased age seem to support the progress of Alzheimer. In the end, an explanation which mechanisms in detail are changed due to age, could not be given at the moment. As our current lack of knowledge is a major reason for an insufficient treatment of Alzheimer´s disease, more effort is necessary. A better understanding of the CSF outflow and the potential elimination of the senile plaques would be significant progress to invent new therapeutic solutions.

2.3. The current debate raised by new imaging methods

2.3.1. Overview of technological tools available for cerebrospinal fluid investigation

The current process in the knowledge of CSF outflow is mainly explained by the invention of new technological methods allowing a more detailed and in vivo observation. The first studies until the beginning of the 20th century were dominated by tracer injection with post-mortem observation (WEED, 1914a, b, c). This method has the disadvantage to ignore post-mortem tracer movement which falsifies the results. In the 1930th, the in vivo imaging by X-ray was a great technical progression to demonstrate the CSF outflow not only in post-mortem slides (MORTENSEN, 1933; WUSTMANN, 1933). However, X-ray is characterized by the high density of bone. Therefore, it lacks an efficient visualization of the neuronal exit points at the base of the skull which appears important for the CSF outflow. Moreover, in competition with progressed methods like MRI, the X-ray fails to give details about the soft tissue which makes it hard for the scientist to define the anatomical structure of tracer accumulation.

NIR imaging is a more advanced version of in vivo imaging with a contrast agent. The method requires a compatible contrast agent and detects the movement of the tracer by measuring the optical density. The injected tracer has other, defined optical characteristics than the surrounding tissue. This allows the detection of our tracer and the demonstration of the CSF outflow in a non-harmful noninvasive way. In addition to that, the NIR imaging offers a high image rate with intervals of only a few seconds while MRI takes several minutes. However, MRI has the advantage to have a better tissular resolution creating a better anatomical orientation where the detected tracer is accumulating. Both techniques can be detected digitally and objectively, by using software for the exact quantification of the tracer amount which the two-photon imaging is unable to offer (ILIFF et al., 2012; LOUVEAU et al., 2015). The detailed, but limited visualization of the NIR imaging fails to demonstrate an observation of the complete brain structures. Moreover, it demonstrates a relatively superficial level of imaging reaching only millimeters compared to MRI. The MRI creates a wider and deeper overview of the CSF outflow by demonstrating the time-correlated outflow of the tracer. Moreover, the high resolution of soft-tissue structures allows a detailed, anatomical localization of the tracer and allows to identify the anatomical structures presenting the CSF outflow pathway (MA et al., 2019b).

MRI allows in vivo imaging of a wider area than the other methods. The sequential image taking allows a chronological interpretation by demonstrating the contrast agent movement on several time points. A big advantage against the NIR imaging which focuses on a narrow window. However, NIR-imaging gives nearly all-time imaging while the MRI image requires more time and is limited to sequences every 4-5 min. The less resolute images compared to the NRI imaging are another disadvantage. Figure 2 shows an overview of the three major technical methods that a relevant for the demonstration of the CSF outflow. It is clear, that the different methods distinguish between different points creating specific advantages and disadvantages. However, we decided that the advantages of a wield and deep view predominate the moderate improved temporal resolution that the NIR imaging offers.

Characteristic	Magnetic resonance imaging	Near-infrared imaging	2-photon imaging
Depth of region imaged	+++	++	+
High spatial resolution	+++	+++	+
Cellular resolution	+	++	+++
Temporal resolution	++	+++	+++
Brain activity	+++	+++	+++
Anesthetized mouse	+++	+++	+++
Awake mouse	-	++	+++

Figure 2: Overview of the benefits and disadvantages of the different imaging methods

The table shows the characteristics of the most common imaging methods which are used in studies concerning CSF outflow. These methods include MRI, NIR imaging, and 2-photon imaging. At the left, the features of imaging are summarized while the number of „+" indicates the quality of imaging. Three „+" are the best value that a method could require, while one + indicates that the feature is not optimized in this method. The „–" at the end should show that the combination of awake mice and the imaging method is not possible as it requires at least a narcotic condition.

A publication that supports the glymphatic pathway worked mainly with the 2-photon imaging (HEISEY et al., 1962). Two-photon imaging method requires a compatible contrast agent which is injected into the CSF. The low energy and the limitation on a focal area are less damaging for the tissue and especially useful for living samples. The infrared light concentrates only in the focal area to collect enough photons for excitation. The concentrated energy allows a high spatial resolution. The lack of out-of-focus light and the high wavelengths allow a visualization without image blurry and photodamage resulting in a high-quality resolution (BENNINGER, PISTON, 2013). As shown in Figure 2, the narrowed view fails to calculate the CSF outflow in the area around the limited area of observation. However, by using a thinner bone, the skull would be still intact and high-resolute images can be taken until 1-2 mm below the surface of the cortex under physiological conditions. This depth is sufficient for visualization of the perivascular space (PVS) in the cortical hemispheres. The creation of detailed images can be useful to demonstrate the processes and structures around PVS that could be part of CSF (MA et al., 2019b).

2.3.2.   2-Photon imaging-based study

The first important study using this method quantified the CSF flow to the brain parenchyma (ILIFF et al., 2012). After intracisternal injection, the tracer was visible in the PVS of cortical arteries and arterioles. They described tracer at the surface of the cortex and due to the limited depth of imaging with this method, a tracer accumulation 50-120 μm below the cortical surface. As molecules of different weights and sizes were detectable in the cortical PVS, the group claimed that the transport to the PVS occurred by bulk flow. However, only the smaller particles entered the interstitium while the bigger molecules remained in the PVS. However, these observations were limited to the surface of the cortical area. Because of the methodical limitation of deeper imaging, the observation in the deeper brain parenchyma requires a post-mortem visualization. By the use of vibratome sections and genetic-modified mice allowing the distinguishment between veins and arteries, the group detected immediate tracer accumulation along with the whole arterial blood network in the brain parenchyma, especially in the region of the thalamus and basal ganglia. More than one hour later, the tracer was slowly detected in the venous system which seemed to allow the exit of CSF from the skull. These CSF routes outside the skull were dominated by medial internal cerebral veins and the lateral-ventral caudal rhinal veins. However, the post-mortem tracer movement due to unphysiological conditions could falsify these results.

The group of Kipnis found that lymphatic vessels are present around the dural sinuses that are directly connected with the DCLN (LOUVEAU et al., 2015). The process of immunohistochemistry was able to detect lymphatic endothelial cells within the meninges. These seemed to create a distinct lumen around the dural sinuses which enables them to transport fluids independently of the cardiovascular system. Moreover, this method demonstrated that many T-cells were aligned around these lymphatic vessels. Even though the lymphatic vessels in the meninges are characterized by similar structural and morphological aspects as the peripheral lymphatics, the organization is different. The networks drain from the eyes and the olfactory bulb reaching the venous sinuses. However, the lymphatics do not offer the complexity and density as their counterparts in the periphery. Within the meningeal area, the vessels became larger and more complex in the transverse sinus compared with the PSS.

This observation fits with the description of the publication of Ahn et al (AHN et al., 2019). In addition to that, they demonstrated even more density of lymphatic vessels at the base of the skull, while the 2-Photon-imaging is limited to the visualization of the dorsal skull. As a consequence, this study ignores the morphological advanced structures of lymphatics at the base of the skull, which is a major CSF pathway, as explained below.

In their experiments, the contrast agent was injected intraventricularly. By the use of 2-photon imaging, they observed the tracer drainage through the thinned skull. Some contrast agent was detectable in lymphatic vessels surrounding the PSS. As a result, the group suggested that this pathway works parallel

to the glymphatic outflow through the arachnoid projection in the dural sinuses (JOHANSON et al., 2008; WELLER et al., 2009).

To confirm their hypothesis, that the meningeal lymphatic vessels directly drain to the DCLN, they injected intraventricular Evans blue and observed the DCLN over two hours. 30 min post-injection, the tracer was visible in the DCLN and the meningeal vessels, before accumulation in the SCLN. When the group injected the same tracer in the nasal mucosa, no tracer was detectable in the CLN, which is why they claimed that the meningeal lymphatic vessels are the major passage for the CSF instead of the cranial nerves and the cribriform plate. The resection of the lymphatic vessels that drain into the DCLN resulted in the interruption of the physiological pathway as no tracer was evident in these lymph nodes. Instead, an increase in diameter was observed in the meningeal vessels.

However, these findings were challenged by different studies, using NIR imaging or MRI. As described below, the groups of Ma et al. were unable to confirm the tracer uptake in meningeal vessels (MA et al., 2017). These results were replicated by the MRI-based studies of Ahn et al. 2019 (AHN et al., 2019). The narrowed window of visualization and the focus on the meningeal vessels ignores that the tracer could reach the CLN on other routes, like the base of the skull. Moreover, the absence of imaging windows for the cranial nerves ignores another potential pathway, which was demonstrated by several in vivo studies. As a result, the uptake of tracers in the DCLN has been demonstrated more again, while the passage through the dorsal meningeal lymphatic vessels around the PSS and transverse sinus was not confirmed by other studies (MA et al., 2017).

2.3.3. <u>Near-infrared imaging-based studies</u>

Recently, NIR imaging was used in a study from 2017 by Ma et al. (MA et al., 2017). They were the first group that injected intraventricular NIR imaging compatible tracers in lymphatic vessels reporter mice to detect the lymphatic outflow in detail. 10 min post-injection, the animals were euthanatized, and the NIR images were taken 10 min, 30 min and 60 min after infusion. Firstly, the group demonstrated that their method could confirm the hypothesis of CSF outflow along the PNS to the CLN, which was the case. Afterwards, they investigated the relative contribution of the CSF to the systemic circulation in the blood system compared to the outflow in the lymphatic vessels. The results of the study demonstrated a significant difference in CSF outflow between 18-months-old mice versus younger two-month-old animals indicating a decreasing dynamic of CSF outflow with age. From the medical perspective, this physiological lack of CSF dynamic with age could be a potential explanation for many neurodegenerative diseases like Alzheimer´s dementia, which are correlated with increasing age. As described, the focal limitation of the NRI imaging required an observation at several locations. The study identified a tracer accumulation in the CLN and the PNS of the cranial nerves. Moreover, the

cribriform plate showed contrast enhancement indicating that the tracer drains through the pharynx into the DCLN. However, a tracer in the dural lymphatics could not be detected. Focusing on the saphenous vein and the posterior facial vein to detect the role of the venous drainage for the CSF outflow, the dye could be demonstrated in venous vessels 30 min after infusion while we could observe an increase of contrast in the CLN after 10 min. Therefore, it could be assumed that the lymphatic pathway has a major role in the CSF outflow. However, 10 min post-injection, an accumulation of tracer was demonstrated in the PVS of arteries of the Circle of Willis within the SAS spreading along the middle cerebral artery to the cortical hemispheres. After 60 min the PVS of the whole venous and arterial blood system in the brain contained contrast agent. Tracer penetrated in the so-called Virchow-Robin spaces suggesting a glymphatic flow too (ILIFF et al., 2012).

2.3.4. <u>Magnetic resonance imaging-based studies</u>

Ahn et al. used the MRI to show the CSF outflow along the lymphatics at the base of the skull following the cranial nerves which have their exit points there (AHN et al., 2019). They wanted to show the pathway along these nerves and the morphological structure which could explain the detailed passage outside the SAS in the lymphatic system. The base of the skull presents a confusing area of several exit points containing different nerves and vessels of all origins. The MRI with a wider window of visualization can demonstrate the CSF outflow in this region is of major importance in comparison to the dorsal skull. Moreover, the study showed that the morphological structure of the lymphatics in this region is changed with age, a fact that fits with the reduced CSF outflow in elder mice (MA et al., 2017). Investigating the morphology of the meningeal lymphatic vessels in Prox1-GFP lymphatic reporter mice, they concluded that the lymphatics in the meninges around the dorsal sinuses got a less wide lumen and do not have any valves while the lymphatics around the petrosquamosal and sigmoid sinus seems to be morphological like the peripheral lymphatics due to valves and a wider lumen. Moreover, the junctional pattern of the basal lymphatics impresses by loose and discontinuous morphology which enables them for the uptake of macromolecular CSF particles. Instead, the tight junctional pattern in the dorsal meningeal vessels offends this function. The morphological aspects of the basal lymphatic vessels led to the hypothesis, that they appear to offer a dual function due to the uptake and transportation of the CSF (AHN et al., 2019). In addition to that, a thinner dura layer and a loser arachnoid barrier in the basal skull in combination with a higher density of capillaries of lymphatic vessels around the SAS compared to the dorsal area indicated a basal outflow. The parallel exit of lymphatics and cranial nerves through the skull foramina makes a perineural lymphatic drainage plausible (WELCH, POLLAY, 1963). However, the removal of cranial nerves did not affect the function of the surrounding lymphatics which challenges the hypothesis of perineural drainage. The intracisternal bolus injection resulted in a tracer accumulation in the CLN before a detection in the dorsal meningeal lymphatic vessels. After the signal

peak in the cisterna magna, a basal outflow to the lymph nodes was detectable immediately. However, the dorsal lymphatics showed a slowed and reduced tracer accumulation. Referring to the study of Ma et al. 2017 (MA et al., 2017), the group investigated the structural characteristics of meningeal lymphatic vessels. Therefore, they distinguished their observation between a group of 3-months old mice and an elder group which was 24-27 years old. They described that in the elder mice, the density of lymphatic branches around the PSS and the dorsal skull was reduced. However, focusing on the base of the skull, the lymphatics revealed the opposite reaction than in the dorsal area due to a hyperplastic, higher branched lymphatic network. Interestingly, middle-aged mice are characterized by a reduced lymphatic network in the dorsal skull, while the base of the skull did not show any changes compared to young mice. Investigations of the morphological changes indicate that the hyperplastic basal lymphatics in old mice are less functional than in young mice as fewer valves, a dysmorphological collagen exhibition and other aged related restrict efficient drainage. Comparing these findings with lymphatics in peripheral organs, they could not confirm these age-related variations in the periphery. As a result, they assumed that these processes are organ-specific and explain the slowed CSF outflow in aged mice, as they claimed the basal skull as a major CSF pathway.

However, their focus on the basal skull ignores the olfactory with the cribriform plate and nasal cavity as a relevant pathway, which was described by several studies (MA et al., 2017). Moreover, the optic nerves, as another potential route, were not imaged. Therefore, it is impossible to quantify the importance of all described pathways. As illustrated in Figure 3 A, MRI allows to detect the CSF circulation within the whole skull and show all relevant pathways in vivo in one animal. Visualization of the role of the basal skull and the frontal cranial nerves in the same animals in comparison to tracer drainage in the dorsal skull would be possible. The detailed quantification of tracer drainage over time leads to an exact and extensive description of all relevant passages.

The recently published studies require a final MRI-based work that demonstrates the CSF outflow and shows the detailed passage. As shown in Figure 3 B, the NRI-based study by Ma et al. in 2017 has the disadvantage that the mice were euthanized before taking the images (MA et al., 2017). The group demonstrated the flow and accumulation of tracer in the lymph nodes and cranial nerves at different time points, but they were not quantified in the same mice. However, their idea that the CSF drains through the cribriform plate over the pharynx to the CLN seems to be right although the narrowed window of the NRI imaging requires a method offering a chronological overview to confirm this hypothesis.
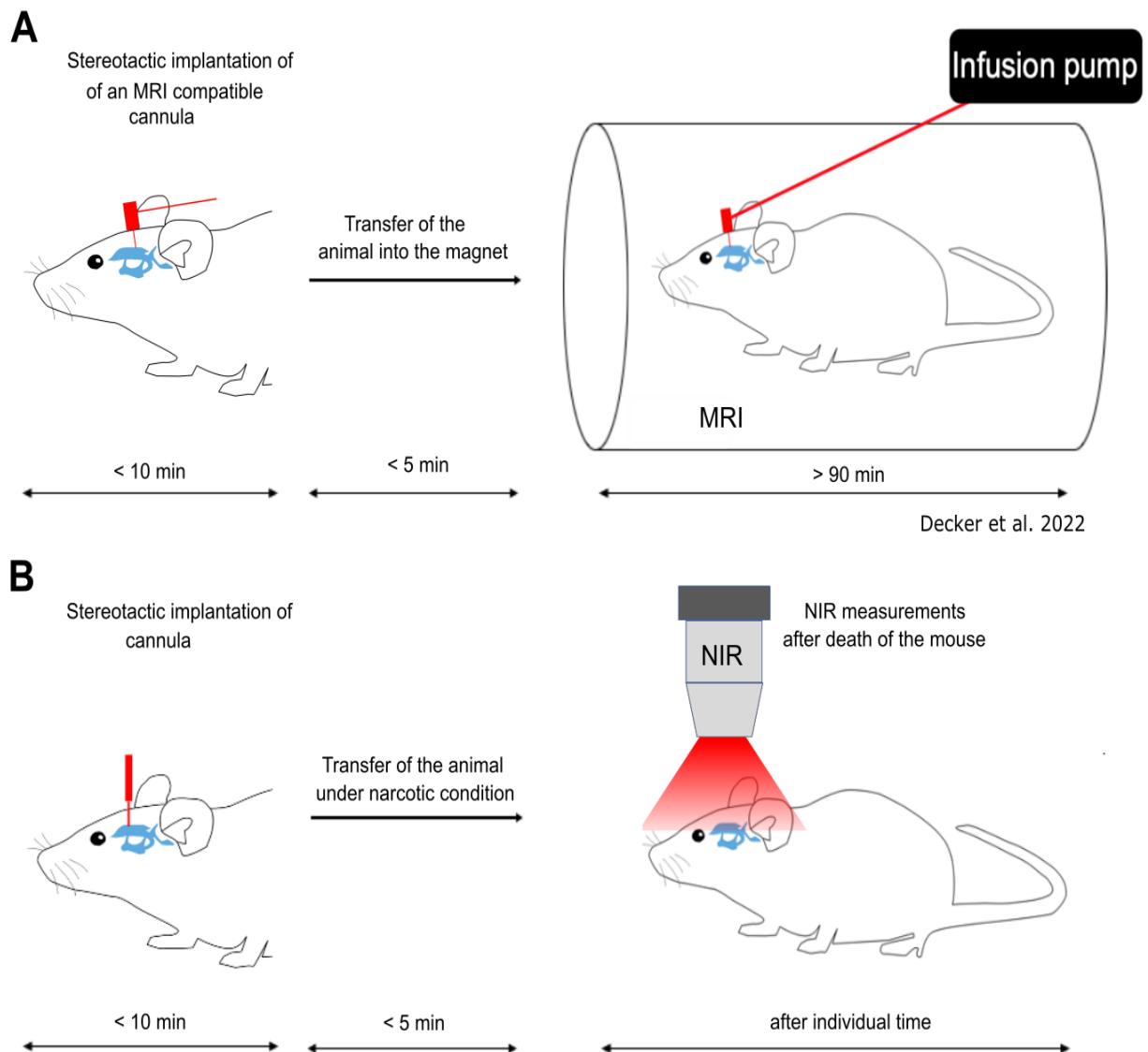
Figure 3: Schematic comparison of magnetic resonance imaging- and near-infrared imaging-based methods for cerebrospinal fluid investigation

A: Intraventricular implantation of an MRI-compatible cannula while fixing the head with a stereotactic frame. Afterward, the animal is transported in the MRI. The 60 min infusion and the MRI measurement are started (DECKER et al., 2022). Reprinted and adapted with permission [JCI Insight], [Decker Y, Krämer J, Xin L, Müller A, Scheller A, Fassbender K, Proulx ST (2022) Magnetic resonance imaging of cerebrospinal fluid outflow after low-rate lateral ventricle infusion in mice. JCI Insight 7:e150881]; https://doi.org/10.1172/jci.insight.150881, permission conveyed through Copyright Clearance Center, Inc. under the license https://creativecommons.org/licenses/by-nc-sa/4.0/legalcode. B: The mouse is intraventricularly injected over x min while fixated in the same stereotactic frame. After the chosen time, the animal is killed, and the near-infrared images are taken. Reprinted and adapted with permission [JCI Insight], [Decker Y, Krämer J, Xin L, Müller A, Scheller A, Fassbender K, Proulx ST (2022) Magnetic resonance imaging of cerebrospinal fluid outflow after low-rate lateral ventricle infusion in mice. JCI Insight 7:e150881]; https://doi.org/10.1172/jci.insight.150881, permission conveyed through Copyright Clearance Center, Inc. under the license https://creativecommons.org/licenses/by-nc-sa/4.0/legalcode.

In a second study, after an intraventricular bolus injection over 2,5 minutes, the group observed mice in different stadiums (MA et al., 2019b). Their findings describe a difference between awake and ketamine-anesthetized mice. While the outflow through the lymphatics seems to be more rapid in the awake mice,

the glymphatic perivascular seems to be the major pathway in the anesthetized mice. They concluded that the faster tracer elimination out of the CSF in awake mice impaired the perivascular pathway.

The PVS contrast seemed to be wider in vivo while the contrast agent was limited on the area near the ventricle and did not drain to the cortical blood vessels. However, when killing the mice, the tracer could be detected in the cortical blood system due to post-mortem vasoconstriction of the middle cerebral artery. This post-mortem tracer movement was confirmed by the same study as tracer accumulation in the cortex parenchyma increased only after the death. However, the detailed mechanism of CSF outflow along PVS remains unsolved as the drainage along veins to the CSF or a direct connection with the dural lymphatics vessels keep discussed (ASPELUND et al., 2015; ILIFF et al., 2015; LOUVEAU et al., 2015). An outflow along PVS could be not demonstrated for awake mice. An important role for the Circle of Willis was described as the anatomical connection of the arteries in this region as stomata within the pia mater could provide a CSF outflow pathway to the PVS (PIZZO et al., 2018; ZERVAS et al., 1982). Rostral of the Circle of Willis, the localization of the optical and olfactory nerve could explain the outflow from the basal cisterns either to the Circle of Willis or the cranial nerves depending on the physiological conditions. The group concluded that even in awake mice, a part of the CSF outflow has to appear over the PVS even if they did not understand the anatomical conditions in detail.

Another MRI-based study injected the tracer into the cisterna magna. The mice were distinguished into two groups by using different narcotics. The anesthesia was processed with isoflurane in one group, while the other group was anesthetized by ketamine/xylazine (STANTON et al., 2021).

The tracer was first detectable in the Circle of Willis and the subarachnoid cisterns. Afterward, the CSF drained along with the middle cerebral artery in the parenchyma from where it reached the olfactory bulb. An increase of contrast had been shown 1,5 mm dorsally of the middle cerebral artery, while 3 mm dorsal of the artery no increase was observed. Moreover, the tracer could be found in the basal foramina and Basilary artery. An increase of contrast along with the olfactory bulb and the nasal turbinate fits with the findings in our work. In addition to that, the pharyngeal lymphatics indicate a significant contrast enhancement. Under isoflurane, the contrast enhancement along with the arterial structures like the middle cerebral artery, the Circle of Willis, or the Basilary artery was significantly decreased compared to the ketamine/xylazine group. It was concluded that under ketamine/xylazine, the CSF transport appears to dominate through the spinal cord or along with the olfactory bulb and the nasal turbinate to the pharyngeal pathway (MA et al., 2019a; MA et al., 2017). Under the anesthesia with isoflurane, the CSF outflow seemed to follow the vagus nerve and leave the skull by the basal foramina.

2.4. Different pathway concepts of cerebrospinal fluid drainage to cervical lymph nodes

The recently published studies have in common that they focus on three models of the CSF outflow pathways to the DCLN. On the one hand, several publishers are convinced by a dominant CSF drainage along the glymphatic pathway that drains through the brain parenchyma and along the dorsal aspect of the skull, as illustrated in Figure 4 A. This model of glymphatic CSF outflow was especially postulated by the group of Iliff et al. (ILIFF et al., 2012; LOUVEAU et al., 2018; LOUVEAU et al., 2015; OLIVER et al., 2020; RUSTENHOVEN et al., 2021). However, these observations are challenged by several studies describing a predominantly outflow along the ventral and basal aspect of the skull (AHN et al., 2019; MA et al., 2019a).

As recent publications rediscovered the presence of lateral ventricle within the dura (AHN et al., 2019; ASPELUND et al., 2015; LOUVEAU et al., 2015) and a discussion was started on a potential CSF outflow along these. As a consequence, it was claimed that the major CSF outflow drains along with the dorsal venous sinuses like the PSS and transverse sinus (HEISEY et al., 1962; HOFFMANN, THIEL, 1956). These studies claim the presence of a glymphatic pathway meaning that the tracer drains along with the PVS through the brain parenchyma, as illustrated in Figure 4 A. After the passage of the arachnoid projections, the tracer drains to the PVS of the venous sinuses. Afterward, the contrast agent would flow in the dural lymphatic vessels along with these sinuses. Therefore, the CSF outflow to the DCLN would dominate along the dorsal aspect of the skull.

Other findings challenged this model of CSF outflow, as they described tracer drainage to the DCLN along the cranial nerves at the base and the front of the skull which is shown in Figure 4 B (MA et al., 2019a; MA et al., 2017; PIZZO et al., 2018; STANTON et al., 2021). By using NIR imaging and MRI to reevaluate the CSF outflow in mice, they described a major pathway along the PNS to the nasal cavity and orbital space. After reaching the front of the skull, the tracer follows the lymphatic vessels draining in the DCLN. Moreover, the base of the skull with several foramina, working as an exit point for other cranial nerves, is described as a parallel outflow pathway (MA et al., 2019a).

The third model, which is shown in Figure 4 C, illustrates the work of Ahn et al. By using MRI, they focused on the role of the base of the skull. On the microscopic view, they observed a more branched network of lymphatics with an advanced morphological structure for a potential CSF outflow at the base of the skull compared to the lymphatics around the venous sinus at the dorsal skull. In their opinion, the morphological characteristics of basal meningeal lymphatics and the localization close to the exit points of the cranial nerves that allows a CSF outflow from the SAS defines the basal region of the skull as a major pathway (AHN et al., 2019).
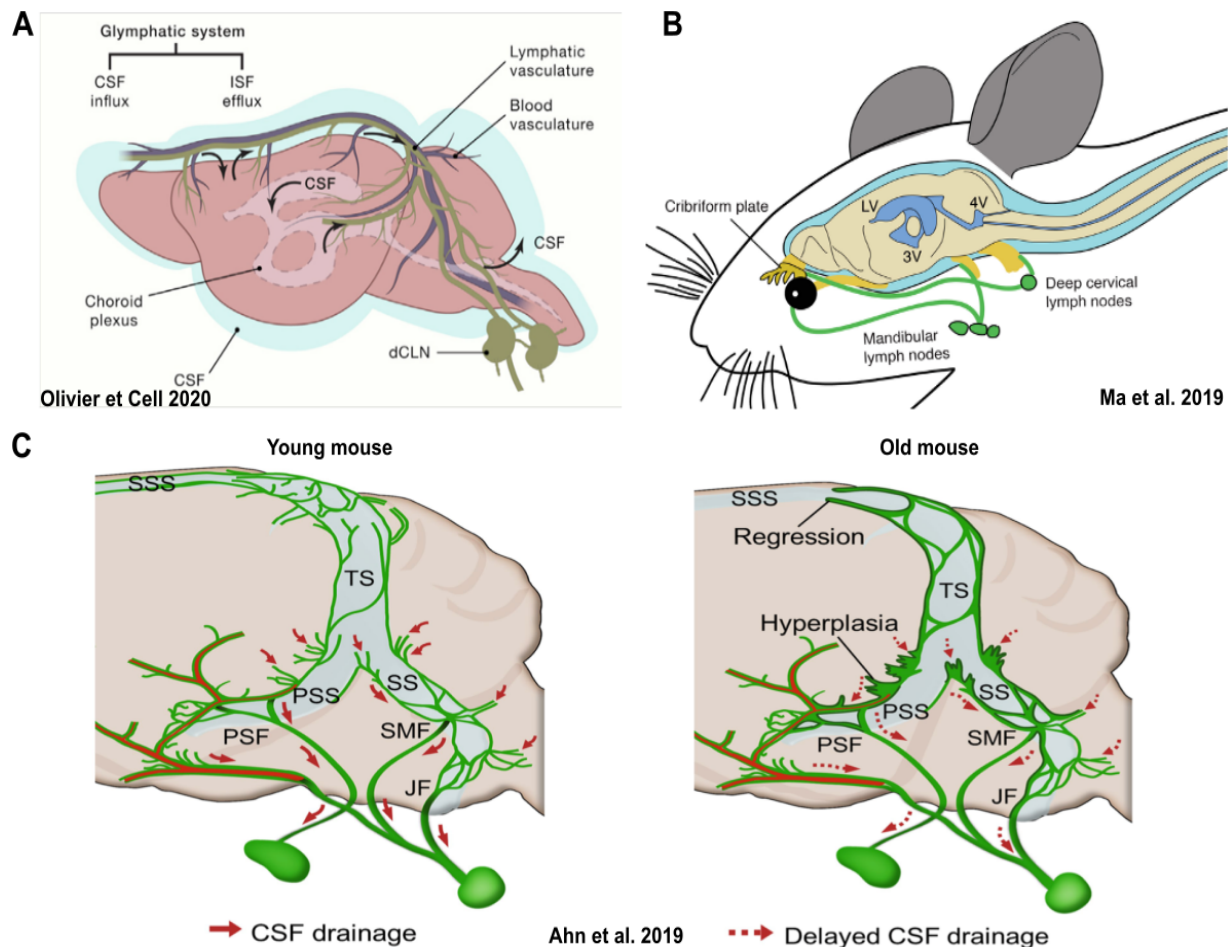
Figure 4: A consensus exists on cerebrospinal fluid outflow to the deep cervical lymph nodes, although the pathways to the deep cervical lymph nodes are still under debate

A: According to hypothesis 1, CSF drains with the glymphatic pathway through the brain parenchyma. The tracer next flows along the perivascular meningeal lymphatics at the dorsal side of the skull and reaches the DCLN (OLIVER et al., 2020). Reprinted with permission of Cell; Volume 182, Issue 2; Oliver G, Kipnis J, Randolph GJ, Harvey NL; The Lymphatic Vasculature in the 21st Century: Novel Functional Roles in Homeostasis and Disease. Page 270-296; Copyright Elsevier (2020). B: According to hypothesis 2, the tracer outflow dominates through the front and the base of the skull along PNS, leaving the skull through the neuronal exit points. From there, the CSF reaches the CLN (MA et al., 2019c). Reprinted with permission [ROCKEFELLER UNIVERSITY PRESS], © 2019, Ma et al.; Originally published in Journal of Experimental Medicine. https://doi.org/10.1084/jem.20190351. C: According to hypothesis 3, the CSF drains along with the basal venous sinuses in the PVS. Especially the PSS and the transverse sinus dominate in this pathway. With increased age, the CSF outflow is slowed down in the PVS leading to a reduced accumulation in the DCLN (AHN et al., 2019). Reprinted with permission of [Springer Nature]: [Ahn JH, Cho H, Kim J-H, Kim SH, Ham J-S, Park I, Suh SH, Hong SP, Song J-H, Hong Y-K, Jeong Y, Park S-H, Koh GY (2019) Meningeal lymphatic vessels at the skull base drain cerebrospinal fluid. Nature 572:62–66], https://doi.org/10.1038/s41586-019-1419-5, permission conveyed through Copyright Clearance Center, Inc. under the license https://creativecommons.org/licenses/by-nc-sa/4.0/legalcode.

2.5. <u>Aim of study</u>

As described previously, recent studies have challenged historical views regarding CSF outflow. Anatomical pathways of CSF outflow are under intense debate in the scientific community and no consensus has been reached.

In this study, using newly developed methods that combine slow-rate infusion of contrast agent associated with dynamic contrast-enhancement MRI), we have tried to clarify conflicting observations.

1. Our first aim was to identify the different anatomic routes used by CSF.

   To do so we aimed at developing a method to preserve the physiological integrity of CSF circulation by developing a slow-rate infusion method that avoids the creation of artificial, pressure-related CSF movement.

   We also aimed at optimizing the method to image by MRI the whole head including the surrounding tissue of the CLN with high spatial and temporal resolution.

2. After the determination of the different CSF outflow routes, our second aim was to identify which ones were the major route(s).

   In dynamic contrast-enhancement MRI, it is not able to estimate the relative contribution of each clearance pathway and determine the major outflow routes. For example, a site with slower dynamics would appear to have more overall flux than an area with rapid transport of contrast agent and a faster washout.

   We used the advantage, that the differences in CSF outflow between young and aged mice were already known as aged mice show a reduced outflow. This development can only be explained at major outflow pathways for CSF that would show the expected differences between young and aged animals. By this observation, it would be possible to reveal the major CSF outflow route(s).

3. <u>Material and method</u>
3.1. <u>Mice</u>

Female, wild-type mice (Janvier, France) that are characterized on the C57BL/6 background were used. For the experiment, the mice were distinguished into a group of 2-3 months old animals and a group at 24 months of age. Although the group of elder mice is described as aged mice in our work, this age is declared as mid-aged. Aged mice are defined as animals older than 24 months. However, we used the term aged mice in this work. The animals were kept in a closed, pathogen-free environment until their use for the experimental process. The experiments with the animals are approved by the Landesamt für Gesundheit und Verbraucherschutz, Saarbruecken, Germany (license number 31/2018 and 45/2019).

3.2. <u>Anesthesia</u>

In the morning before the surgery, the mouse is transported to the operation room. Then, it got time to adapt to the new environment.

The anesthesia is reached through intraperitoneal injection of ketamine (100mg/kg) and xylazine (20mg/kg), which guarantee sufficient pain relief and anesthesia. While the surgery, the infusion, and the MRI, we applied isoflurane through the inhalation mask in oxygen-enriched air. The used isoflurane doses were adjusted to the depth of the narcotic stadium. Generally, the isoflurane doses were kept steady between 0,5 and 1% with 98% O2 to prevent and respiratory rate lower than 140 breaths per minute. The animals could breathe spontaneously in the whole experimental procedure. The monitoring of the vital parameters as the respiratory rate and the body temperature were measured non-invasive (SA Instruments, Stony Brook, NY). A body temperature between 36,5°C and 37,5°C was the aim. To keep the animal at a physiological temperature, the mouse was planted on water bath-operated thermal pads too.

Figure 5 shows the used stereotactic frame (Kopf Instruments, Tujunga, CA) that allows to fix the head between the two ear bars on both sides. The frontal side of the skull is localized in the nose bare, where the anesthesia is applied.
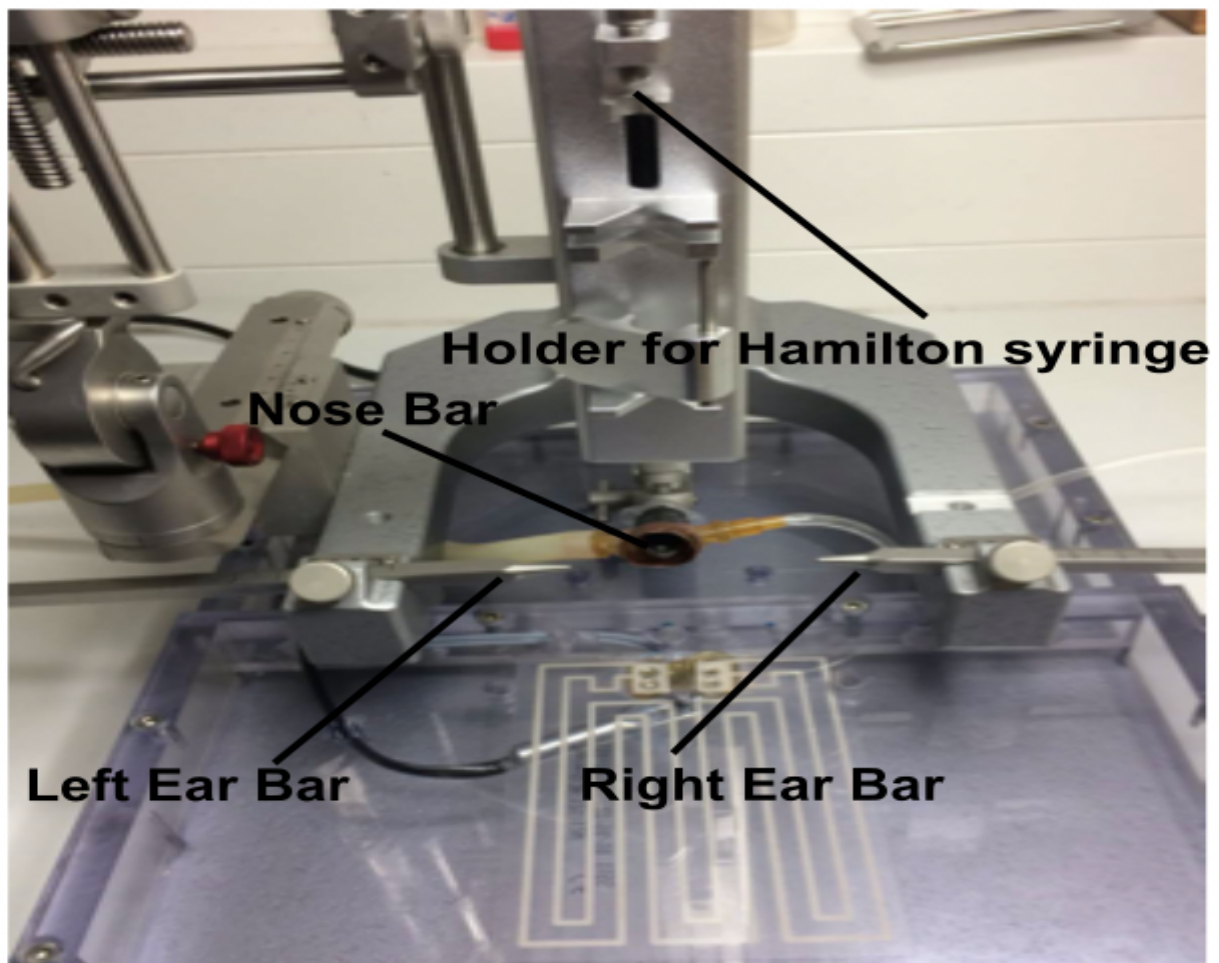

Figure 5: Stereotactic surgery tool

Illustration of the used stereotactic frame (Kopf Instruments, Tujunga, CA). Descriptions are made to show the several functional parts of the stereotactic frame. The mouse is fixed between the ear bars on the side of the skull while the nose is placed in the nose bar. Above, the holder for the Hamilton syringe can be moved in 3 dimensions. This enables the user to place the cannula at the exact position.

3.3. <u>Surgical operation</u>

The skull was shaved to get a free view of the periost of the skull. Afterward, the head of the mouse was fixed in a stereotactic frame (Kopf Instruments, Tujunga, CA). To uncover the scull, a small incision along at the occipital suture sagittal was made. By using some tweezers, the skin was pulled up. Under the stereomicroscope, a 1,2 cm long, longitudinal incision from the anterior to the occipital side of the skull was done by using feather scissors. Around the suture cross, the cut was extended along the suture coronals with the same method. Afterward, the flaps of skin were removed by the tweezers. As a consequence, we got a free view of the suture cross. The operation protocol was copied from DeVos et al. 2013 (DEVOS et al., 2013).

A mixture of bupivacaine and lidocaine was put on the uncovered periost (mixture of 1:1). Then, the bone was thinned with a Proxxon GG 12 Engraving drill (Proxxon, Niersbach, Germany). With the help of the stereotactic frame, the exact position to insert the 2,5 mm long, MRI-compatible 28G microcannula (#328OP/PK/Spc; Plastics One) was calculated.

Firstly, the bregma was the point of orientation on the skull. The correct position for the insertion of the cannula is reached 0,95 mm at lateral and 0,22 mm caudal from the bregma. Then, the cannula was localized above the lateral ventricle and inserted 2,5 mm ventral of the skull surface (MA et al., 2019a). The successfully placed cannula was sealed with cyanoacrylate glue. The skin was replaced over the infusion area and reconnected by 2-3 stitching. The implanted and anesthetized animal is transported in prone position to the MRI cradle (BioSpec Avance III 94/20; Bruker Biospin GmbH, Ettlingen, Germany) and was examined without application of the contrast agent. Afterward, Gadospin D (nanoPET Pharma GmbH, Germany) solution with at a Gadolinium G concentration of 25 mM was filled in a 1-1,5m long polyethylene catheter. The catheter was connected to the microcannula and a 10 µL syringe which is regulated by NanoJet syringe pump (Chemyx Inc., Stafford, TX, USA). The microcannula and the syringe pump are MRI-compatible.

The skin was closed with a medical adhesive bandage around the microcannula.

For the surgical operations, 15-25 minutes were calculated.

3.4. Dynamic magnetic resonance imaging

The imaging of the CSF circulation was performed by horizontal-bore 9,4 T animal scanner (BioSpec Avance III 94/20; Bruker Biospin GmbH, Ettlingen, Germany) with a BGA12S gradient system with ParaVision 6.0.1 (Bruker Biospin GmbH) and a lineary polarized coil with an inner diameter of 40 mm (Bruker Bipspin GmbH). Immediately after the infusion of the contrast agent the MRI was performed on anesthetized, prone-positioned animals. To detect the contrast enhancement, a three-dimensional time of flight gradient recalled echo sequence (3D-TOF-GRE) was adapted from previous imaging processes of lymphatic vessels. The recovery time of 12,0 ms, echo time of 2,5 ms, flip angle 25 °, matrix 600 x 432 x 180, a field of view 36,00 mm x 25,92 mm x 18,00 mm, one average, and a scan time of 4 min 19 s 200 ms were the chosen imaging parameters. Furthermore, next to the animal´s head, a phantom was planted to calculate the intensity normalization over time. The phantom contained a dilution of 5 mM Gadolinium and 0,9 % NaCl.

Firstly, a baseline scan was taken to control the position of the implanted cannula and to guaranty the physiological anatomy of the CNS. The Gadospin D solution of 25 mM was infused constantly at a rate of 0,1 µL/min for 60 minutes. This rate means around 1/3 of the estimated CSF production rate in mice (Davson and Segal, 1996; 29867199). In the end, 6 µL of a solution based on 25mM Gadospin D (nanoPET Pharma GmbH, Germany) were injected in lateral ventricle.

The performed 3D images were analyzed by Horos software (version 3.3.6, Horos Project). In the software, the ROIs were drawn manually in two sections for each mouse. The data from the sections were averaged. For each section, the contrast of the phantom was quantified and the measured ROI´s were normalized.

3.5. Statistics

Other successful, reproducible studies were the reference for the size of the two groups (Ma et al. 2017, 30306266). The statistical analyses were done with GraphPad Prism 5 (GraphPad). All values are presented as mean +- Standard error of the mean (SEM). The means were compared by common unpaired two-tailed Student´s t-test. For the comparison of measured values, two-way ANOVAs followed by Bonferroni´s posthoc test were used. A p-value below 0,05 indicated statistical significance. As explained, the ROIs were drawn manually in the HOROS software (version 3.3.6, Horos Project), shown in Figure 6. Figure 6 A illustrates the manually placed ROI on the lateral ventricle. The contrast enhancement was quantified in the contralateral lateral ventricle of the infusion site. The massive contrast enhancement at the site of infusion leads to black spots creating artificially reduced values. The lateral ventricles are separated by a permeable membrane and show a comparable increase. However, the contralateral ventricle did not produce artificial black spots. Therefore, it was taken as ROI and the

measured values are more reliable. After the correct positioning of the ROIs, the HOROS software calculated the contrast enhancement. This process was done for each slide of the MRI images.
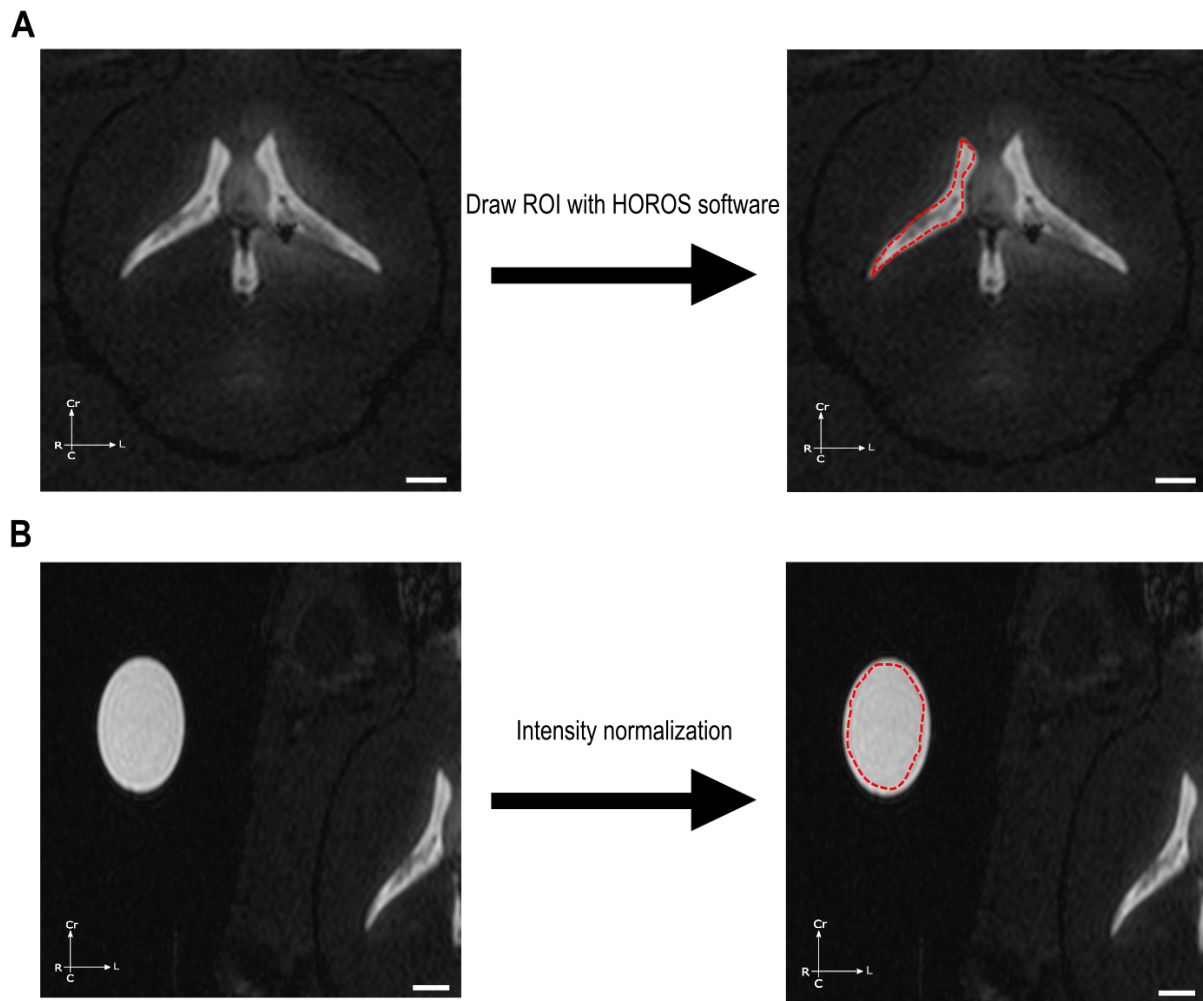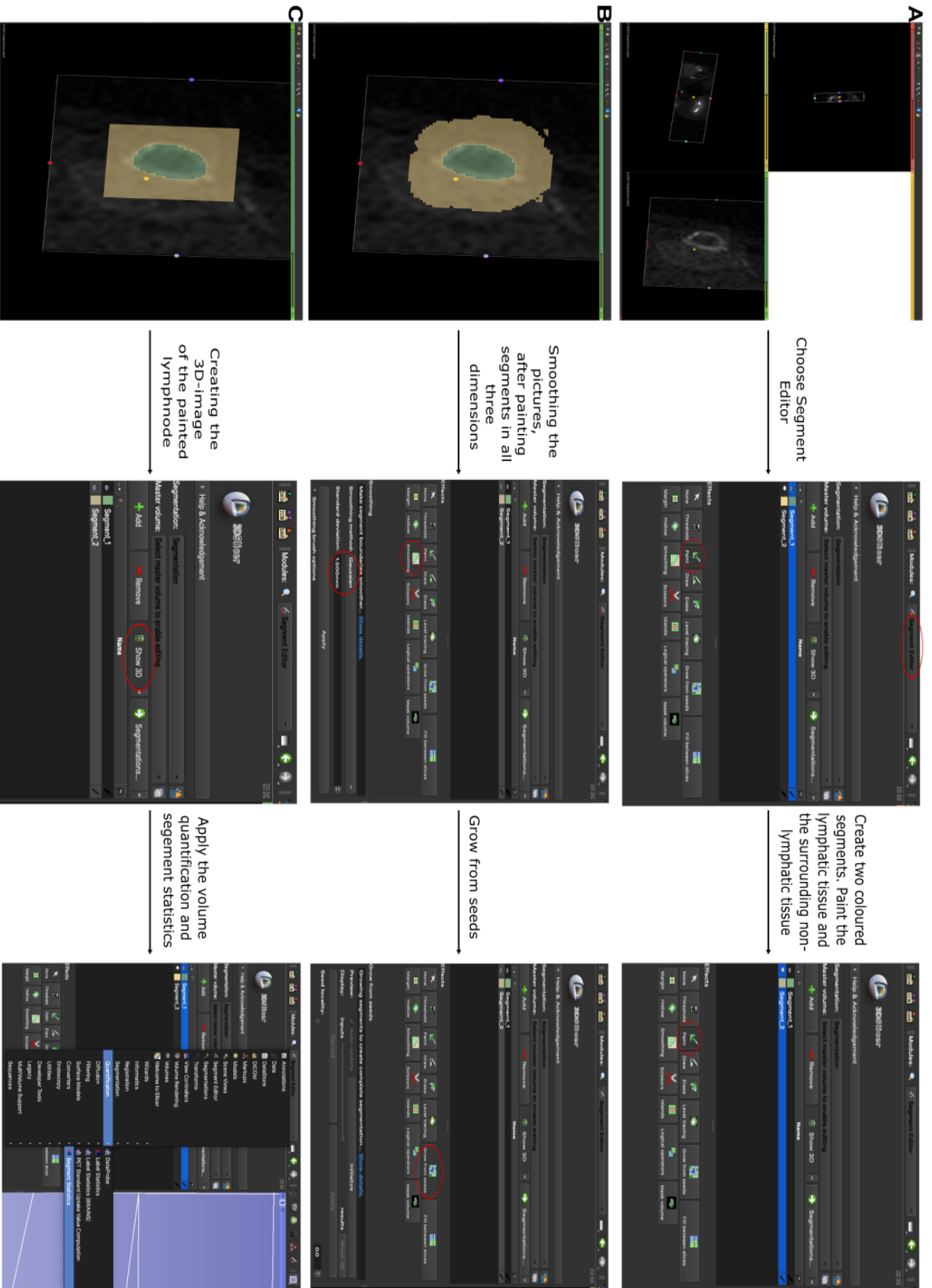

Figure 6: Data processing of the magnetic resonance imaging

A: ROIs were drawn manually in the HOROS software in the correct position. Here, the lateral ventricle is taken as an example. The HOROS software calculates the contrast value at this region. B The ROI was drawn on the phantom, the polyethylene tubing that contains the contrast agent. This quantification was necessary to normalize the ROI value of measured regions. It was calculated in every slide.
Scale bar 1 mm.

To achieve the normalized value of contrast increase over time, the quantified value of the ROI was divided by the measured value of the phantom. The measurement of the phantom is illustrated in Figure 6 B. For the calculation of the percentage change, the pre-infusion ROI was taken as the basis. This value was substrate from the measured contrast increase in the slide of interest. As a result, the absolute change was quantified and was divided by the baseline value. For getting the percentage change, it was multiplicated by 100. At the end, the percentage change of contrast enhancement over time is calculated by the following equation: [(normalized signal intensity – normalized pre-infusion intensity) / (normalized pre-infusion intensity)] x 100.

For the calculation of the volume of the lateral ventricle and the lymph nodes, the software 3DSlicer, version 4.11 (www.slicer.org), was used. All MRI images were imported from Horos software. The used slides for each animal were standardized, as the slide with the highest intensity in the lateral ventricle. or lymph node was taken. Figure 7 demonstrates the applicated steps in the software on the example of a DCLN as region of interest. At first, as shown in Figure 7 A, two segments were chosen to paint the lymph node and the surrounding, non-lymphatic tissue. The painting was done for all three dimensions with the segment editor module. As shown in Figure 7 B, the painted segments required a smoothing with Gaussian 1,500 mm and the application of „Grow from seeds". Finally, a 3D construction of the lymph node was designed, and the software calculated the volume with segment statistics module, illustrated by Figure 7 C.

Figure 7: Volume quantification in Slicer 3D

Screenshots from the different steps in the software Slicer 3D 4.11 (www.slicer.org). The red circles illustrate the applicated buttons. The left side shows the change of painting after the implementation of the processes. A: Through the segment editor module two segments were chosen. One segment paints the tissue of interest (lateral ventricle or lymph node) and the other segment the surrounding tissue for better definability. B: The two segments

require smoothing, which was applied with Gaussian 1,500 mm. The implementation of „Grow from seeds" generates the final reconstruction of the structure which is ready for reconstruction. These steps were performed in the segment editor module, too. C: The 3D model is calculated in segment statistics module by the software. As marked in blue, „Quantification" and „Segment statistics" were applied and the volume was quantified.

All statistical analyses were done by GraphPad Prism (GraphPad). The contrast values are presented as mean +-SEM. Unpaired two-tailed Student´s test was used to compare two groups. Two-way ANOVA was applied to compare with age as a between-subject factor and time points as a within-subject factor. Then, Bonferroni´s posthoc test was done. Statistical significance was reached by a p-value <0,05.

4. <u>Results</u>

4.1. <u>Validation of the experimental method</u>

At first, it is necessary to confirm the findings that are already accepted as the accumulation in the CLN (MA et al., 2019a; MA et al., 2017; MA et al., 2019b). As the study is the first that works with the MRI-based, slow-rate infusion, a confirmation of previous descriptions is required that showed tracer accumulation after bolus injection (MA et al., 2019a; MA et al., 2017; MA et al., 2019b). As the mouse produces around 35 µL CSF per day (DAVSON, SEGAL, 1966), bolus injections of 5-10 µL could create an unphysiological elevated ICP. As a result, I decided to establish a method with a slower and physiological tracer application. However, the establishment of a new method of tracer infusion requires confirmation as a valid method. Therefore, the demonstration of tracer accumulation in the CLN after tracer infusion is necessary. As shown in Figure 8 A, the quantification of the contrast enhancement in the DCLN indicates a similar increase compared to bolus injection illustrated by Figure 8 B (MA et al., 2019a; MA et al., 2017; MA et al., 2019b). Moreover, Figure 8 illustrates, that the tracer accumulation in the CLN is delayed and reduced in aged mice as observed after bolus injection (BRADY et al., 2020; LIU et al., 2020; MA et al., 2017). As a result, my experimental setup of slow rate infusion and imaging is valid.
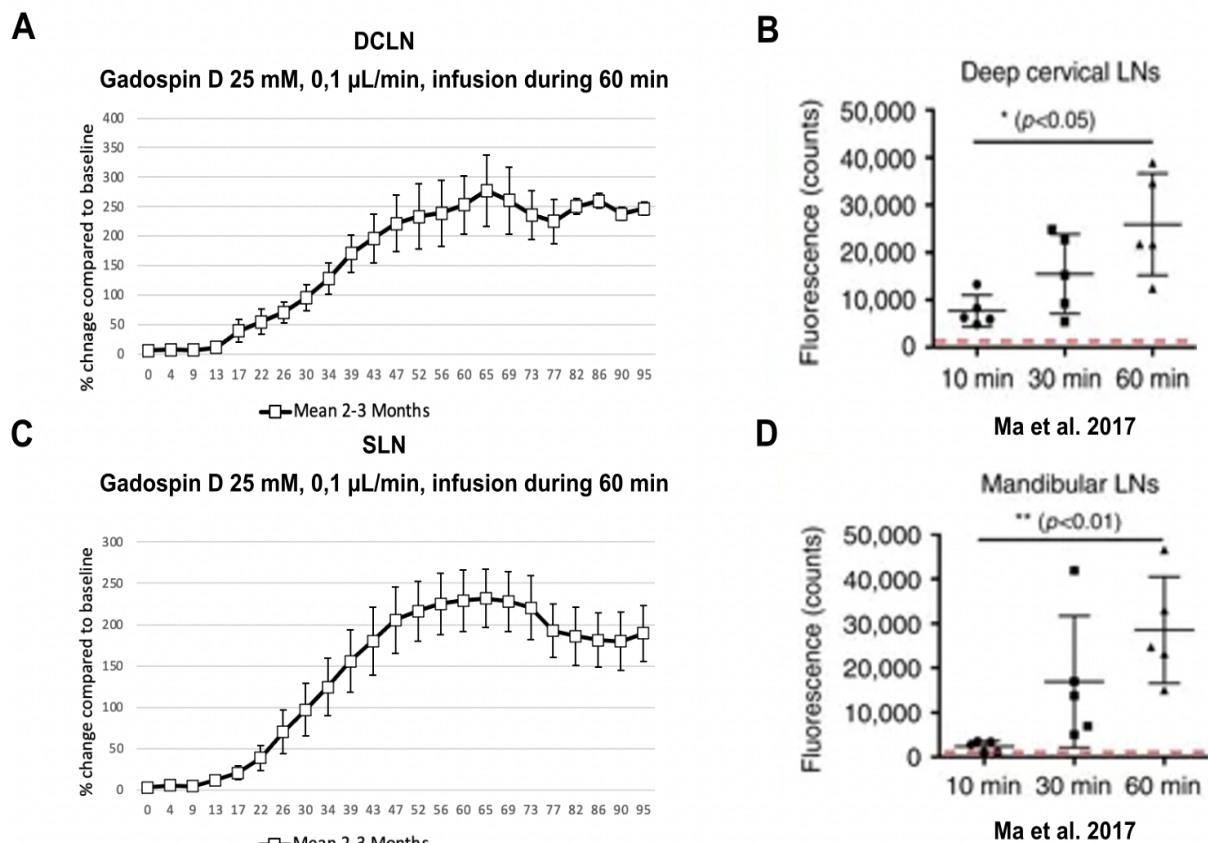
Figure 8: Tracer detection in cervical lymph nodes by magnetic resonance imaging is in accordance with previously published near-infrared imaging observations

A: The signal in the DCLN increases 15 min post-infusion for the whole time of infusion duration of 60 min. After the infusion, the contrast keeps steady on a high level. B: The MRI-based study found a similar increase as the near-infrared imaging-based study. C: The contrast in the SLN increases slower over the same time and peaks below the quantification of the DCLN. Reprinted with permission of [Springer Nature]: [Ma Q, Ineichen BV, Detmar M, Proulx ST (2017) Outflow of cerebrospinal fluid is predominantly through lymphatic vessels and is reduced in aged mice. Nat Commun 8:1434], https://doi.org/10.1038/s41467-017-01484-6, permission conveyed through Copyright Clearance Center, Inc. under the license https://creativecommons.org/licenses/by-nc-sa/4.0/legalcode. D: The other study found a slower and reduced increase compared to the DCLN too. Reprinted with permission of [Springer Nature]: Outflow of cerebrospinal fluid is predominantly through lymphatic vessels and is reduced in aged mice. Nat Commun 8:1434], https://doi.org/10.1038/s41467-017-01484-6, permission conveyed through Copyright Clearance Center, Inc. under the license https://creativecommons.org/licenses/by-nc-sa/4.0/legalcode.
Data are expressed as mean ± SEM of n=7 young mice and are representative of three independent experiments.

Observations of the CLN show that the peak of contrast enhancement is significantly reduced in elder mice compared to the younger animals. As shown for the DCLN in Figure 9 A and the SLN in Figure 10 A, the magnetic resonance images show a significantly slowed increase of contrast enhancement in aged mice. In lymph nodes, the contrast agent peaks at the surface of the nodes while the inner tissue shows less contrast enhancement. The illustrations in Figure 9 B and Figure 10 B indicate that the volume of the SLN and DCLN between aged and young mice is not significantly reduced. Therefore, the possibility of an artificially reduced contrast enhancement due to increased volume of the CLN is

eliminated. As a consequence, the physiological process of aging seems to be responsible for this change in CSF dynamics. However, the details of this process keep unsolved.

Moreover, as shown in Figure 9 C, the increase of contrast in DCLN starts around 15 min post-injection in both groups while the acceleration is significantly reduced in elder mice. The SLN, as shown in Figure 10 C, demonstrate a similar finding as the acceleration is significantly slower in the aged group. However, the increase of contrast starts for the young mice around 15 min too. However, in the group of elder mice, a contrast enhancement is observed after nearly 30 min. The application of bolus injection and NIR imaging demonstrated similar findings (MA et al., 2017). As described before, the contrast quantification in young mice is significantly increased 30 min post-injection and still higher than in aged mice 60 min post-infusion in the CLN.

Figure 9 D and 10 D shows the decreased and slowed contrast enhancement in the CLN that is detectable after bolus-injection and NIR imaging too (MA et al., 2017). Therefore, the method of slow rate infusion and MRI confirms common knowledge and is valid.
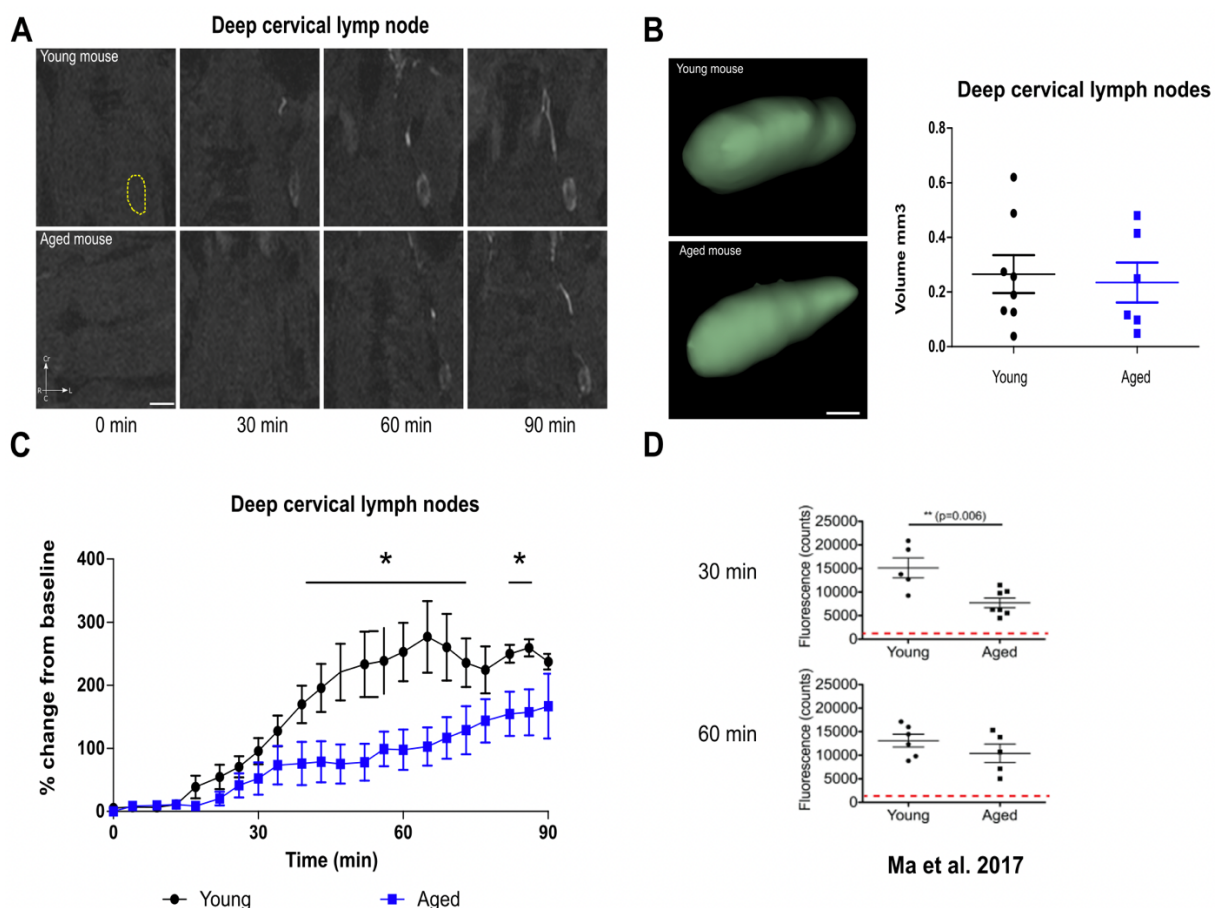

Figure 9: Reduced tracer detection in deep cervical lymph nodes of elder mice by magnetic resonance imaging is in accordance with previously published near-infrared imaging-based observations

A: Magnetic resonacne images directly post-infusion and 30 min, 60 min, and 90 min post-infusion. The upper series shows an example for a young mouse and the series below for an elder mouse. The subjective view indicates a reduced contrast for the aged mouse. B: The 3D reconstruction by Slicer 3D of the DCLN in both groups shows a similar macroscopic size. The volume calculation for all used mice shows no significant difference due to age. The volumes are compared with a two-tailed Student´s t-test. Scale bars: 0,3 mm. C: The increase of contrast is

significantly delayed and reduced in elder mice. However, the acceleration of tracer accumulation starts in both groups around 15 min. Quantifications of the different ROIs are expressed as the mean ± SEM of n= 7 young mice vs n=6 aged mice and are representative of three independent experiments. *$p<0.05$ (two-way ANOVA followed by Bonferroni's posthoc test). Reprinted and adapted with permission [JCI Insight], [Decker Y, Krämer J, Xin L, Müller A, Scheller A, Fassbender K, Proulx ST (2022) Magnetic resonance imaging of cerebrospinal fluid outflow after low-rate lateral ventricle infusion in mice. JCI Insight 7:e150881]; https://doi.org/10.1172/jci.insight.150881, permission conveyed through Copyright Clearance Center, Inc. under the license https://creativecommons.org/licenses/by-nc-sa/4.0/legalcode. D: NIR imaging demonstrates a significantly reduced accumulation 30 min post-injection in aged mice. The contrast decreases after 60 min in the young mice while the aged group shows still an increase. Reprinted with permission of [Springer Nature]: [Ma Q, Ineichen BV, Detmar M, Proulx ST (2017) Outflow of cerebrospinal fluid is predominantly through lymphatic vessels and is reduced in aged mice. Nat Commun 8:1434], https://doi.org/10.1038/s41467-017-01484-6, permission conveyed through Copyright Clearance Center, Inc. under the license https://creativecommons.org/licenses/by-nc-sa/4.0/legalcode.
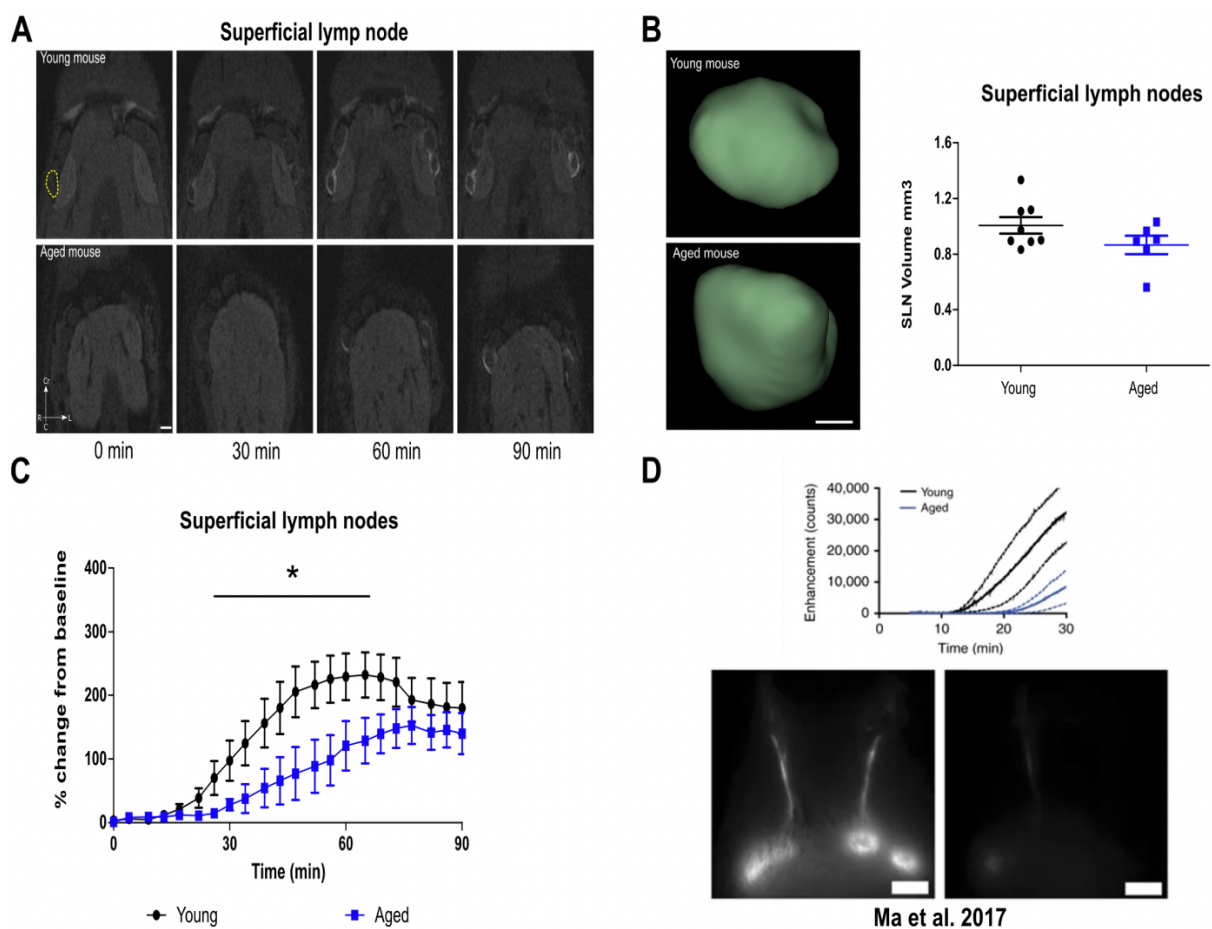

Figure 10: Reduced tracer detection in submandibular lymph nodes of elder mice by magnetic resonance imaging is in accordance with previously published near-infrared imaging-based observations

A: Magnetic resonance images directly post-infusion and 30 min, 60 min, and 90 min post-infusion. The upper series shows an example for an elder mouse and the series below a young mouse. The subjective view indicates a reduced contrast for the aged mouse. B: The 3D reconstruction of the DCLN in both groups by SLICER-3D shows a similar macroscopic size. The volume calculations for all used mice show no significant difference due to age. The volumes are compared with a two-tailed Student´s t-test. Scale bars: 0,3 mm. C: The increase of contrast is significantly slowed and reduced in elder mice. However, the acceleration of tracer accumulation starts in both groups around 20 min. Quantifications of the different ROIs are expressed as the mean ± SEM of n= 7 young mice vs n=6 aged mice and are representative of three independent experiments. *$p<0.05$ (two-way ANOVA followed by Bonferroni's posthoc test). Reprinted and adapted with permission [JCI Insight], [Decker Y, Krämer J, Xin L, Müller A, Scheller A, Fassbender K, Proulx ST (2022) Magnetic resonance imaging of cerebrospinal fluid outflow after low-rate lateral ventricle infusion in mice. JCI Insight 7:e150881]; https://doi.org/10.1172/jci.insight.150881,

Therefore, as shown in Figure 11, the tracer distribution can be tracked back after the infusion by MRI. Figure 11 A highlights all the relevant regions, that play a role in the CSF outflow. As shown in Figure 11 B, an overview was created that demonstrates the tracer accumulation at several time points and enabled us to visualize the tracer accumulation in three dimensions. 15 minutes after infusion the tracer is detectable at the basal cisterns and the olfactory bulbs. After passing more time, contrast enhancement is detectable in the nasopharyngeal region. Moreover, an increase in the CLN starts 20 minutes after infusion. The observation of the overview in Figure 11 indicates a continuous anatomical pathway from the nasal cavity along with the nasopharyngeal region to the DCLN. Moreover, a connection between the SLN and the DCLN is detectable, which was described by another publication too (MA et al., 2017). In Figure 11 C, further descriptions of relevant anatomical structures in the MRI are visible.
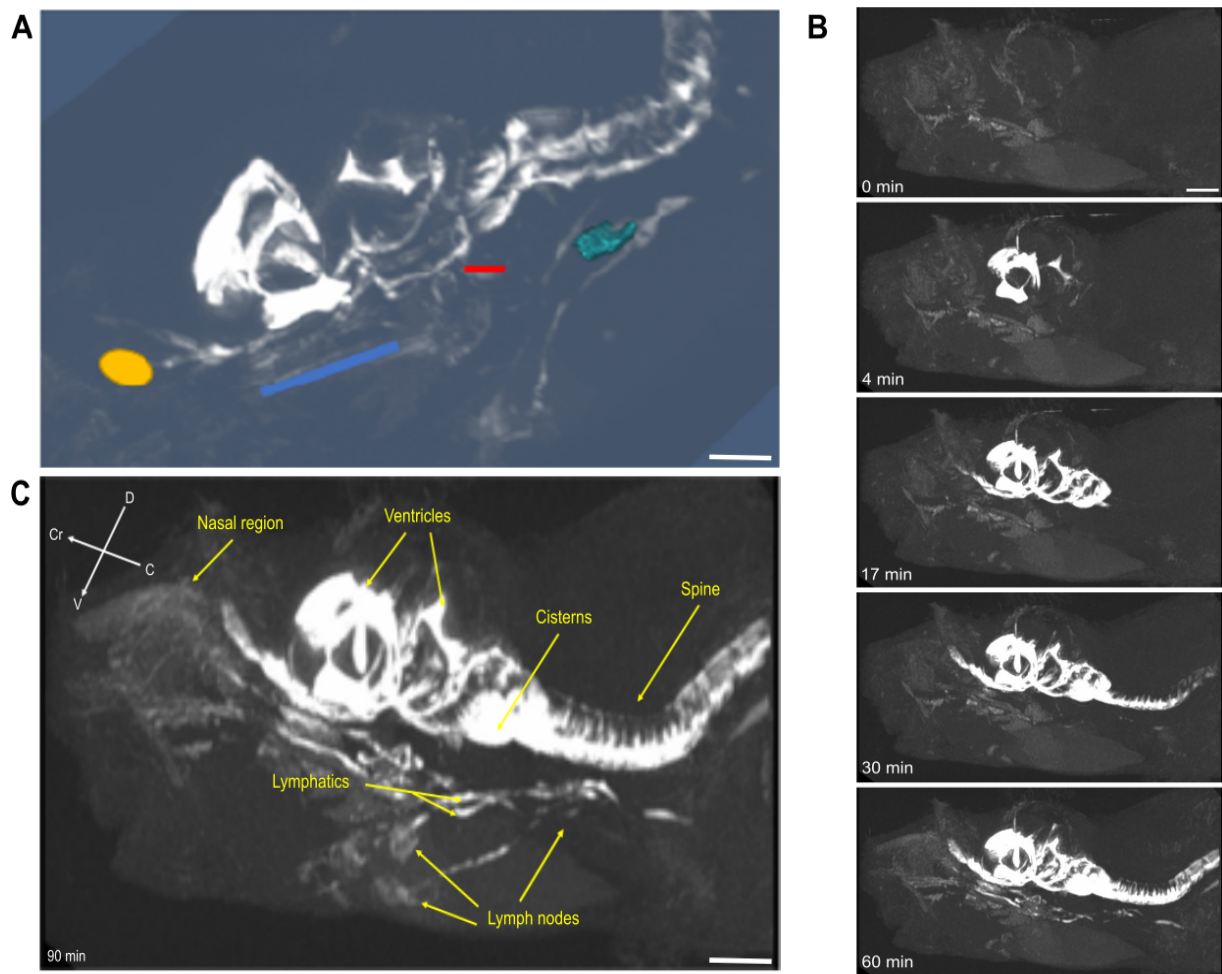
Figure 11: Dynamic contrast-enhanced magnetic resonance imaging showed a continuous efflux of contrast agent from the nasal region through lymphatic vessels toward cervical lymph nodes following slow-rate infusion

A: Maximum intensity projection of the mural head with HOROS software. The quantified regions are highlighted. The yellow color shows the nasal cavity, blue color shows the lymphatics in the pharyngeal region draining to the CLN in green color. The red line demonstrates the location of the jugular foramen. B: Timeline demonstrates the mural head before injection and the tracer flow 4-, 30-, 60- and 90-min post-infusion. The tracer was infused successfully without any leakage or diffusion after 4 min. The CSF system is filled with the tracer after 30 min. An hour post-infusion, increased contrast in the nasal region and the lymphatics around the CLN are detectable. Moreover, the CLN are recognizable due to tracer accumulation. After 90 min, the tracer accumulation in the named regions after 60 min increases even more. C: MRI overview on the CNS and a mural head and neck after intraventricular injection 90 min post-infusion. The arrows indicate the relevant regions for CSF outflow. A massive tracer accumulation is detectable within the CSF system in the spine and in basal part of the brain. Moreover, a diffuse contrast was visible in the nasal region. The CLN are significantly filled with contrast agent. Data are representative of n = 7 mice and three independent experiments. Scale bars: 3 mm.

4.2.   Perivascular space at the base of the skull as a potential pathway

The recent demonstrations of decreased tracer outflow in aged mice compared to younger animals could be confirmed by this study (BRADY et al., 2020; MA et al., 2017). As shown in Figure 12 A, the contrast enhancement on the infusion site was determined firstly. The group of aged mice indicate a significantly delayed increase although the peak values are higher for the aged animals. The decrease of contrast agent starts around 40 min post-infusion while it peaks around 60 min in the group of aged mice. Figure 12 B demonstrates that a potential increased size of the lateral ventricle due to age is not detectable. The volume of the lateral ventricle in both groups of mice was quantified by the software SLICER 3D as visualized below (Figure 12 B). Neither the 3D reconstruction nor the calculation of the volumes lead to a significant difference. As a result, the delayed increase and higher peak values in aged mice are explained by a reduced CSF dynamic due to a lower flow rate to the third ventricle. Observation of the third ventricle shows a similar contrast enhancement (Additional data). The delayed peak of contrast confirms the observations of a reduced CSF dynamic in aged mice (BRADY et al., 2020; MA et al., 2017).
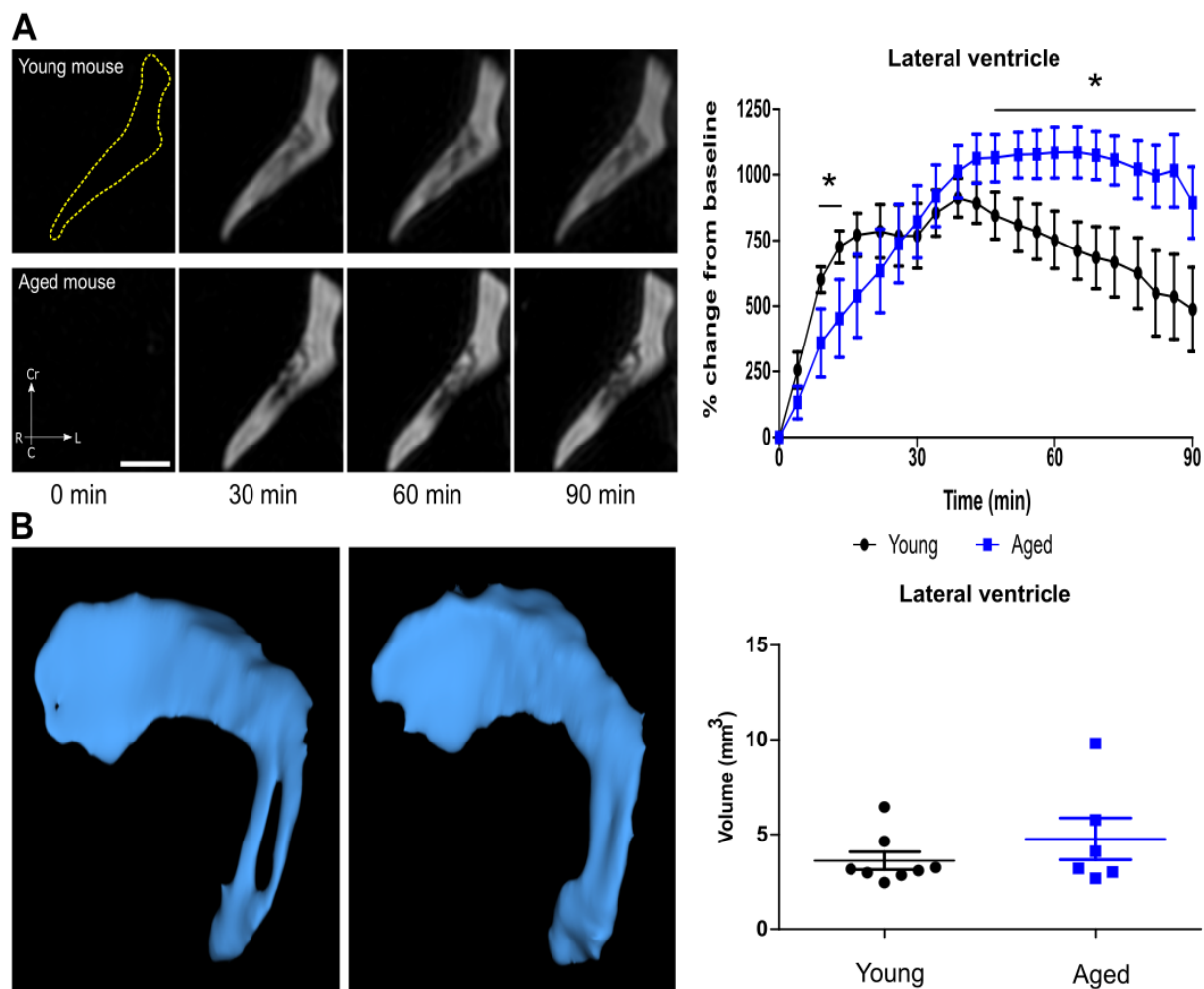
Figure 12: Quantification of the contrast increase over time at the injection site and comparison of the ventricular size depending on the age

A: Intraventricular contrast enhancement in the contralateral ventricle of infusion site. A massive contrast increase can be detected. The graphical illustration indicates a reduced acceleration with a higher contrast increase. Quantifications of the different ROIs are expressed as the mean ± SEM of n= 7 young mice vs n=6 aged mice and are representative of three independent experiments. *p<0.05 (two-way ANOVA followed by Bonferroni's posthoc test). B: The size of the lateral ventricle is compared between young and aged mice leading to no significant difference by illustrating and measurement with the software SLICER 3D. Ventricle volumes of young and aged mice are compared with an unpaired two-tailed Student's t-test.

Reprinted and adapted with permission [JCI Insight], [Decker Y, Krämer J, Xin L, Müller A, Scheller A, Fassbender K, Proulx ST (2022) Magnetic resonance imaging of cerebrospinal fluid outflow after low-rate lateral ventricle infusion in mice. JCI Insight 7:e150881]; https://doi.org/10.1172/jci.insight.150881, permission conveyed through Copyright Clearance Center, Inc. under the license https://creativecommons.org/licenses/by-nc-sa/4.0/legalcode.

Moreover, the relevant arterial network at the base of the skull was quantified which is presented by the Circle of Willis and the Carotid cistern. As illustrated in Figure 13 B/C, in both regions, a massive increase of contrast was visible (> 700% compared to baseline, Figure 13 B/C), which was delayed again in the group of elder mice. Besides, the young mice peaked between 30 and 60 min and started to decrease after 60 min. However, the aged mice demonstrated a quantitatively weaker contrast enhancement at the beginning compared to young animals. These results indicate a major role for this

area in the CSF outflow pathway. Anatomically, the area around this network of blood vessels is characterized by cranial nerves leaving the skull with these arteries. As described, in the study by Ma et al 2019, the Circle of Willis may play a role in the CSF outflow, because of an anatomical connection between the arteries and the CSF (MA et al., 2019b). In the pia mater around these arteries, stomata exist and provide a pathway for CSF outflow to the PVS (PIZZO et al., 2018; ZERVAS et al., 1982). The massive increase in the PVS around the Circle of Willis and Carotid cistern confirms this hypothesis.

Another important motivation of my work is the evaluation of CSF outflow at the dorsal aspect of the skull along with the PVS of the venous sinuses within the meninges. In 2012, Iliff et al. published the concept of the glymphatic pathway describing a CSF flow along the cerebral arteries to the interstitial space (HOFFMANN, THIEL, 1956). From there, CSF would drain to the PVS of the venous system, and after the penetration of the arachnoid barrier draining along with the venous sinuses within the meninges where it enters the lymphatic system (ILIFF et al., 2012). Therefore, the dorsal brain parenchyma was quantified which should show an increase in contrast following this model. Moreover, the PVS around the PSS should show a tracer accumulation too. However, the MRI images indicate only a minimal amount of tracer drains through this claimed pathway. Referring to Figure 12 D and E, in no mouse, the quantified ROI´s showed a significant amount of contrast agent around the venous sinus at the dorsal aspect of the skull. As a consequence, the glymphatic pathway was not observed in our study. The tracer drainage appears to dominate along the basal and ventral aspect of the skull as these regions showed significant contrast enhancement. This observation fits with the morphological advantages of lymphatics at the base of the skull compared to the counterparts at the dorsal part of the skull (AHN et al., 2019).
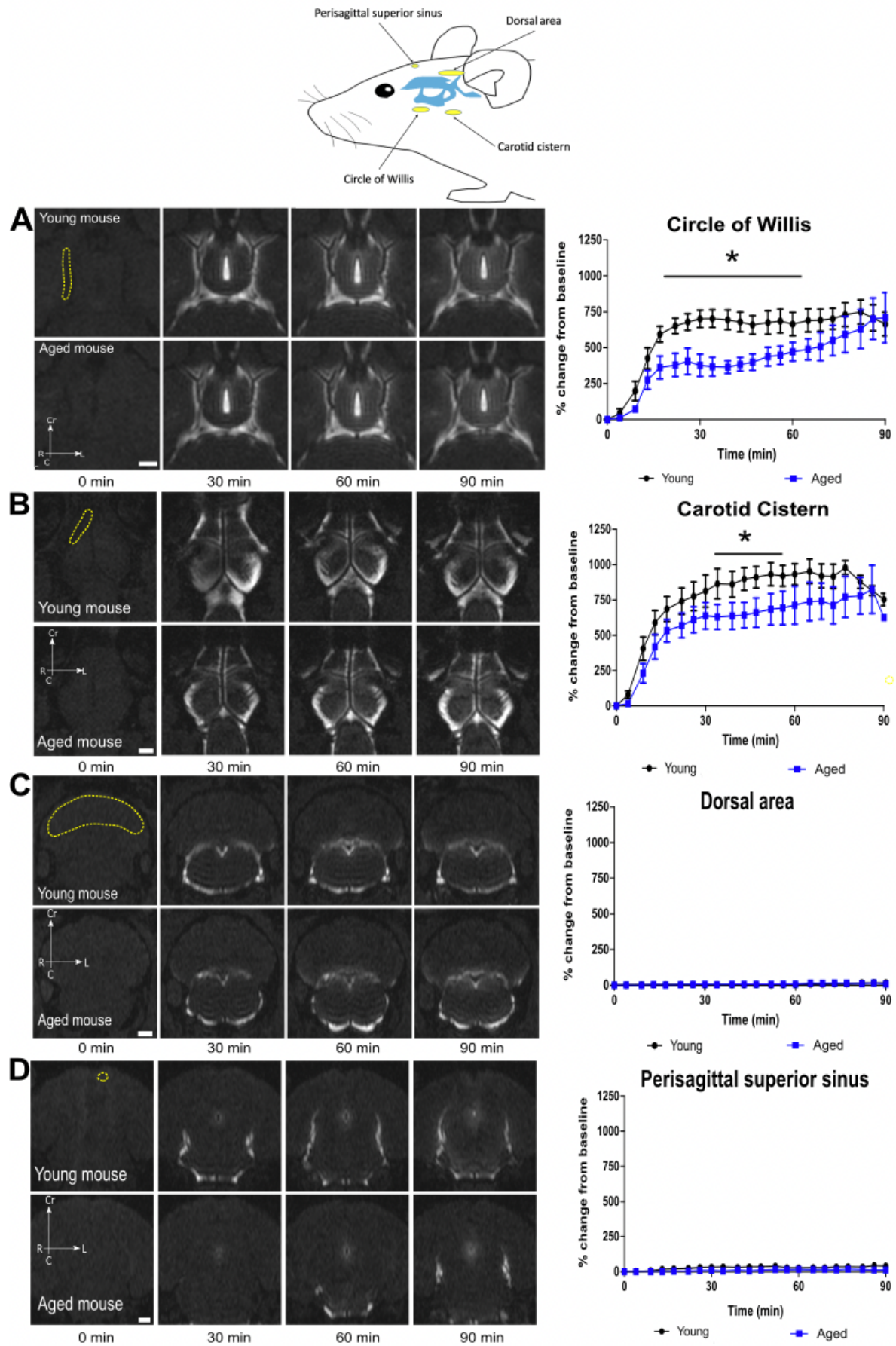
Figure 13: Cerebrospinal fluid outflow drains along within the cranium at the base of the skull

At the top overview of the anatomic localization of the ROIs is illustrated by the yellow marks. Illustrations show the MRI images at several timepoints added by the graphs with the temporal contrast acceleration. The images are taken before injection, directly post-injection, and afterward in an interval of 30-, 60-, and 90-min post-injection. The upper row demonstrates an example for a young mouse while below an elder mouse is shown. In the graphs, the group of old mice is demonstrated by the blue color, while the young mice are shown black. A: The Circle of Willis shows a significant contrast accumulation that accelerates stronger in young mice over the whole observation time. After 60 min in young mice, the contrast is slightly decreasing, and the aged mice show still an increase. B: The Carotid Cistern shows a similar behavior as the Circle of Willis. C: The upper dorsal brain parenchyma is flat for both groups. D: The PSS shows no significant contrast enhancement for both groups. Quantifications of the different ROIs are expressed as the mean ± SEM of n= 7 young mice vs n=6 aged mice and are representative of three independent experiments. *p<0.05, (two-way ANOVA followed by Bonferroni's posthoc test). Scale bars: 1 mm.

4.3. Perineural cerebrospinal fluid outflow along with cranial nerves

After the quantification of the role of the base of the skull, the previously mentioned CSF transport along with the cranial nerves through the frontal aspect of the skull has to be quantified. The transport along with the olfactory nerves to the nasal cavity and the passage along the optical nerves to the orbital region was described before (BRADY et al., 2020; MA et al., 2019a; MA et al., 2017; PIZZO et al., 2018; STANTON et al., 2021). Therefore, the ROIs were placed at the anatomical routes of these nerves. In Figure 14 B, the nasal turbinates as the drainage location of the olfactory nerve and the nasopharyngeal region are quantified. Comparing the nasal turbinates to other quantified regions of major CSF outflow, a moderate increase of contrast is detectable (young mice: 170%; aged mice: 85%). Facing the circumstances of quantification, it is obvious that the anatomical structure of the nasal cavity is the explanation for these artificial low values. Its twisted system of mucosal tissue and air-filled respiratory capacities leads to a massive tracer diffusion. Moreover, the placed ROI quantifies not only the enhanced mucosal tissue but the air-filled space too. Therefore, the nasal cavity plays a more important role in the CSF outflow as the low increase of contrast agent suggests.

A recent study by Ma et al. demonstrated drainage of contrast agent through the nasopharyngeal area (MA et al., 2017). Our findings demonstrated in Figure 14 C, indicate a massive increase of contrast for both groups of mice (Young mice: 710%; aged mice: 570%). Therefore, the quantification indicates that the tracer distributes along with the olfactory nerve to the nasal cavity and the nasopharyngeal region to the DCLN. Referring back to Figure 8, the increase of contrast in the DCLN appeared around 20 min post-infusion. This chronological increase of contrast in the described areas confirms this model, as the nasal turbinates and the nasopharyngeal region show a contrast enhancement around 10-15 min post-injection.

The jugular foramen at the base of the skull was of particular interest for the group of Ahn et al. and is accepted as a potential CSF pathway by several groups (AHN et al., 2019; MA et al., 2017). As a result, this region is quantified too, as shown in Figure 14 D. Contrary to other quantified areas, the jugular region indicates a stronger increase of contrast in aged mice compared to the young mice. In both groups, the contrast enhancement was observed immediately post-infusion which does not suggest a correlation between the jugular region and the model of CSF outflow along with the olfactory and optical nerves. Instead, it appeared that the jugular region is an area of tracer accumulation rather than a point of CSF efflux. Moreover, a passage from the jugular foramen to the DCLN is not visible in the MRI.
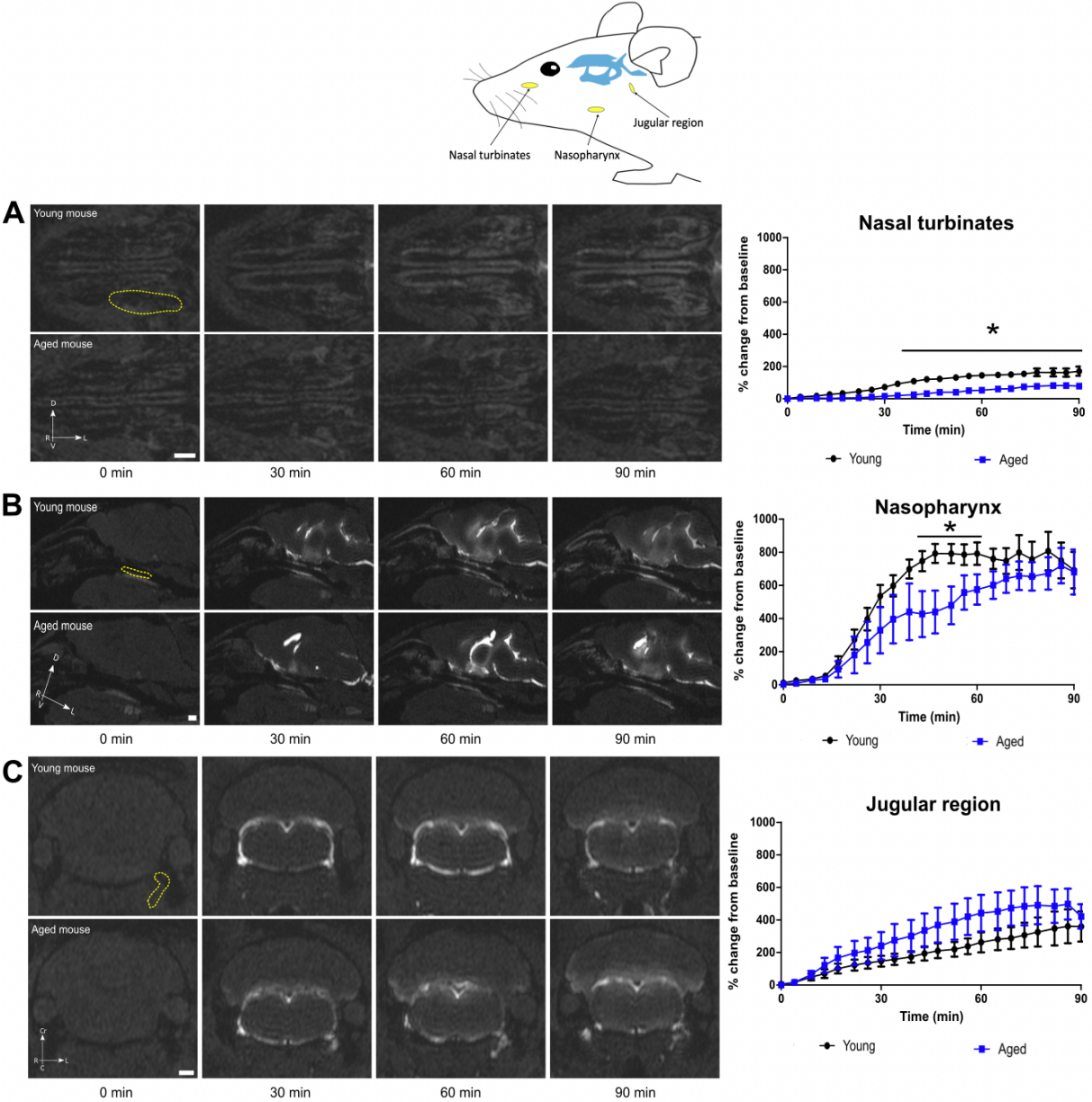
Figure 14: Cerebrospinal fluid outflow from the cranium is reduced for elder mice in the nasal turbinates and the nasopharynx but not in the jugular region

The top overview of the anatomic localization of the ROIs is illustrated by the yellow marks. Illustrations show the MRI images at several timepoints added by the graphs with the temporal contrast acceleration. The images are taken before injection, directly post-injection, and afterward at intervals of 30-, 60-, and 90-min post-injection.

The upper row demonstrates an example of a young mouse. Below that, an elder mouse is shown. In the graphs, the group of old mice is demonstrated by the blue color, while the young mice are shown as black. A: The nasal cavity shows a contrast enhancement that diffuses within the whole mucosa of the region. An contrast increase is visible, even if not as massive as in other regions. The contrast acceleration is reduced in old mice compared to the younger group. B: The lymphatics along the pharyngeal area indicate a massive increase with even more a delay in the old mice. In the young mice, the contrast starts decreasing slightly after 60 min, in elder mice and rising increase is still visible. C: The jugular foramen shows an opposite behavior of increase. The group of the old mice shows a higher and accelerated rise of contrast compared to the young mice.

Quantifications of the different ROIs are expressed as the mean ± SEM of n= 7 young mice vs n=6 aged mice and are representative of three independent experiments. *p<0.05 (two-way ANOVA followed by Bonferroni's posthoc test). Scale bars: 1 mm.

5. Discussion

5.1. Experimental setup

As described in previous studies I confirmed a significantly reduced CSF outflow in the group of aged mice compared to younger mice. In vivo, MRI demonstrates a major outflow through the ventral aspect of the skull through the basal cisterns and the cribriform plate which drains to the CLN.

The method of the experimental setup by MRI is established by previous studies in rodents (AHN et al., 2019; PIZZO et al., 2018; STANTON et al., 2021). However, these studies injected the contrast agent through a cannula in the cisterna magna and observed the efflux to the CLN. Instead, the infusion of contrast agent in the lateral ventricle follows the physiological CSF flow, as the lateral ventricle contains the choroid plexus that produces the CSF. The CSF circulation was demonstrated within the ventricular system and the following outflow from the SAS to the CLN. Moreover, my method does not show any manipulation of the animals that could lead to artificial tracer distribution. However, other publications described a strong manipulation after the tracer injection in the cisterna magna, as „the muscle was pinched to apply some pressure on the cisterna magna prior to the needle removal" (LOUVEAU et al., 2018). This artificial pressure could explain the discrepancy between their observation of a tracer accumulation within the brain parenchyma while I failed to demonstrate it with slow rate infusion under physiological pressure.

The separation in two groups of mice of different ages allows a confirmation of the reduced CSF outflow with age that was described by previous groups (AHN et al., 2019; BRADY et al., 2020; MA et al., 2019c; NAGRA, JOHNSTON, 2007). A delayed contrast enhancement is visible for several locations on the CSF pathway like the lateral ventricle, the basal cisterns, the nasal turbinate, and the nasopharyngeal collecting lymphatic vessels leading to a delayed increase in the CLN as well. As a result, the dynamics of CSF circulation are impaired in aged mice. Several publications tried to answer

the question of which anatomical and structural changes influence CSF dynamics with aging. A reduced production rate of CSF in the choroid plexus results in a decreased volume of CSF (LIU et al., 2020; PRESTON, 2001), as well as morphological changes in the lymphatic vessels within the dura (AHN et al., 2019) or an impaired function of the lymphatic vessels that drain the CSF outside the brain (KARAMAN et al., 2015; PROULX et al., 2017), are proposed. The role of the decreased CSF dynamics with age in the pathology of neurodegenerative diseases remains discussed (AHN et al., 2019).

However, we take advantage of the differences in the CSF outflow between the two groups of mice to work out the relative importance of several potential CSF pathways. The delayed contrast enhancement in the CLN of aged mice has to be explained by a reduced bulk flow in the major CSF passages. As our findings are unable to demonstrate a relevant outflow along the dorsal aspect of the skull, we concluded that the CSF passage dominance along the ventral part of the skull like the cribriform plate (ERLICH et al., 1986; FABER, 1937; MA et al., 2017; NORWOOD et al., 2019; SCHWALBE, 1869; WEED, 1914c), the PNS of the optic nerves (ERLICH et al., 1989; LUDEMANN et al., 2005; MA et al., 2017), and the jugular foramina (AHN et al., 2019; ASPELUND et al., 2015; MA et al., 2017; SCHWALBE, 1869; STANTON et al., 2021). The expected contrast enhancement at the front of the skull confirms this hypothesis as well as the delayed increase of contrast in aged mice in this region (Figure 14). The model of CSF drainage through the cribriform plate to the DCLN follows the results of several other publications (BRADBURY, WESTROP, 1983; BRADY et al., 2020; JOHNSTON et al., 2004; KIDA et al., 1993). Blocking the cribriform plate resulted in increased ICP and a decreased tracer elimination from the CNS which is strong evidence for this pathway (BRADBURY, WESTROP, 1983; MOLLANJI et al., 2001).

Another factor that influences the CSF outflow is the chosen type of anesthesia. A recent study demonstrated that under isoflurane anesthesia, the amount of contrast agent around the cribriform plate is significantly decreased indicating a reduced CSF outflow through this region compared to other types of anesthesia. The contrast enhancement was increased along the cranial nerves in the jugular foramen under 1,5 % anesthesia (STANTON et al., 2021). These differences in CSF dynamics under several types of anesthesia were demonstrated in earlier studies too (HABLITZ et al., 2019; MA et al., 2019a; MA et al., 2019b). Therefore, a shift of CSF flow direction under different conditions has to be considered. Moreover, many pathologies like glioblastoma or hydrocephalus could block CSF pathways and redirect the CSF flow (MA et al., 2019c; VOELZ et al., 2007).

5.2.   Limitations of the current study

The used method of imaging by MRI is limited in the visualization of microscopic processes that enable CSF outflow. As MRI gives us an overview of the major localizations for CSF circulation while we cannot determine for sure within which microscopic anatomical structure the CSF drains. Histological observations are required for detailed observation of perivascular lymphatic vessels or the CSF drainage through the cribriform plate. Our study shows the major CSF pathways but cannot deliver an explanation for the physiological processes that enable this flow. Therefore, our study should be understood as the basis for further histological investigation.

Moreover, the contrast quantification using the MRI approach reveals disadvantages whe the amount of contrast agent that drains through the nasal turbinate is measured. Due to the anatomical characteristics of the nasal tissue, the wide diffusion of tracer within the nasal tissue led to artificially reduced values of contrast increase. Although the use of a macromolecular tracer should limit the diffusion within the nasal mucosal tissue, only a further histological investigation could elucidate the exact anatomical routes that CSF is passing in this region. Only these histological are able to clarify the major role of the cribriform plate.

5.3.   Experimental results compared with recent studies and cerebrospinal fluid concepts

The quantification of the ROIs planted on the dorsal aspect of the skull like around the PSS or above the cortical hemispheres indicates a minimal increase of contrast. However, these findings challenge the concepts that are published in recent studies. These publications claim that a major CSF outflow appears through the dorsal dura (ILIFF et al., 2012; LOUVEAU et al., 2018; LOUVEAU et al., 2015; OLIVER et al., 2020; RUSTENHOVEN et al., 2021) which was extended to the human species (RINGSTAD, EIDE, 2020). The dynamics of contrast enhancement in our study demonstrate a major CSF pathway through the basal cisterns and the SAS along with the Circle of Willis. The hypothesis of the ventral aspect of the skull as a major CSF pathway agrees with several publications (AHN et al., 2019; GAKUBA et al., 2018; MA et al., 2019b; PIZZO et al., 2018; STANTON et al., 2021; YAMADA et al., 2005). As a consequence, the minimal increase of contrast at the cortical hemisphere and around the dural sinuses indicates that some contrast agent reaches the dorsal aspect of the skull (MA et al., 2019a; PIZZO et al., 2018), although the role of the dorsal aspect of the skull remains unclear.

However, the arachnoid layer provides a strong barrier that opposes a bulk flow of CSF(ALKSNE, LOVINGS, 1972; WEED, 1914a, b, c). Several studies were unable to confirm an in vivo CSF drainage through the arachnoid barrier although ex vivo studies showed an artificial contrast enhancement

(FABER, 1937; SPERANSKY AD, 1943). Therefore, the details of the described tracer passage from the CNS to the dural lymphatics keep unexplained. As a result, the studies supporting the glymphatic pathway failed to deliver a detailed explanation of how the tracer reaches the dural lymphatics at the dorsal aspect of the skull due to the technical limitation of the imaging methods (HEISEY et al., 1962). The arachnoid barrier provides strong anatomical evidence that opposed the theory of a glymphatic pathway, as the presence of arachnoid projections in the dural sinuses could not be validated (ALKSNE, LOVINGS, 1972; DAVSON et al., 1970). However, the exit points of the cranial nerves at the basal and frontal aspect of the skull provide a discontinuity of the arachnoid layer (ANTILA et al., 2017; ASPELUND et al., 2015).

These findings challenge the study published by Ahn et al. which claims that CSF drains mostly along the basal meningeal lymphatic vessels through the jugular foramen. However, the study ignores completely the nasal region and the cribriform plate which were not observed. Therefore, the relative importance of the nasal region compared to the jugular foramen was not demonstrated. Moreover, the different experimental conditions like another location of injection and the different injection rates are a possible explanation for this discrepancy between this study and mine.

However, the dynamic imaging by MRI requires further histological investigation as we still do not understand the microscopic processes that enable an outflow of CSF to the lymphatic vessels. To get further knowledge about these processes, another histological experiment was established following this work to investigate how CSF tracer flow through the cribriform plate into the lymphatic vessels appears (DECKER et al., 2022). Using the same infusion protocol as the MRI-based method, Alexa Fluor 647-labeled ovalbumin (AF647-OVA) was infused, and the amount of tracer measured at decalcified DCLN and cranium. The lymphatic vessels were marked by anti-lymphatic vessel endothelial hyaluronan receptor 1 (anti LYVE-1) antibodies. At the two coronal sections of the nasal cavity shown in Figure 15 A/B, the tracer flow is strictly associated with olfactory nerves that drain through the cribriform plate and spreads throughout the nasal mucosal tissue. The detailed microscopic view of the nasopharynx, illustrated in Figure 15 C to E, demonstrates the presence of lymphatic vessels on both sides containing AF647-OVA. Figure 15 F-J shows the drainage of tracer within the sinuses of lymphatic vessels that assess the DCLN. As a result, the histological approach confirms the CSF pathway that was demonstrated by MRI. Therefore, in vivo dynamic MRI and immunochemistry prove the CSF pathway along with the cribriform plate and nasopharynx to the DCLN.
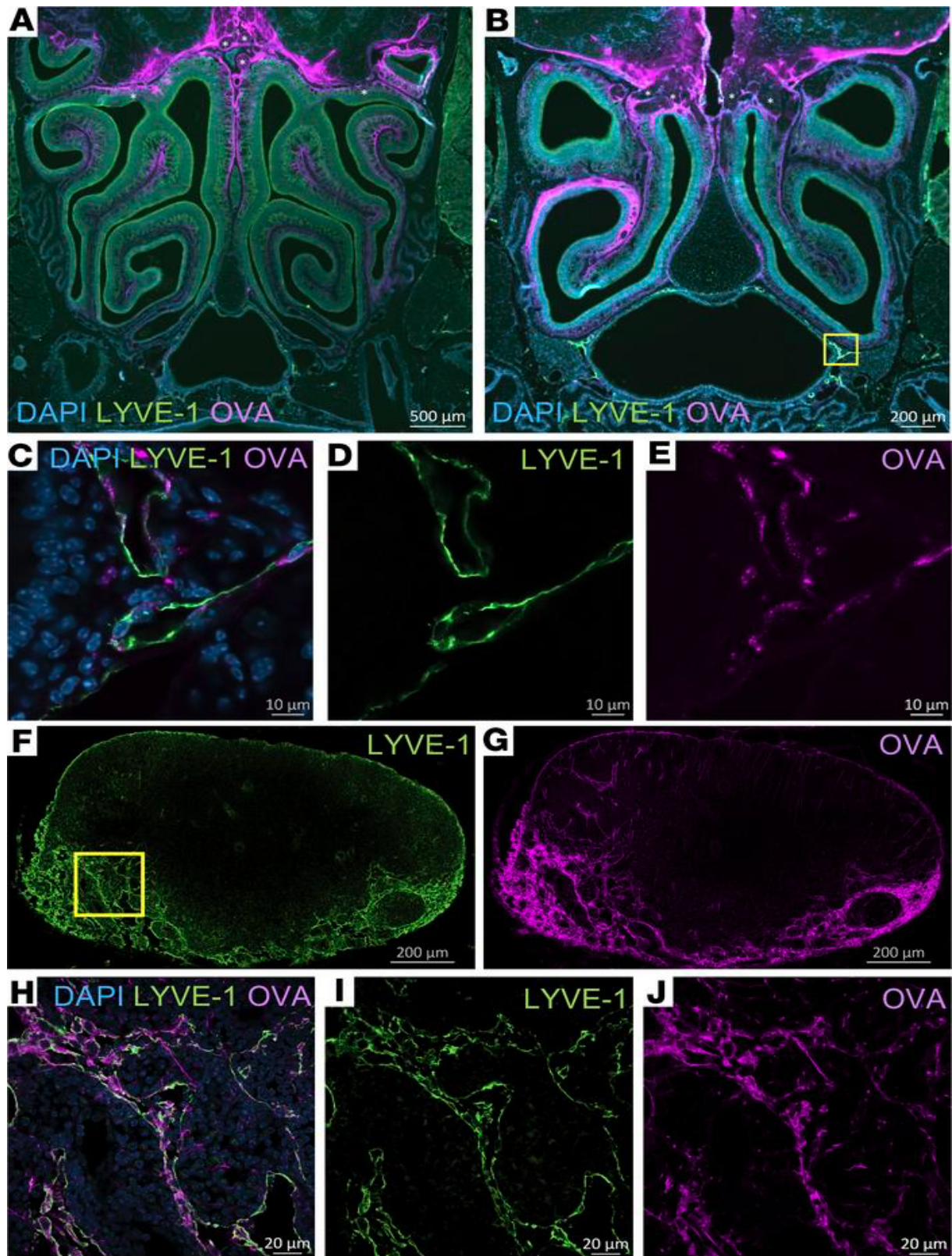
Figure 15: Histological validation of cerebrospinal fluid tracer drainage through the cribriform plate and nasopharyngeal lymphatics to deep cervical lymph nodes

Fluorescently labeled ovalbumin was low-rate infused intraventricularly (0.1 µL/min for 60 minutes), and the mice were analyzed of tracer efflux postmortem after 90 minutes. (**A** and **B**) Coronal sections of decalcified skulls show significant outflow of ovalbumin into the nasal mucosal tissues. Ovalbumin (purple) can be observed crossing the cribriform plate alongside several olfactory nerve bundles (indicated with *). Lymphatic vessels (stained with LYVE-1 in green) can be detectable near the nasopharynx under the nasal turbinates. Scale bars: 500 µm (**A**), 200 µm (**B**). (**C–E**) High-magnification view of the nasopharyngeal region is marked by the yellow box in **B**,

demonstrating ovalbumin signal within the LYVE-1$^+$ lymphatic vessels. Scale bars: 10 μm. (**F** and **G**) Sections of deep cervical lymph nodes show a close association of ovalbumin signal within lymphatic sinuses stained with LYVE-1. Scale bars: 200 μm. (**H**–**J**) High-magnification view of the region is marked by the yellow box in **F**, demonstrating ovalbumin signal within the LYVE-1$^+$ lymphatic sinuses.
Scale bars: 20 μm. Data are representative of n = 6 mice and 2 independent experiments.

Other recent publications concerning the neuropathology of many neuronal disorders refer to the glymphatic pathway as a CSF clearance passage along with the arterial PVS through the brain parenchyma to the venous PVS. These vessels are described as penetrating veins and arteries on the superficial brain (ILIFF et al., 2012; LOUVEAU et al., 2015). However, this theory faces several issues. On the one hand, the studies based on 2-photon imaging lack a sufficient depth of imaging, which allows perfect detection of tracer within the PVS on the superficial brain and a moderate accumulation along the deeper veins. These observations were interpreted as a CSF drainage along the parenchymal vessels (ILIFF et al., 2012; LOUVEAU et al., 2015). After intraventricular tracer injection, the groups following this experimental setup did not report tracer circulation (BEDUSSI et al., 2017; ZHANG et al., 1990). A study that injected tracer intraventricular in awake mice reported no tracer circulation (XIE et al., 2013) which led to the conclusion that CSF does not circulate after intraventricular and intrathecally application (ILIFF et al., 2012; XIE et al., 2013). Even though intraventricular injection is a common method for the observation of distribution, clearance, and activity of intrathecally applied drugs and therapeutics (GLASCOCK et al., 2011).

Therefore, there is a misconception under the supporters of the glymphatic pathway (FERRIS, 2021) as our findings after intraventricular infusion demonstrates massive CSF dynamics. Moreover, the tracer dynamics are shown in awake and anesthetized mice with the same injection location, Corresponding to my findings, no contrast enhancement is detectable in the subcortical brain parenchyma. Instead, their findings demonstrate that the anesthesia blocks the tracer in the SAS and superficial cerebral hemispheres and the death of the animals promotes the tracer influx in the PVS (MA et al., 2019b). As a consequence, the death and the following preparation is the only reason for the tracer detection in the deeper layers of the cortical hemispheres (ILIFF et al., 2012; LOUVEAU et al., 2015). The hypothesis of the glymphatic pathway has to be reconsidered as it faces several challenging findings that are unable to show evidence for this model.

5.4.   **Clinical relevance for humans**

The situation in humans remains unsolved as recent studies published results that once show a significant CSF flow along with the cribriform plate while others were unable to demonstrate this pathway (DE LEON et al., 2017; JOHNSTON et al., 2004; LÖWHAGEN et al., 1994; MELIN et al., 2020). One of these studies injected a low-weight molecular Gadolinium tracer intrathecal at the lumbar spine of patients with various CSF disorders. Afterward, the contrast enhancement at the nasal turbinates was measured at several time points. As no significant increase appeared, it was concluded that the CSF outflow drains along another route although contrast enhancement below the nasal cavity was shown (MELIN et al., 2020). However, as explained before, the quantification of contrast enhancement in the nasal cavity is technically difficult with the MRI because the tracer spreads diffusely in the nasal mucosal tissue. This technical problem can explain the difficulty of the signal detection in the nasal area after the crossing of the cribriform plate. However, even the infusion of a macromolecular contrast agent in our study, which should be cleared dominantly through the nasal pathway, did not solve that technical problem sufficiently.

As Alzheimer´s dementia is one of the most challenging diseases that the human species is facing, several publications were made. A recent study ablated the meningeal lymphatic vessels within the dura at the dorsal aspect of the skull (DA MESQUITA et al., 2021). The ablation was absolved by Visudyne injection and transcranial photoconversion. The animals were characterized by the genetic expression of typical mutations in familial Alzheimer´s disease. After the ablation of these vessels, a significant increase of ß-plaques within the brain parenchyma was observed, compared to a group of physiological, unablated mice. Moreover, increased mobilization of myeloid cells was observable. The increased neuroinflammation and accumulation of amyloid plaques could be explained by a general inflammation through the injection of Visudyne and transcranial photoconversion. The expression of proinflammatory cytokines leading to general neuroinflammation induced the accumulation of amyloid, as a casualty between neuroinflammation and Alzheimer´s disease was described (CAI et al., 2014; TUPPO, ARIAS, 2005). In the second group of mice, a vascular endothelial growth factor was applicated and the group showed neither increased neuroinflammation nor accumulation of plaques. However, the missing irritation of the Visudyne injection prevents a circle of inflammation and amyloid accumulation. As a consequence, the role of meningeal lymphatic vessels as a major drainage pathway for CSF and metabolites has to be reevaluated. In addition to that, the missed observation of the frontal aspect of the skull and the base of the skull is a point of criticism. These regions were demonstrated as major CSF outflow pathways by several groups and have to evaluate (AHN et al., 2019; GAKUBA et al., 2018; MA et al., 2019b; PIZZO et al., 2018; STANTON et al., 2021; YAMADA et al., 2005).
Another recent publication indicates that the MRI-based method for the detection of CSF drainage can be adopted on a wider clinical application (EIDE et al., 2021). The hydrophilic contrast agent gadobutrol

was injected into the lumbar CSF and the contrast enhancement was measured with parallel quantification of the gadobutrol quantification in taken blood samples for 48 hours. The human participants are divided into two groups. On the one hand, the patients suffered from various neurological diseases like idiopathic normal pressure hydrocephalus or idiopathic intracranial hypertension. On the other hand, a reference group with no recognizable CSF disturbance was established. The study demonstrates a positive linear correlation between the tracer enrichment in the cisterna magna and the blood for the reference group. The various neurological diseases resulted in a change in CSF outflow dynamics depending on the individual CSF disorder. These findings fit with other publications that observed the CSF dynamics under specific neurological issues like glioblastoma (MA et al., 2019c). The contrast enhancement in the blood peaks before the parasagittal sinus confirms our findings that the CSF efflux along this route has a minor role. The correlation between tracer enrichment at the cisterna magna and the blood increases with age. As a result, the differences in CSF outflow between different ages can be demonstrated in the human species too.

As a consequence, a different CSF outflow depending on the age was shown for humans too. Moreover, the minor role of the parasagittal sinus at the dorsal aspect of the skull can be transferred to humans. The tracer enrichment peaked in the lymph nodes before a peak in the blood was observed, indicating a CSF drainage to the lymphatic system independently from the blood system (EIDE et al., 2021).

Moreover, current observations in humans describe a major role of the CSF regarding the immunological processes within the brain (CROESE et al., 2021). The authors claim the presence of immunological niches within the CNS that release immunological active cells and cytokines. The choroid plexus, the meningeal layers, and the CSF are defined as such niches. After releasing these cells in the CSF, they drain within the CSF to the CLN. Their observations describe a major CSF drainage along the cranial nerves at the base of the skull and the nasal region to the CLN which maintains the CSF pressure. These findings confirm our model of a bulk flow along these routes. However, the meningeal sinuses are described as a pathway for immune cells supported by channels within the arachnoid projections. As explained at the beginning, the active transport by channels delivers an insufficient mechanism that opposes the theory of a bulk flow.

5.5.   Conclusion

To conclude, the slow rate infusion of a macromolecular gadolinium contrast agent combined with dynamic MRI shows a tracer distribution from the lateral ventricle predominantly through the cribriform plate along the nasal region to the collection of lymphatic vessels in the nasopharyngeal region that drain the CLN. These CSF dynamics are reduced with aging as the contrast enhancement at the nasal region was delayed and reduced. The experimental setup allows further MRI-based studies in mice with

neurological disorders to the relevance for the neuropathology. However, the ideal experimental setup that allows a transformation on the human species is not available yet. As many questions are raised concerning the reliability and validity of experiments in animals, more effort must be made. Before any experimental method is transferred to humans, the findings and experimental methods must be successfully replicated several times by other groups to guarantee reliability and validity. However, the establishment of this method in human patients could generate new findings on the drug delivery within the CNS through the BBB. As a result, the effectiveness of intrathecal drug application can be detected which could help to invent new therapies for various neurological disorders. As the intrathecal application of drugs avoids the restriction of the BBB, a significant advantage compared to systemically applicated drugs is the consequence (PARDRIDGE, 2005). Many intrathecal therapeutics are under current investigation to treat neurodegenerative diseases like spinal muscular atrophy (FINKEL et al., 2016; WURSTER et al., 2019), amyotrophic lateral sclerosis, spinocerebellar ataxia, and dementia (CHEN et al., 2020; HARDCASTLE et al., 2018; MCCAMPBELL et al., 2018; NGUYEN et al., 2018; NIU et al., 2018).

6. <u>References</u>

1. Absinta M, Ha S-K, Nair G, Sati P, Luciano NJ, Palisoc M, Louveau A, Zaghloul KA, Pittaluga S, Kipnis J, Reich DS (2017) Human and nonhuman primate meninges harbor lymphatic vessels that can be visualized noninvasively by MRI. eLife 6:e29738
2. Ahn JH, Cho H, Kim J-H, Kim SH, Ham J-S, Park I, Suh SH, Hong SP, Song J-H, Hong Y-K, Jeong Y, Park S-H, Koh GY (2019) Meningeal lymphatic vessels at the skull base drain cerebrospinal fluid. Nature 572:62-66
3. Alksne JF, Lovings ET (1972) Functional ultrastructure of the arachnoid villus. Archives of Neurology 27:371-377
4. Andres KH, von Düring M, Muszynski K, Schmidt RF (1987) Nerve fibres and their terminals of the dura mater encephali of the rat. Anatomy and Embryology 175:289-301
5. Antila S, Karaman S, Nurmi H, Airavaara M, Voutilainen MH, Mathivet T, Chilov D, Li Z, Koppinen T, Park J-H, Fang S, Aspelund A, Saarma M, Eichmann A, Thomas J-L, Alitalo K (2017) Development and plasticity of meningeal lymphatic vessels. The Journal of Experimental Medicine 214:3645-3667
6. Aspelund A, Antila S, Proulx ST, Karlsen TV, Karaman S, Detmar M, Wiig H, Alitalo K (2015) A dural lymphatic vascular system that drains brain interstitial fluid and macromolecules. The Journal of Experimental Medicine 212:991-999
7. Attems J, Jellinger K, Thal DR, Van Nostrand W (2011) Review: sporadic cerebral amyloid angiopathy. Neuropathology and Applied Neurobiology 37:75-93
8. Bedussi B, van der Wel NN, de Vos J, van Veen H, Siebes M, VanBavel E, Bakker EN (2017) Paravascular channels, cisterns, and the subarachnoid space in the rat brain: A single compartment with preferential pathways. Journal of Cerebral Blood Flow and Metabolism: Official Journal of the International Society of Cerebral Blood Flow and Metabolism 37:1374-1385
9. Benninger RKP, Piston DW (2013) Two-photon excitation microscopy for the study of living cells and tissues. Current Protocols in Cell Biology Chapter 4:Unit 4.11.11-24
10. Boulton M, Armstrong D, Flessner M, Hay J, Szalai JP, Johnston M (1998) Raised intracranial pressure increases CSF drainage through arachnoid villi and extracranial lymphatics. The American Journal of Physiology 275:R889-896
11. Bradbury M (1979) The concept of a blood-brain barrier.
12. Bradbury MW, Cole DF (1980) The role of the lymphatic system in drainage of cerebrospinal fluid and aqueous humour. The Journal of Physiology 299:353-365
13. Bradbury MW, Westrop RJ (1983) Factors influencing exit of substances from cerebrospinal fluid into deep cervical lymph of the rabbit. The Journal of Physiology 339:519-534
14. Brady M, Rahman A, Combs A, Venkatraman C, Kasper RT, McQuaid C, Kwok W-CE, Wood RW, Deane R (2020) Cerebrospinal fluid drainage kinetics across the cribriform plate are reduced with aging. Fluids and barriers of the CNS 17:71
15. Brøchner CB, Holst CB, Møllgård K (2015) Outer brain barriers in rat and human development. Frontiers in Neuroscience 9:75
16. Cai Z, Hussain MD, Yan L-J (2014) Microglia, neuroinflammation, and beta-amyloid protein in Alzheimer's disease. The International Journal of Neuroscience 124:307-321
17. Chen W, Hu Y, Ju D (2020) Gene therapy for neurodegenerative disorders: advances, insights and prospects. Acta Pharmaceutica Sinica B 10:1347-1359
18. Courtice FC, Simmonds WJ (1951) The removal of protein from the subarachnoid space. The Australian Journal of Experimental Biology and Medical Science 29:255-263
19. Croese T, Castellani G, Schwartz M (2021) Immune cell compartmentalization for brain surveillance and protection. Nature Immunology 22:1083-1092
20. Cserr HF, Bundgaard M (1984) Blood-brain interfaces in vertebrates: a comparative approach. The American Journal of Physiology 246:R277-288
21. Czerniawska A (1970) Experimental investigations on the penetration of 198Au from nasal mucous membrane into cerebrospinal fluid. Acta Oto-Laryngologica 70:58-61
22. Da Mesquita S, Papadopoulos Z, Dykstra T, Brase L, Farias FG, Wall M, Jiang H, Kodira CD, de Lima KA, Herz J, Louveau A, Goldman DH, Salvador AF, Onengut-Gumuscu S, Farber E,

Dabhi N, Kennedy T, Milam MG, Baker W, Smirnov I, Rich SS, Network DIA, Benitez BA, Karch CM, Perrin RJ, Farlow M, Chhatwal JP, Holtzman DM, Cruchaga C, Harari O, Kipnis J (2021) Meningeal lymphatics affect microglia responses and anti-Aβ immunotherapy. Nature 593:255-260

23. Dandy WE (1929) Where is cerebrosponal fluid absorbed? Journal of the American Medical Association

24. Davson H, Segal MB (1966) Physiology of the CSF and blood-brain barriers. CRC Press

25. Davson H, Hollingsworth G, Segal MB (1970) The mechanism of drainage of the cerebrospinal fluid. Brain: A Journal of Neurology 93:665-678

26. de Leon MJ, Li Y, Okamura N, Tsui WH, Saint-Louis LA, Glodzik L, Osorio RS, Fortea J, Butler T, Pirraglia E, Fossati S, Kim H-J, Carare RO, Nedergaard M, Benveniste H, Rusinek H (2017) Cerebrospinal Fluid Clearance in Alzheimer Disease Measured with Dynamic PET. Journal of Nuclear Medicine: Official Publication, Society of Nuclear Medicine 58:1471-1476

27. Decker Y, Kramer J, Xin L, Muller A, Scheller A, Fassbender K, Proulx ST (2022) Magnetic resonance imaging of cerebrospinal fluid outflow after low-rate lateral ventricle infusion in mice. JCI Insight 7

28. DeVos SL, Goncharoff DK, Chen G, Kebodeaux CS, Yamada K, Stewart FR, Schuler DR, Maloney SE, Wozniak DF, Rigo F, Bennett CF, Cirrito JR, Holtzman DM, Miller TM (2013) Antisense reduction of tau in adult mice protects against seizures. The Journal of Neuroscience: The Official Journal of the Society for Neuroscience 33:12887-12897

29. Eide PK, Mariussen E, Uggerud H, Pripp AH, Lashkarivand A, Hassel B, Christensen H, Hovd MH, Ringstad G (2021) Clinical application of intrathecal gadobutrol for assessment of cerebrospinal fluid tracer clearance to blood. JCI insight 6:147063

30. Eisenberg HM, McLennan JE, Welch K (1974) Ventricular perfusion in cats with kaolin-induced hydrocephalus. Journal of Neurosurgery 41:20-28

31. Erlich SS, McComb JG, Hyman S, Weiss MH (1986) Ultrastructural morphology of the olfactory pathway for cerebrospinal fluid drainage in the rabbit. Journal of Neurosurgery:466-473

32. Erlich SS, McComb JG, Hyman S, Weiss MH (1989) Ultrastructure of the orbital pathway for cerebrospinal fluid drainage in rabbits. Journal of Neurosurgery:926-931

33. Faber WM (1937) The nasal mucosa and the subarachnoid space. American Journal of Anatomy:121-148

34. Faulhauer K, Donauer E (1985) Experimental hydrocephalus and hydrosyringomyelia in the cat. Radiological findings. Acta Neurochirurgica 74:72-80

35. Ferris CF (2021) Rethinking the Conditions and Mechanism for Glymphatic Clearance. Frontiers in Neuroscience 15:624690

36. Finkel RS, Chiriboga CA, Vajsar J, Day JW, Montes J, De Vivo DC, Yamashita M, Rigo F, Hung G, Schneider E, Norris DA, Xia S, Bennett CF, Bishop KM (2016) Treatment of infantile-onset spinal muscular atrophy with nusinersen: a phase 2, open-label, dose-escalation study. Lancet (London, England) 388:3017-3026

37. Foldy M, Gatai G, Zoltan TO (1959) The removal of iodine 131-labeled serum albumin from the subarachnoid space in the dog. Naunyn Schniedebergs Arch Exp Pathol Pharmakol:65-70

38. Gakuba C, Gaberel T, Goursaud S, Bourges J, Di Palma C, Quenault A, Martinez de Lizarrondo S, Vivien D, Gauberti M (2018) General Anesthesia Inhibits the Activity of the "Glymphatic System". Theranostics 8:710-722

39. Glascock JJ, Osman EY, Coady TH, Rose FF, Shababi M, Lorson CL (2011) Delivery of therapeutic agents through intracerebroventricular (ICV) and intravenous (IV) injection in mice. Journal of Visualized Experiments: JoVE:2968

40. Hablitz LM, Vinitsky HS, Sun Q, Stæger FF, Sigurdsson B, Mortensen KN, Lilius TO, Nedergaard M (2019) Increased glymphatic influx is correlated with high EEG delta power and low heart rate in mice under anesthesia. Science Advances 5:eaav5447

41. Hardcastle N, Boulis NM, Federici T (2018) AAV gene delivery to the spinal cord: serotypes, methods, candidate diseases, and clinical trials. Expert Opinion on Biological Therapy 18:293-307

42. Hardy J, Selkoe DJ (2002) The amyloid hypothesis of Alzheimer's disease: progress and problems on the road to therapeutics. Science (New York, NY) 297:353-356

43.   Heisey SR, Held D, Pappenheimer JR (1962) Bulk flow and diffusion in the cerebrospinal fluid system of the goat. The American Journal of Physiology 203:775-781

44.   Hoffmann E, Thiel W (1956) [Studies of the supposed and real channels of egress from the subdural and subarachnoid spaces]. Zeitschrift Fur Anatomie Und Entwicklungsgeschichte 119:283-301

45.   Iliff JJ, Wang M, Liao Y, Plogg BA, Peng W, Gundersen GA, Benveniste H, Vates GE, Deane R, Goldman SA, Nagelhus EA, Nedergaard M (2012) A paravascular pathway facilitates CSF flow through the brain parenchyma and the clearance of interstitial solutes, including amyloid β. Science Translational Medicine 4:147ra111

46.   Iliff JJ, Goldman SA, Nedergaard M (2015) Implications of the discovery of brain lymphatic pathways. The Lancet Neurology 14:977-979

47.   Jackson RT, Tigges J, Arnold W (1979) Subarachnoid space of the CNS, nasal mucosa, and lymphatic system. Archives of Otolaryngology (Chicago, Ill: 1960) 105:180-184

48.   Jain RK, di Tomaso E, Duda DG, Loeffler JS, Sorensen AG, Batchelor TT (2007) Angiogenesis in brain tumours. Nature Reviews Neuroscience 8:610-622

49.   Jenny B, Harrison JA, Baetens D, Tille J-C, Burkhardt K, Mottaz H, Kiss JZ, Dietrich P-Y, De Tribolet N, Pizzolato GP, Pepper MS (2006) Expression and localization of VEGF-C and VEGFR-3 in glioblastomas and haemangioblastomas. The Journal of Pathology 209:34-43

50.   Johanson CE, Duncan JA, Klinge PM, Brinker T, Stopa EG, Silverberg GD (2008) Multiplicity of cerebrospinal fluid functions: New challenges in health and disease. Cerebrospinal Fluid Research 5:10

51.   Johnston M, Zakharov A, Papaiconomou C, Salmasi G, Armstrong D (2004) Evidence of connections between cerebrospinal fluid and nasal lymphatic vessels in humans, non-human primates and other mammalian species. Cerebrospinal Fluid Research 1:2

52.   Karaman S, Buschle D, Luciani P, Leroux J-C, Detmar M, Proulx ST (2015) Decline of lymphatic vessel density and function in murine skin during aging. Angiogenesis 18:489-498

53.   Karran E, Mercken M, De Strooper B (2011) The amyloid cascade hypothesis for Alzheimer's disease: an appraisal for the development of therapeutics. Nature Reviews Drug Discovery 10:698-712

54.   Key AaR (1875). Studien in der Anatomie des Nervensystems und des Bindegewebes (Stockholm: Samson & Waller)

55.   Kida S, Pantazis A, Weller RO (1993) CSF drains directly from the subarachnoid space into nasal lymphatics in the rat. Anatomy, histology and immunological significance. Neuropathology and Applied Neurobiology 19:480-488

56.   Krisch B, Leonhardt H, Oksche A (1983) The meningeal compartments of the median eminence and the cortex. A comparative analysis in the rat. Cell and Tissue Research 228:597-640

57.   le Gros Clark WE (1920) On the Pacchionian Bodies. Journal of Anatomy 55:40-48

58.   Liu G, Mestre H, Sweeney AM, Sun Q, Weikop P, Du T, Nedergaard M (2020) Direct Measurement of Cerebrospinal Fluid Production in Mice. Cell Reports 33:108524

59.   Louveau A, Smirnov I, Keyes TJ, Eccles JD, Rouhani SJ, Peske JD, Derecki NC, Castle D, Mandell JW, Lee KS, Harris TH, Kipnis J (2015) Structural and functional features of central nervous system lymphatic vessels. Nature 523:337-341

60.   Louveau A, Herz J, Alme MN, Salvador AF, Dong MQ, Viar KE, Herod SG, Knopp J, Setliff JC, Lupi AL, Da Mesquita S, Frost EL, Gaultier A, Harris TH, Cao R, Hu S, Lukens JR, Smirnov I, Overall CC, Oliver G, Kipnis J (2018) CNS lymphatic drainage and neuroinflammation are regulated by meningeal lymphatic vasculature. Nature Neuroscience 21:1380-1391

61.   Löwhagen P, Johansson BB, Nordborg C (1994) The nasal route of cerebrospinal fluid drainage in man. A light-microscope study. Neuropathology and Applied Neurobiology 20:543-550

62.   Ludemann W, von Rautenfeld DB, Samil M, Brinker T (2005) Ultrastructure of the cerebrospinal fluid outflow along the optic nerve into the lymphatic system. Childs Nervous System:96-103

63.   Lun M, Lok E, Gautam S, Wu E, Wong ET (2011) The natural history of extracranial metastasis from glioblastoma multiforme. Journal of Neuro-Oncology 105:261-273

64. Ma Q, Ineichen BV, Detmar M, Proulx ST (2017) Outflow of cerebrospinal fluid is predominantly through lymphatic vessels and is reduced in aged mice. Nature Communications 8:1434

65. Ma Q, Decker Y, Müller A, Ineichen BV, Proulx ST (2019a) Clearance of cerebrospinal fluid from the sacral spine through lymphatic vessels. The Journal of Experimental Medicine 216:2492-2502

66. Ma Q, Ries M, Decker Y, Müller A, Riner C, Bücker A, Fassbender K, Detmar M, Proulx ST (2019b) Rapid lymphatic efflux limits cerebrospinal fluid flow to the brain. Acta Neuropathologica 137:151-165

67. Ma Q, Schlegel F, Bachmann SB, Schneider H, Decker Y, Rudin M, Weller M, Proulx ST, Detmar M (2019c) Lymphatic outflow of cerebrospinal fluid is reduced in glioma. Scientific Reports 9:14815

68. Mack AF, Wolburg H, Fallier-Becker P (2017) In Brain edema (ed Nikolaus Plesnila Jérôme Badaut). Academic Press:293-313

69. Martinez J, Duma RJ, Nelson EC, Moretta FL (1973) Experimental naegleria meningoencephalitis in mice. Penetration of the olfactory mucosal epithelium by Naegleria and pathologic changes produced: a light and electron microscope study. Laboratory Investigation; a Journal of Technical Methods and Pathology 29:121-133

70. McCampbell A, Cole T, Wegener AJ, Tomassy GS, Setnicka A, Farley BJ, Schoch KM, Hoye ML, Shabsovich M, Sun L, Luo Y, Zhang M, Comfort N, Wang B, Amacker J, Thankamony S, Salzman DW, Cudkowicz M, Graham DL, Bennett CF, Kordasiewicz HB, Swayze EE, Miller TM (2018) Antisense oligonucleotides extend survival and reverse decrement in muscle response in ALS models. The Journal of Clinical Investigation 128:3558-3567

71. Melin E, Eide PK, Ringstad G (2020) In vivo assessment of cerebrospinal fluid efflux to nasal mucosa in humans. Scientific Reports 10:14974

72. Mollanji R, Bozanovic-Sosic I, Silver I, Li B, Kim C, Midha R, Johnston M (2001) Intracranial pressure accommodation is impaired by blocking pathways leading to extracranial lymphatics. American Journal of Physiology Regulatory, integrative and comparative physiology:R1573-1581

73. Mortensen AOS, W. E. (1933) The cerebrospinal fluid and the cervical lymph nodes. Anatomical Record:359-363

74. Nagra G, Johnston MG (2007) Impact of ageing on lymphatic cerebrospinal fluid absorption in the rat. Neuropathology and Applied Neurobiology 33:684-691

75. Nguyen AD, Nguyen TA, Zhang J, Devireddy S, Zhou P, Karydas AM, Xu X, Miller BL, Rigo F, Ferguson SM, Huang EJ, Walther TC, Farese RV (2018) Murine knockin model for progranulin-deficient frontotemporal dementia with nonsense-mediated mRNA decay. Proceedings of the National Academy of Sciences of the United States of America 115:E2849-E2858

76. Niu C, Prakash TP, Kim A, Quach JL, Huryn LA, Yang Y, Lopez E, Jazayeri A, Hung G, Sopher BL, Brooks BP, Swayze EE, Bennett CF, La Spada AR (2018) Antisense oligonucleotides targeting mutant Ataxin-7 restore visual function in a mouse model of spinocerebellar ataxia type 7. Science Translational Medicine 10:eaap8677

77. Norwood JN, Zhang Q, Card D, Craine A, Ryan TM, Drew PJ (2019) Anatomical basis and physiological role of cerebrospinal fluid transport through the murine cribriform plate. eLife 8:e44278

78. Oliver G, Kipnis J, Randolph GJ, Harvey NL (2020) The Lymphatic Vasculature in the 21st Century: Novel Functional Roles in Homeostasis and Disease. Cell 182:270-296

79. Pardridge WM (2005) The blood-brain barrier: bottleneck in brain drug development. NeuroRx: The Journal of the American Society for Experimental NeuroTherapeutics 2:3-14

80. Pardridge WM (2016) CSF, blood-brain barrier, and brain drug delivery. Expert Opinion on Drug Delivery 13:963-975

81. Pizzo ME, Wolak DJ, Kumar NN, Brunette E, Brunnquell CL, Hannocks M-J, Abbott NJ, Meyerand ME, Sorokin L, Stanimirovic DB, Thorne RG (2018) Intrathecal antibody distribution in the rat brain: surface diffusion, perivascular transport and osmotic enhancement of delivery. The Journal of Physiology 596:445-475

82.   Preston JE (2001) Ageing choroid plexus-cerebrospinal fluid system. Microscopy Research and Technique 52:31-37

83.   Prins RM, Liau LM (2004) Cellular immunity and immunotherapy of brain tumors. Frontiers in Bioscience: A Journal and Virtual Library 9:3124-3136

84.   Proulx ST, Ma Q, Andina D, Leroux J-C, Detmar M (2017) Quantitative measurement of lymphatic function in mice by noninvasive near-infrared imaging of a peripheral vein. JCI insight 2:e90861

85.   Ringstad G, Eide PK (2020) Cerebrospinal fluid tracer efflux to parasagittal dura in humans. Nature Communications 11:354

86.   Rogers J, Strohmeyer R, Kovelowski CJ, Li R (2002) Microglia and inflammatory mechanisms in the clearance of amyloid beta peptide. Glia 40:260-269

87.   Rustenhoven J, Drieu A, Mamuladze T, de Lima KA, Dykstra T, Wall M, Papadopoulos Z, Kanamori M, Salvador AF, Baker W, Lemieux M, Da Mesquita S, Cugurra A, Fitzpatrick J, Sviben S, Kossina R, Bayguinov P, Townsend RR, Zhang Q, Erdmann-Gilmore P, Smirnov I, Lopes M-B, Herz J, Kipnis J (2021) Functional characterization of the dural sinuses as a neuroimmune interface. Cell 184:1000-1016.e1027

88.   Schwalbe G (1869) Die Arachnoidalraum ein Lymphraum und sein Zusammenhang mit den Perichorioidalraum [The arachnoidal space as a lymphatic space with connection to the perichoroidal compartment.]. Zbl med Wiss:465-467

89.   Shen JY, Kelly DE, Hyman S, McComb JG (1985) Intraorbital cerebrospinal fluid outflow and the posterior uveal compartment of the hamster eye. Cell and Tissue Research 240:77-87

90.   Speransky AD AC (1943) A basis for the theory of medicine. New York: International Publishers

91.   Stanton EH, Persson NDÅ, Gomolka RS, Lilius T, Sigurðsson B, Lee H, Xavier ALR, Benveniste H, Nedergaard M, Mori Y (2021) Mapping of CSF transport using high spatiotemporal resolution dynamic contrast-enhanced MRI in mice: Effect of anesthesia. Magnetic Resonance in Medicine 85:3326-3342

92.   Tuppo EE, Arias HR (2005) The role of inflammation in Alzheimer's disease. The International Journal of Biochemistry & Cell Biology 37:289-305

93.   Voelz K, Kondziella D, von Rautenfeld DB, Brinker T, Lüdemann W (2007) A ferritin tracer study of compensatory spinal CSF outflow pathways in kaolin-induced hydrocephalus. Acta Neuropathologica 113:569-575

94.   Weed LH (1914a) Studies on Cerebro-Spinal Fluid. No. II : The Theories of Drainage of Cerebro-Spinal Fluid with an Analysis of the Methods of Investigation. The Journal of Medical Research 31:21-49

95.   Weed LH (1914b) Studies on Cerebro-Spinal Fluid. No. III : The pathways of escape from the Subarachnoid Spaces with particular reference to the Arachnoid Villi. The Journal of Medical Research 31:51-91

96.   Weed LH (1914c) Studies on Cerebro-Spinal Fluid. No. IV : The dual Source of Cerebro-Spinal Fluid. The Journal of Medical Research 31:93-118.111

97.   Welch K, Pollay M (1963) The spinal arachnoid villi of the monkeys Cercopithecus aethiops sabaeus and Macaca irus. The Anatomical Record 145:43-48

98.   Welch K (1977) Selected topics relating to hydrocephalus. Experimental Eye Research 25 Suppl:345-375

99.   Weller RO, Djuanda E, Yow H-Y, Carare RO (2009) Lymphatic drainage of the brain and the pathophysiology of neurological disease. Acta Neuropathologica 117:1-14

100.   Weller RO, Sharp MM, Christodoulides M, Carare RO, Møllgård K (2018) The meninges as barriers and facilitators for the movement of fluid, cells and pathogens related to the rodent and human CNS. Acta Neuropathologica 135:363-385

101.   Woollam DH (1957) The historical significance of the cerebrospinal fluid. Medical History 1:91-114

102.   Wurster CD, Winter B, Wollinsky K, Ludolph AC, Uzelac Z, Witzel S, Schocke M, Schneider R, Kocak T (2019) Intrathecal administration of nusinersen in adolescent and adult SMA type 2 and 3 patients. Journal of Neurology 266:183-194

103. Wustmann O (1933) Experimentelle Untersuchungen über die Reliefdarstellung (Umrißzeichnung) des Zentralnervensystems im Röntgenbild durch Thoriumkontrastmittel. Deutsche Zeitschrift für Chirurgie:529-567

104. Xie L, Kang H, Xu Q, Chen MJ, Liao Y, Thiyagarajan M, O'Donnell J, Christensen DJ, Nicholson C, Iliff JJ, Takano T, Deane R, Nedergaard M (2013) Sleep drives metabolite clearance from the adult brain. Science (New York, NY) 342:373-377

105. Yamada S, Shibata M, Scadeng M, Bluml S, Nguy C, Ross B, McComb JG (2005) MRI tracer study of the cerebrospinal fluid drainage pathway in normal and hydrocephalic guinea pig brain. The Tokai Journal of Experimental and Clinical Medicine 30:21-29

106. Zervas NT, Liszczak TM, Mayberg MR, Black PM (1982) Cerebrospinal fluid may nourish cerebral vessels through pathways in the adventitia that may be analogous to systemic vasa vasorum. Journal of Neurosurgery 56:475-481

107. Zhang ET, Inman CB, Weller RO (1990) Interrelationships of the pia mater and the perivascular (Virchow-Robin) spaces in the human cerebrum. Journal of Anatomy 170:111-123

7. Publication

Magnetic resonance imaging of cerebrospinal fluid outflow after low-rate lateral ventricle infusion in mice

Yann Decker,[1] Jonas Krämer,[1] Li Xin,[2] Andreas Müller,[3] Anja Scheller,[4] Klaus Fassbender,[1] and Steven T. Proulx[2]

[1]Department of Neurology, Saarland University Medical Center, Homburg, Germany. [2]Theodor Kocher Institute, University of Bern, Bern, Switzerland. [3]Clinic for Diagnostic and Interventional Radiology and [4]Molecular Physiology, Center for Integrative Physiology and Molecular Medicine, University of Saarland, Homburg, Germany.

RESOURCE AND TECHNICAL ADVANCE

The anatomical routes for the clearance of cerebrospinal fluid (CSF) remain incompletely understood. However, recent evidence has given strong support for routes leading to lymphatic vessels. A current debate centers upon the routes through which CSF can access lymphatics, with evidence emerging for either direct routes to meningeal lymphatics or along cranial nerves to reach lymphatics outside the skull. Here, a method was established to infuse contrast agent into the ventricles using indwelling cannulae during imaging of mice at 2 and 12 months of age by magnetic resonance imaging. As expected, a substantial decline in overall CSF turnover was found with aging. Quantifications demonstrated that the bulk of the contrast agent flowed from the ventricles to the subarachnoid space in the basal cisterns. Comparatively little contrast agent signal was found at the dorsal aspect of the skull. The imaging dynamics from the 2 cohorts revealed that the contrast agent was cleared from the cranium through the cribriform plate to the nasopharyngeal lymphatics. On decalcified sections, we confirmed that fluorescently labeled ovalbumin drained through the cribriform plate and could be found within lymphatics surrounding the nasopharynx. In conclusion, routes leading to nasopharyngeal lymphatics appear to be a major efflux pathway for cranial CSF.

Conflict of interest: The authors have declared that no conflict of interest exists.

Introduction

Cerebrospinal fluid (CSF) is produced within the ventricles by the choroid plexuses and circulates within the subarachnoid spaces around the brain and spinal cord. Historically, it was concluded that CSF leaves the central nervous system (CNS) via direct pathways through outcroppings of arachnoid tissue into the venous sinuses of the dura mater (1, 2). However, in recent decades it has become commonly accepted that lymphatic vessels play a significant role in the process of CSF drainage (3–6). Recent studies in rodents have demonstrated that lymphatic vessels appear to be the exclusive clearance route for tracers injected into the CSF, even for low–molecular weight solutes (7, 8). An active area of research has focused upon the anatomical routes of outflow that CSF takes to access the lymphatic vessels. Support exists for access of CSF to lymphatic vessels that have been recently rediscovered in the dura mater (9–11) and for efflux along cranial or spinal nerves to reach extracranial lymphatics (7, 12–15). Of the perineural routes, evidence in many different species exists for routes along olfactory nerves through the cribriform plate (5, 10, 16–20).

Imaging techniques have long been utilized to assess CSF outflow of tracers (6). Traditionally, these techniques have employed x-ray or scintigraphic measurements (21, 22). Recently, 2-photon and near-infra- red fluorescence techniques (7–9, 13, 14, 23) have been developed to allow sensitive in vivo readouts to allow sensitive in vivo readouts within the CNS (imaging through skull or through spine), at specific efflux path- ways (imaging through vomeronasal bones into the nasal region or imaging of lymphatic vessels draining to the superficial cervical or

mandibular lymph nodes), or to the systemic blood from multiple efflux pathways. However, these methods can only allow assessments at one particular region at a relatively superficial level. On the other hand, contrast-enhanced magnetic resonance imaging (CE-MRI) techniques have the advan- tage of 3D imaging of the entire cranial or spinal regions in the context of the surrounding soft tissue anat- omy, with sufficient temporal resolution to track the dynamics of contrast agent outflow, and have a more immediate translational potential to the clinic (8, 11–13, 15, 24).

1

One valid criticism of tracer injection studies is that they may inherently introduce artifacts because of relatively large acute volumes introduced into the CSF. In the mouse, with an estimated CSF volume of 35 μL (2), injections of 5 to 10 μL made within a short period likely introduce elevated pressure conditions that will affect the dynamics and routes of outflow (8, 25). Our group has attempted to address this issue by establishment of an indwelling cannula into the lateral ventricle of mice that allows slow infusion during imaging acquisition (13) at rates below the published rates for CSF production (2, 26). We have utilized this cannula system to allow MRI measurements of spinal CSF distribution and sacral outflow during the infusion of contrast agent (13). Similar cisterna magna infusion setups have also recently been employed by other groups to examine cranial CSF distribution (12, 15).

Alterations in CSF circulation may have significant effects on the pathogenesis of neurological condi- tions associated with the aging process, including dementia and stroke. Many research groups have now demonstrated that a slower overall efflux of CSF occurs during the aging process (7, 11, 14). Thus, we have utilized this expected difference in CSF turnover dynamics between younger (2–3 months old) and older (12 months old) mice to aid in validation of MRI quantifications. Second, we have investigated potential efflux routes by analyzing the contrast agent signal dynamics at several locations within the CNS and the cervical lymph nodes. We hypothesized that differences in signal dynamics quantified between the 2 age groups would be apparent only at the major site(s) of efflux.

Results

Tracer infused into the lateral ventricle follows a continuous outflow route from the nasal cavity to the draining cervical lymph nodes. Since CSF is principally produced by the choroid plexuses that are located in the ventricles, we decided to analyze the flow of tracer following an intraventricular low-rate infusion of a 17 kDa dendritic gadolinium-based contrast agent, GadoSpin D (Figure 1A). We chose GadoSpin D rather than a low–molec- ular weight contrast agent to limit potential diffusion into the brain parenchyma from the ventricular injection site. After stereotactic implantation of an indwelling cannula in the right lateral ventricle, mice were posi- tioned in a prone position on a horizontal MRI platform. A polyethylene line filled with contrast agent was subsequently connected at one end to the cannula and at the other end to an infusion pump. After a baseline precontrast scan, an infusion of the contrast agent was started at a rate of 0.1 μL/min for 60 minutes, and a series of CE-MRI images were collected over the course of 90 minutes. This experimental setup allowed us to acquire images of the animal throughout the infusion of a macromolecular contrast agent at rates not excessive beyond physiological levels.

We first determined the general pattern of the spread of GadoSpin D by generating maximum-in- tensity projection images at each time point to allow a 3D dynamic visualization of the contrast agent (Supplemental Video 1; supplemental material available online with this article; https://doi.org/10.1172/ jci.insight.150881DS1). An initial filling of the ventricular system was apparent, spreading ventrally to the basal cisterns and under the olfactory bulbs within the first 15 minutes after the start of the infusion. With increasing time, the signal intensity of the tracers was progressively detectable in the nasal cavity, in the nasopharyngeal region, and in the deep and superficial lymph nodes (Figure 1B). Moreover, as observed in Figure 1C and Supplemental Video 1, it was possible to identify a continuous anatomic route along the nasopharynx that emerged from the nasal cavity and connected to the deep cervical lymph nodes. Con- nections also were apparent from the deep cervical lymphatics to the superficial cervical (or mandibular) lymph nodes, as previously shown using near-infrared imaging (7).

Reduced tracer clearance from the ventricles and slower efflux to draining lymph nodes in older mice. It has recently been demonstrated that CSF production and drainage are both reduced in aged mice, suggesting that the overall CSF turnover is slower with aging (7, 14, 27). During and immediately after the low-rate intraventricular infusion, we investigated the clearance of GadoSpin D from the ventricular system in 2 groups of mice of either 2–3 months ($n = 7$) or 12 months of age ($n = 6$). While the low-rate infusion of contrast agent took place during the first 60 minutes, we observed that the signal intensity in the con- tralateral ventricles reached a peak at around 40 minutes and then progressively decreased in both age groups (Figure 2A and Supplemental Figure 1A). At later time points, we could observe significantly stronger decreased signal intensity in the contralateral ventricles of the group of younger mice. As no significant difference was observed in the volume of the contralateral ventricles (Figure 2B) between the 2

groups, we concluded that a decrease in the rate of CSF turnover was responsible for the reduced con- trast agent clearance observed in the 12-month-old mice.
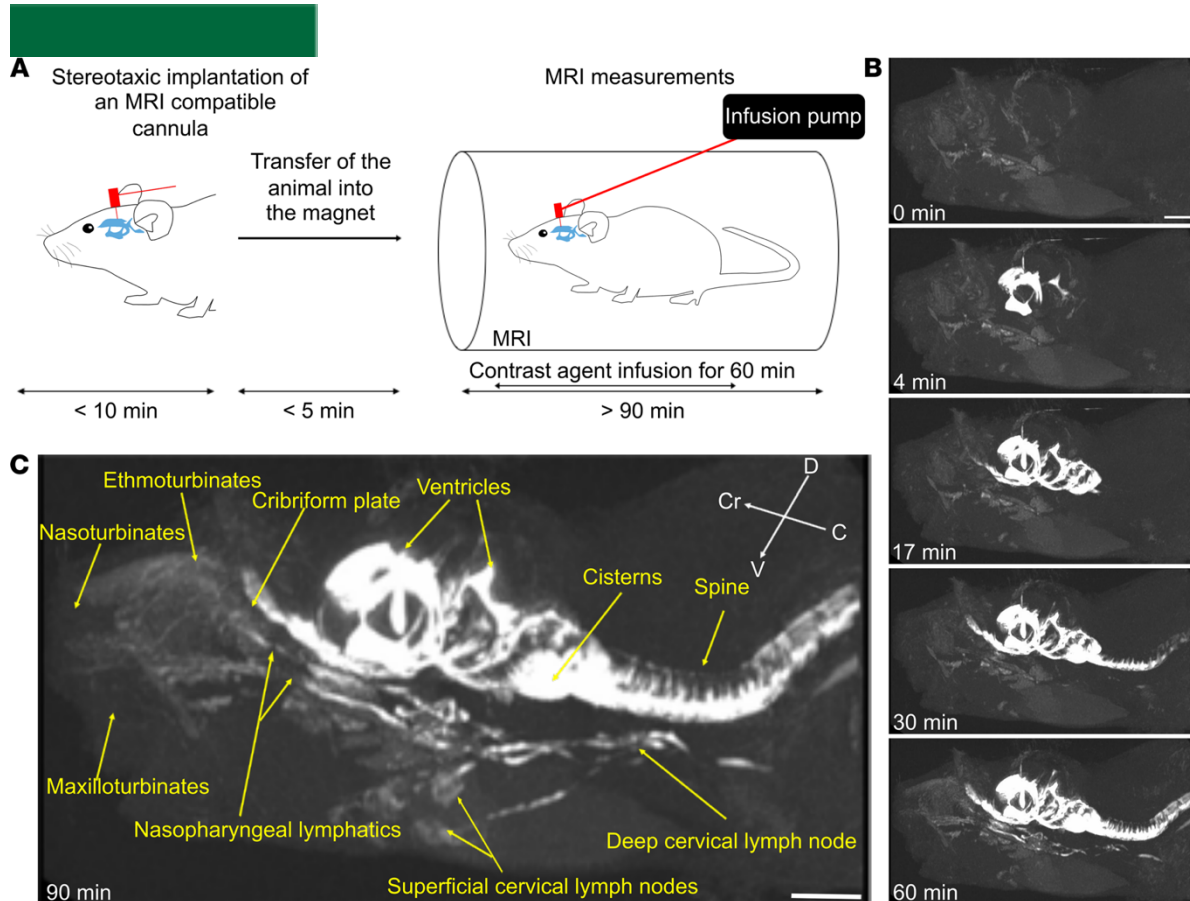
RESOURCE AND TECHNICAL ADVANCE

Figure 1. Dynamic CE-MRI shows continuous efflux of contrast agent from the nasal region through lymphatic vessels to cervical lymph nodes following low-rate ventricular infusion. (**A**) Schematic representation of the experimental setup. MRI-compatible cannulae were stereotactically implanted into the ventricle of 2- to 3-month-old C57BL/6J mice anesthetized with ketamine/xylazine. The animals were then transferred into a horizontal-bore 9.4 T MRI. Polyethylene tubing containing the contrast agent (GadoSpin D solution from nanoPET Pharma GmbH at 25 mM Gd)
was attached connecting the cannula and the infusion pump. Before contrast agent infusion, T1-weighted (3D time-of-flight gradient recalled echo sequence) MRI measurements were started and followed by intraventricular low-rate infusion (0.1 μL/min) of the contrast agent while MRI acqui- sitions continued. (**B**) Representative signal dynamics using maximum-intensity projections visualizing the entire head-neck region. Following the beginning of contrast agent infusion, enhancement of the signal intensity in the ventricle is detectable at 4 minutes, in the nasal cavity at 17 min- utes, and in the neck lymph nodes at 30 and 60 minutes. (**C**) Visualization of the spread of contrast agent after 90 minutes demonstrating continu- ous signal enhancement from the cribriform plate to the nasopharyngeal lymphatic vessels to cervical lymph nodes. Data are representative of *n* = 7 mice and 3 independent experiments. Scale bars: 3 mm.

Our previous studies have shown that lymphatic outflow from CSF is reduced in 18-month-old mice compared with 2-month-old mice following a bolus injection of a macromolecular fluorescently labeled tracer (7). We tested whether this difference would be apparent by MRI in 12-month-old mice by quan- tifying the signal intensity of the contrast agent in regions of interest (ROIs) positioned in the deep and superficial cervical lymph nodes. Dynamic CE-MRI quantification revealed less contrast agent signal in both groups of cervical lymph nodes in the 12-month-old mice compared with the group of younger mice (Figure 2, C and D; and Supplemental Figure 1, B and C). Quantifications of the volume of 3D reconstructions of the cervical lymph nodes also did not show significant differences between the 2 age groups (Supplemental Figure 1, D and E).

In sum, we observed that with aging, a low-rate infusion of a macromolecular contrast agent was asso- ciated with reduced clearance from the ventricles and a delayed transport to draining lymph nodes, which is consistent with previous studies by our group and others. Thus, we next aimed to exploit these differences in CSF turnover dynamics

between the 2 age groups of mice to help identify major efflux routes from the ventricular system to the lymphatic system.

Contrast agent flows along the ventral aspect of the brain and down the spine. CSF has recently been proposed to reach the dura mater on the dorsal aspect of the skull, where it is hypothesized to be either directly or indirectly drained by meningeal lymphatic vessels leading to the deep cervical lymph nodes (9, 28–30). Previous work

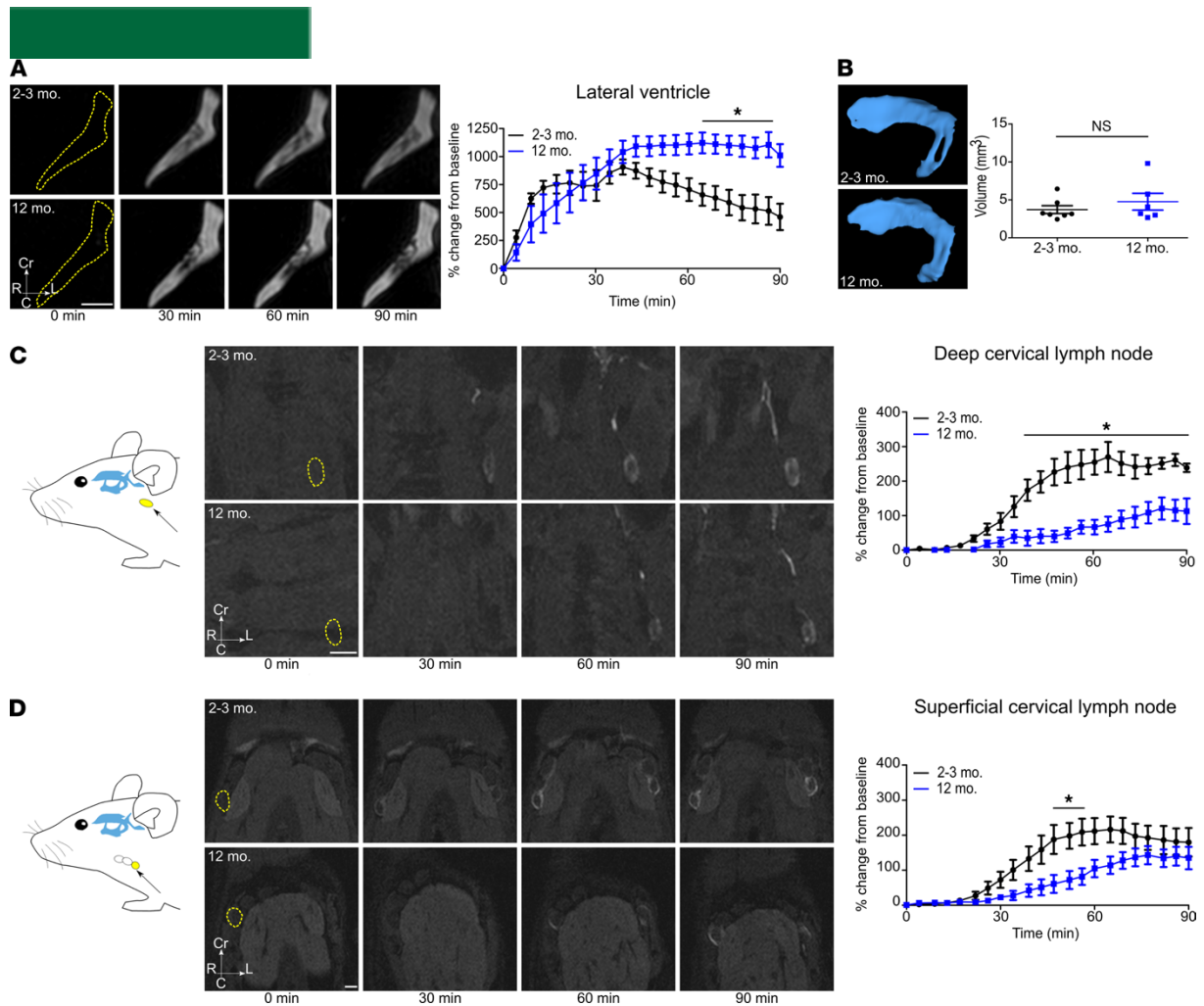### RESOURCE AND TECHNICAL ADVANCE

Figure 2. Clearance from ventricles and efflux to lymph nodes are reduced in 12-month-old mice. Visualization of tracer spread after low-rate intraven- tricular infusion (0.1 μL/min) of a GadoSpin D solution at 25 mM Gd; data acquired with a series of T1-weighted MRI measurements (3D time-of-flight gradient recalled echo sequence). (**A**) Signal dynamics of GadoSpin D contrast agent showing clearance from the contralateral ventricles in the horizon- tal plane in young (2–3 months) and 12-month-old mice. (**B**) Representative images of 3D reconstruction of the contralateral ventricles of young and 12-month-old mice. Ventricle volumes of young and 12-month-old mice were compared with 2-tailed Student's t test. (**C** and **D**) Signal dynamics in the horizontal plane of GadoSpin D tracer efflux to deep and superficial cervical lymph nodes in young and 12-month-old mice. ROIs shown in yellow. Data are expressed as mean ± SEM of 2- to 3-month-old mice (n = 7) vs. 12-month-old mice (n = 6) and are representative of 3 independent experiments. *P < 0.05 (2-way ANOVA followed by Bonferroni's post hoc test). Scale bars: 1 mm.

has highlighted lymphatic vessels in the dural tissue surrounding the sagittal and the transverse sinuses to be "hotspots" for uptake from the CSF. Thus, following intraventricular infusion of GadoSpin D, we quantified the signal intensity in 2 ROIs of the dorsal aspect of the skull in proximity to these regions. In both areas, we could observe only a limited maximum change in signal intensity compared to baseline (sagittal sinus ROI: <42%; quadrigeminal cistern ROI: <120%) and no significant differences at any time point between the groups of 2-month-old and 12-month-old mice (Figure 3, A–C; and Supplemental Figure 2, A and B).

On the other hand, quantifications of ROIs in the ventral region (at the basal cisterns around the circle of Willis and the internal carotid artery) showed a substantial increase in maximum change in signal intensity compared with baseline (circle of Willis ROI: >700%; internal carotid ROI: >700%), suggesting that this area is a major site of contrast agent bulk flow (Figure 3, A, D, and E; and Supplemental Figure 2, C and D). Moreover, in the 2 regions investigated, the signal intensity was quantitatively significantly higher at earlier time points in young mice compared with the group of 12-month-old mice. These results indicate that an infused macromolec- ular tracer principally flows with the CSF through the ventral, rather than dorsal, aspect of the skull.

RESOURCE AND TECHNICAL ADVANCE

Because CSF leaving the ventricles has free communication with the subarachnoid space around the spinal cord, we also quantified the dynamics in the ventral aspect of the cervical spine (Supplemental Fig- ure 3A). We observed a rapid increase in signal intensity, in the group of young mice, that reached a max- imum percentage change of more than 600%. Conversely, in the group of 12-month-old mice, the signal intensity increase was delayed and only reached approximately half of the value observed in young mice. Thus, CSF tracer flow from the ventricular system to the spine can be easily demonstrated with CE-MRI and exhibits the expected decline with aging.

Recent work has introduced the concept of glymphatic flow that would theoretically aid in CSF/solute penetration into the brain parenchyma along para-arterial spaces. Recent MRI studies have shown that low–molecular weight contrast agents, such as gadoteric acid, do indeed demonstrate signal enhancement within the parenchyma (31–36). However, we were unable to confirm a significant influx of the GadoSpin D contrast agent (17 kDa) into the brain cortex in either group (maximum percentage change of 17%) (Supplemental Figure 3B). This limited signal enhancement of a macromolecular contrast agent within the brain is consistent with our earlier study (8) and others (12).

Thus, we conclude from this study that bulk flow routes to the basal cisterns and the subarachnoid space of the spinal canal are major pathways for CSF macromolecular distribution from the ventricular system.

Dynamics of CSF contrast agent outflow support route(s) leading to the nasopharyngeal lymphatics. After observing that a substantial portion of the tracer reached the basal cisterns, we aimed to elucidate the potential anatom- ical pathways from this location that might be used to reach the cervical draining lymph nodes. Based on our observation that the bulk of the contrast agent appeared to flow continuously from the region of the olfactory bulbs to the nasopharynx and to the draining lymph nodes, we first quantified the changes in signal intensity in ROIs localized in the nasal turbinates and the nasopharynx (Figure 4, A–C; and Supplemental Figure 4, A and B). Dynamic imaging showed, in the group of 12-month-old mice, a delayed and significantly reduced transport of contrast agent in these 2 regions.

At other regions suggested to be efflux sites from the skull, CSF contrast agent signal could be detected in the jugular region below the skull and around the optic nerves (Figure 4, A, D, and E; and Supplemental Figure 4, C and D). However, at these 2 regions, our quantifications revealed that no significant differences in the signal intensity at any time point were observed between the young and 12-month-old groups. In fact, the jugular region appeared to show a trend toward increased signal intensity over time in the 12-month-old mice compared with the young mice, indicating that this region may be a site of accumulation of contrast agent. An earlier report has shown that dural lymphatic vessels of this region become more hyperplastic with age (11).

Thus, because the expected differences in signal dynamics between young and older animals were only detectable in the nasal turbinates and the nasopharyngeal areas, we conclude that this route is a major path- way for CSF clearance from the cranium to the cervical lymph nodes.

Histological confirmation of CSF outflow route(s) to the nasopharyngeal lymphatics. Interestingly, the signal quantifications revealed that only a minimal increase of signal (170% in young mice, 85% in 12-month- old mice) could be detected within the turbinates themselves in either group, whereas much larger signal increases were detected at the nasopharynx (710% in young mice, 570% in 12-month-old mice). This may suggest that the contrast agent distributes to a large area throughout the nasal cavity after effluxing through the cribriform plate before draining to the lymphatic vessels near the nasopharynx leading to the lymph nodes, as appears to be evident from the sagittal view in Supplemental Video 1.

To further evaluate how CSF tracers drain through the cribriform plate to reach lymphatics sur- rounding the nasopharynx, we injected Alexa Fluor 647–labeled ovalbumin (AF647-OVA) using the same slow infusion protocol

employed within the MRI and then assessed the presence of tracer on sec- tions from decalcified craniums and deep cervical lymph nodes. Lymphatic vessels were identified using anti–lymphatic vessel endothelial hyaluronan receptor 1 (anti–LYVE-1) antibodies. As seen in Figure 5, A and B, which were taken from 2 coronal sections at different levels of the nasal cavity, AF647-OVA was clearly associated with olfactory nerves crossing the cribriform plate and was distributed throughout a wide volume of nasal mucosal tissue. A rich network of LYVE-1+ lymphatic vessels exists laterally on both sides of the nasopharynx, and these vessels could be found to contain AF647-OVA signal (Figure 5, C–E). Deep cervical lymph nodes located downstream of this site also contained AF647-OVA that was found within LYVE-1+ lymphatic sinuses (Figure 5, F–J). Thus, this serves as histological confirmation of the CSF drainage route visible on MRI.
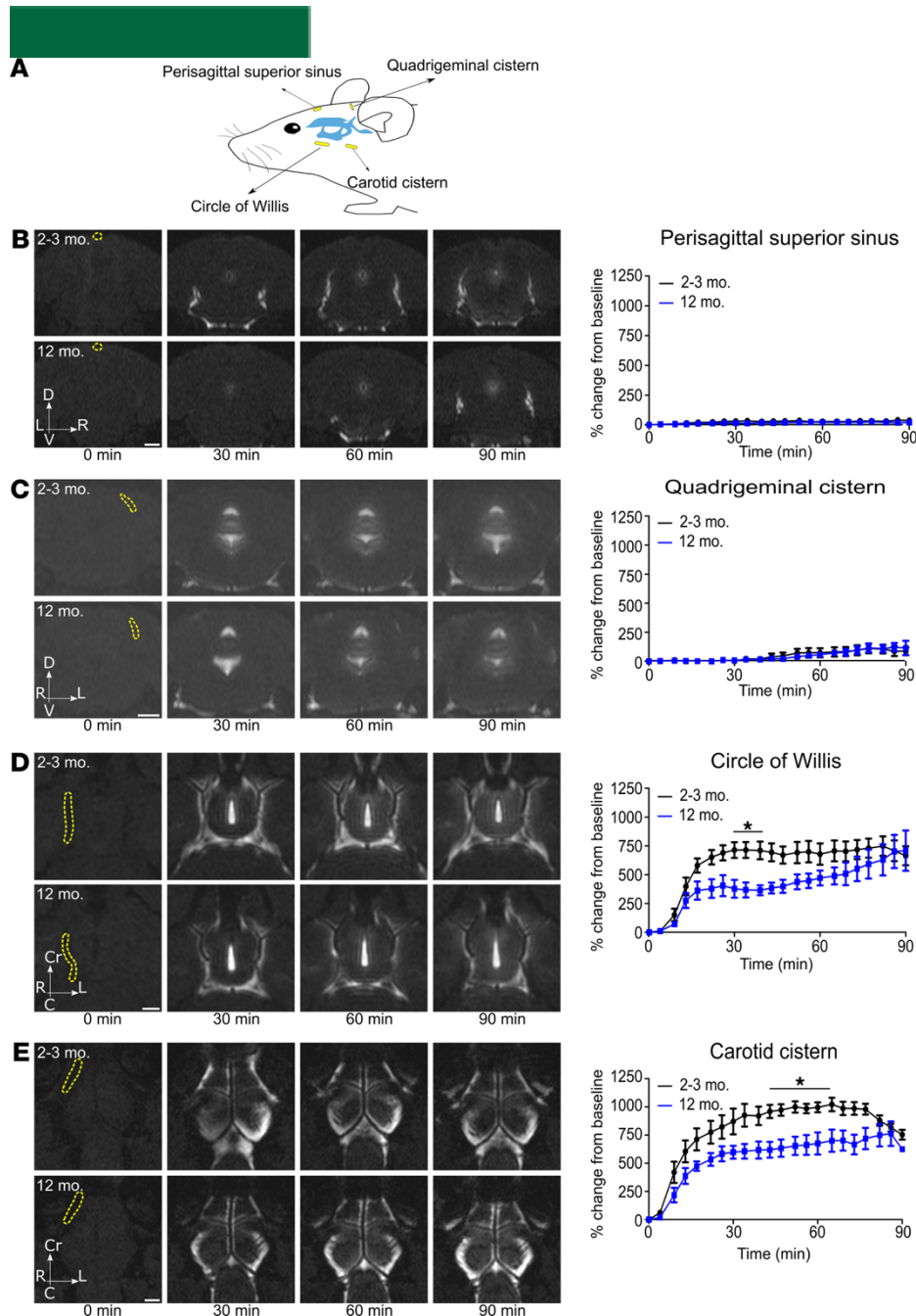
RESOURCE AND TECHNICAL ADVANCE

Figure 3. CSF predominantly clears along the ventral aspect of the skull. Visualization of tracer clearance after low-rate intraventricular infusion (0.1 μL/min) of GadoSpin D solution at 25 mM Gd. Data were acquired with a series of T1-weighted MRI measurements (3D time-of-flight gradient recalled echo sequence). (**A**) Overview scheme of ROI location. (**B** and **C**) Coronal sections demonstrating in 2- to 3-month- and 12-month-old mice the dynamics of CSF efflux in representative ROIs (shown in yellow) of the

dorsal aspect of the skull: in the perisagittal superior sinus and the quadrigeminal cisterns. (**D** and **E**) Horizontal sections showing the dynamics of CSF efflux in the ventral aspect of the skull in 2- to 3-month- and 12-month-old mice: around the circle of Willis and around the internal carotid (ROIs in yellow). Quantifications of the different ROIs are expressed as the mean ± SEM of 2- to 3-month-old mice (n = 7) vs. 12-month-old mice (n = 6) and are representative of 3 independent experiments. *$P < 0.05$ (2-way ANOVA followed by Bonferroni's post hoc test). Scale bars: 1 mm.

Discussion

In this study, we have assessed CSF outflow by MRI in 2 age groups (2–3 months and 12 months) of mice by utilizing an indwelling catheter system, allowing low-rate infusion of a macromolecular contrast agent during image acquisitions. Similar to previous reports, we found slower dynamics of CSF circulation in the older cohort of mice compared with the younger mice. Imaging of the contrast agent dynamics in the
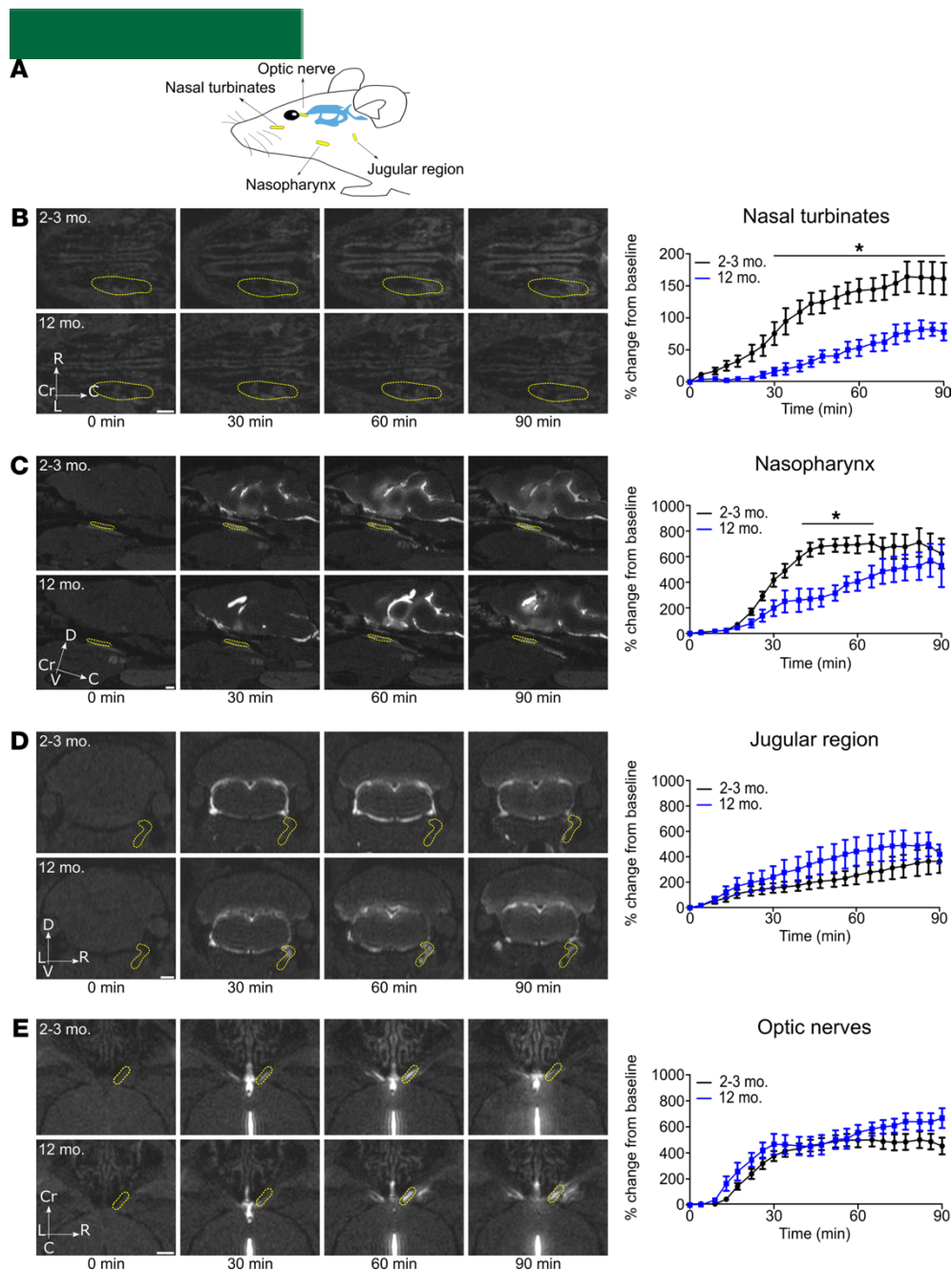
RESOURCE AND TECHNICAL ADVANCE

Figure 4. Clearance of CSF from the cranium is reduced with aging in the nasal turbinates and the nasopharynx but not in the jugular region and around the optic nerves. Imaging of tracer clearance after low-rate intraventricular infusion (0.1 µL/min) of GadoSpin D solution at 25 mM Gd. Data were acquired with a series of T1-weighted MRI measurements (3D time-of-flight gradient recalled echo sequence). (**A**) Overview scheme of ROI location. (**B**) Horizontal sections demonstrat- ing the dynamics of CSF efflux to nasal turbinates in 2- to 3-month- and 12-month-old mice. (**C**) Sagittal sections reveal the dynamics of contrast agent in the nasopharynx in the 2 groups of mice. (**D**) Coronal sections demonstrating the CSF efflux from the jugular region in the groups of mice of different ages. (**E**) Horizontal sections showing CSF efflux along the optic nerves in the groups of mice of different ages. Quantifications of the different ROIs (shown in yellow) are expressed as the mean ± SEM of 2- to 3-month-old mice ($n = 7$) vs. 12-month-old mice ($n = 6$) and are representative of 3 indepen- dent experiments. *$P < 0.05$ (2-way ANOVA followed by Bonferroni's post hoc test). Scale bars: 1 mm.

cranial region revealed that the bulk of the CSF flowed ventrally under the brain through the basal cisterns and exited through the cribriform plate to be collected by lymphatics in the nasopharyngeal region.

Our methods are similar to those in recent publications utilizing MRI for examination of CSF flow in rodents (11, 12, 15). In these studies, the authors infused contrast agents during the MRI acquisi- tion into the cisterna magna through a cannula and examined the efflux routes from the cranial cavity.

RESOURCE AND TECHNICAL ADVANCE

In our study, we chose to infuse into the ventricles, close to the source of production at the choroid plex- uses, which allowed assessment of the clearance from the ventricular system, as well as distribution to and efflux from the subarachnoid space.

We observed minimal contrast agent signal in the dorsal region near the dural sinuses or above the cortical hemispheres. Thus, this is contrary to a concept of a major pathway of CSF outflow at the dorsal dura, as pro- posed in several recent studies in mice (9, 28, 29) and recently extended to the human situation (37). Instead, the dynamics clearly indicated that the majority of contrast agent traversed the basal cisterns with pathways from the cisterna magna to the subarachnoid space around the circle of Willis. This is consistent with both historical data (1, 38) and other recent MRI studies (8, 11, 12, 15, 24, 33). While it is clear that some portion of CSF does reach the surface of the cortical hemispheres as well as the subarachnoid cisterns located near the dural sinuses (12, 13, 39, 40), the significance and ultimate egress route(s) for this flow remain open questions.

As we anticipated, our data indicate a reduction in CSF outflow in older mice consistent with previous reports (7, 11, 14, 41). We were able to detect delays in 12 month-old animals in CSF clearance and transport at several locations along the CSF flow pathways, including the lateral ventricle, basal cisterns, cervical spinal sub- arachnoid space, nasal turbinates, nasopharyngeal lymphatics, and CNS-draining lymph nodes. Thus, the data are indicative of an overall reduction in CSF turnover with aging. The reason for this diminished turnover of CSF is not yet clear; however, it may be related to a reduced CSF production by the choroid plexuses (27, 42), morphological changes in the dural lymphatics (11), or a reduced transport within lymphatic vessels outside the CNS (43–45). Whether this slowed CSF circulation plays a role in the development of neurodegenerative disorders associated with aging, as speculated in many recent studies (11, 46), remains to be determined.

We took advantage of the differences in contrast agent dynamics between the 2 age groups of mice to attempt to elucidate the relative importance of several potential efflux routes. We hypothesized that only along major bulk flow pathways for CSF egress would the patterns of contrast agent dynamics between the 2 age groups mirror those seen at the downstream lymph nodes. Since we found that lim- ited contrast agent signal was apparent along the dorsal aspect of the skull, we focused these efforts on potential efflux routes from the basal cisterns. From this location, evidence exists in the literature for outflow to the lymphatic system through the cribriform plate (1, 5, 7, 16, 17, 19, 47), along the sheaths surrounding the optic nerves (7, 48, 49), through the jugular foramina (7, 10, 11, 15, 47), and from the spinal column (13, 23, 50). Of these routes, in our study, only the spinal and nasal regions appeared to exhibit the expected contrast enhancement dynamics between the 2 age groups of mice. An outflow pathway to the lymphatic system does indeed exist in rodents from the sacral region of the spine; how- ever, our previous work and others have determined that under normal conditions the spinal pathways are minor compared with the cranial efflux routes (13, 51, 52). Thus, the resulting conclusion of a major CSF outflow pathway through the cribriform plate would be in agreement with many previous studies (14, 18, 53, 54). Strong supporting evidence for this conclusion comes from experiments that blocked this pathway, which resulted in dramatic decreases in tracer recovery outside the CNS and increased intracranial pressure during fluid challenge (53, 55). However, we cannot rule out at this point that more direct pathways may exist, extending from the basal skull to reach the nasopharyngeal lymphatics.

This conclusion appears to conflict with that of Ahn et al. in rats (11), who determined using MRI with a macromolecular contrast agent that basal meningeal lymphatic vessels draining through the jugular foram- ina are the main route for CSF macromolecular uptake and drainage. It must be noted that in their study Ahn et al. did not investigate any potential efflux through the cribriform plate region. However, another possible explanation for this discrepancy may be due to different experimental conditions between our study and Ahn et al. In a recent, elegant MRI study by Stanton et al., the authors demonstrated that the choice of anesthesia has a significant effect on the amount of efflux through the cribriform plate, with mice under isoflurane anesthesia demonstrating much less gadolinium diethylenetriaminepentaacetic acid signal in this area (15). This study is consistent with earlier work demonstrating differences in CSF flow dynamics under different types of anesthesia (8, 13, 56). The authors demonstrated that mice under 1.5% anesthesia exhibit- ed more signal at the jugular foramina along the cranial nerves and also within the spinal canal, indicating that shunting of the CSF flow may occur under certain conditions (15). This potential redirection of flow is an important factor to consider, especially in the context of pathological conditions such as hydrocephalus or glioblastoma, which may block CSF outflow pathways at the skull and reroute flow to the spine (57, 58).

The situation in humans remains unresolved (6). Studies have presented evidence both for and against efflux of contrast agent through the cribriform plate (54, 59–61). One recent clinical MRI study concluded
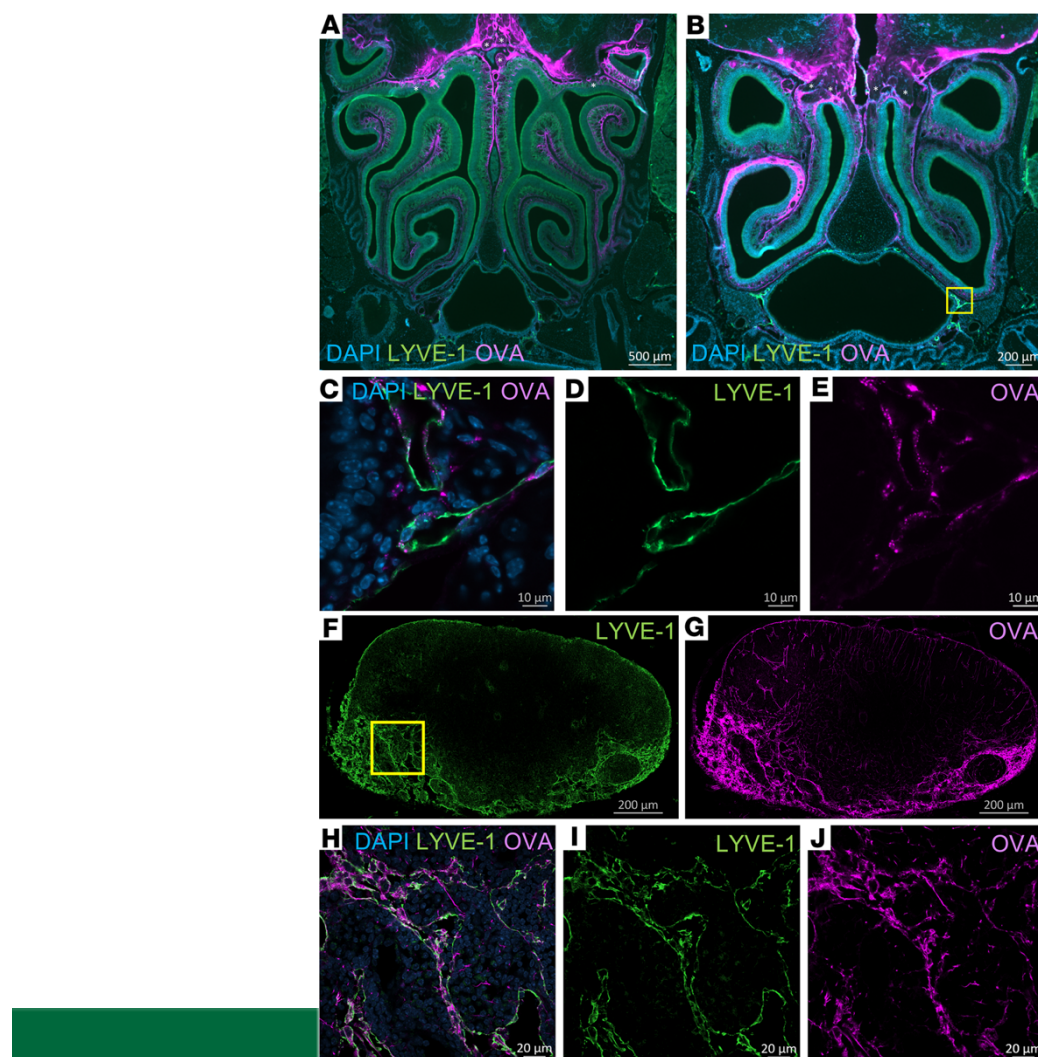
RESOURCE AND TECHNICAL ADVANCE

Figure 5. Histological validation of CSF tracer efflux through the cribriform plate to nasopharyngeal lymphatics and to deep cervical lymph nodes. Fluorescently labeled ovalbumin (OVA) was introduced via low-rate intraventricular infusion (0.1 μL/min for 60 minutes), and at 90 minutes the mice were sacrificed for postmortem analysis of tracer efflux. (**A** and **B**) Coronal sections of decalcified skulls demonstrating substantial efflux of OVA into the nasal mucosal tissues. OVA (purple) can be seen crossing the cribriform plate alongside several olfactory nerve bundles (indicated with *). Lymphatic vessels (stained with LYVE-1 in green) can be found in proximity to the nasopharynx under the nasal turbinates. Scale bars: 500 μm (**A**), 200 μm (**B**). (**C–E**) High-magnification

view of the nasopharyngeal region indicated by the yellow box in **B**, demonstrating OVA signal within the LYVE-1$^+$ lymphatic vessels. Scale bars: 10 µm. (**F** and **G**) Sections of deep cervical lymph nodes indicating close association of OVA signal within lymphatic sinuses stained with LYVE-1. Scale bars: 200 µm. (**H–J**) High-magnification view of the region indicated by the yellow box in **F**, demonstrating OVA signal within the LYVE-1$^+$ lymphatic sinuses. Scale bars: 20 µm. Data are representative of *n* = 6 mice and 2 independent experiments.

that CSF efflux to the nasal region is minimal in humans (61). This study used a low–molecular weight gadolinium contrast agent injected into the lumbar intrathecal space and examined the nasal turbinates at multiple time points in patients with various CSF circulation disorders. Although contrast agent was observable in almost half of the patients below the cribriform plate along the olfactory nerves, the authors were unable to observe a significant increase of signal within the nasal cavity at any time point. Our current study demonstrates the technical difficulty of detecting significant contrast agent signal enhancement with- in nasal tissue using an MRI approach, even though we employed a macromolecular contrast agent that should clear exclusively from the nasal submucosa through lymphatics (53). While the exact anatomical routes remain to be elucidated, it was evident from our decalcified sections after ovalbumin infusion that the tracer spread throughout a wide volume of the nasal tissue after crossing the cribriform plate, which may partially account for the difficulty in detecting signal with MRI in humans.

RESOURCE AND TECHNICAL ADVANCE

In sum, through establishment of a technique allowing dynamic CE-MRI under low-rate infusion of gadolinium contrast agents, we conclude that CSF distributes from the ventricles to the subarachnoid space ventral to the brain and in a caudal direction down the spine. Under our experimental conditions, a major outflow route from the cranium appeared to be through the nasal region to reach lymphatic vessels near the nasopharynx before draining to the cervical lymph nodes. With aging, the dynamics of clearance from the ventricles and flow through the nasal turbinates and nasopharyngeal lymphatics to the lymph nodes were reduced. These experiments have set the stage for further MRI evaluation of CSF outflow in mouse models of neurological disorders.

Methods

Mice. Female wild-type mice (Janvier) on a C57BL/6 background were kept under specific pathogen–free conditions until they were used for experimental studies.

Surgical preparation. Mice were anesthetized by intraperitoneal injection of 100 mg/kg ketamine and 20 mg/kg xylazine and fixed in a stereotaxic frame (Kopf Instruments). Under this anesthesia, the skull was thinned with a Proxxon GG 12 engraving drill. A 28 G, 2.5 mm long, MRI-compatible microcannula (328OP/PK/Spc; Plastics One) was inserted stereotactically 0.95 mm lateral and 0.22 mm caudal to the bregma and 2.50 mm ventral to the skull surface (13). The microcannula was sealed with cyanoacrylate glue. Animals were transferred into the magnet in a prone position on an MRI cradle (BioSpec Avance III 94/20; Bruker BioSpin GmbH). A 1 to 1.5 m long polyethylene catheter filled with a GadoSpin D (nano- PET Pharma GmbH) solution at a Gd concentration of 25 mM was connected to the MRI-compatible microcannula and a 10 µL syringe operated by an MRI-compatible NanoJet syringe pump (Chemyx Inc.). The skin incision was then closed with a medical adhesive bandage around the cannula and the catheter. Animals were allowed to breathe spontaneously during the entire experimental procedure. Respiratory rate and temperature were measured with noninvasive probes (SA Instruments). Throughout the experiment, the body temperature was maintained between 36.5°C and 37.5°C. During the MRI measurement, the initial anesthetic was supplemented as necessary with 0.5%–1% isoflurane delivered in 98% O_2 to keep the breath- ing rate less than 140 breaths/min.

Dynamic CE-MRI of the head and neck. Animals were examined in a horizontal-bore 9.4 T animal scan- ner (BioSpec Avance III 94/20) with a BGA12S gradient system with ParaVision 6.0.1 and a linearly polar- ized coil with an inner diameter of 40 mm (all from Bruker BioSpin GmbH). Contrast-enhanced imaging was achieved with a 3D time-of-flight gradient recalled echo sequence originally adapted for imaging of peripheral lymph vessels (62) with a recovery time of 12.0 ms, echo time of 2.5 ms, flip angle of 25°, matrix of 600 × 432 × 180, field of view of 36.00 mm × 25.92 mm × 18.00 mm, 1 average, and a scan time of 4 minutes, 19 seconds, 200 milliseconds. A phantom placed in the vicinity of the animal's head (solution diluted in 0.9% NaCl at 5 mM Gd) was used for image intensity normalization over the time series. Follow- ing a precontrast scan, a GadoSpin D solution at 25 mM Gd was infused at a constant rate of 0.1 µL/min for 60 minutes. Total scan time was between 95 and 99 minutes.

Data processing. ROIs were manually drawn around the different anatomical regions investigated with Horos (version 3.3.6, Horos Project). Signal intensity was normalized using the reference phan- tom. The normalized ROI value

(provided in Supplemental Figures 1–4) was calculated by dividing the original ROI value by the phantom value of the same scan. Contrast agent efflux over time was deter- mined by calculating the percentage change of signal intensity as a function of time after infusion of the contrast agent using the following equation: [(normalized signal intensity – normalized precontrast intensity)/(normalized precontrast intensity)] × 100. Ventricle and lymph node volumes were quanti- fied using semiautomatic segmentation tools in 3DSlicer, version 4.11 (https://www.slicer.org). All the Digital Imaging and Communications in Medicine (DICOM) image files were imported into 3DSlicer for segmentation and 3D modeling. The ROI was first defined and segmented with the segment editor module. The model maker module was used to create the 3D model. Finally, the volume was deter- mined via the segment statistics module.

Histological analysis of tracer efflux to lymphatics. For experiments where ventricular infusions were followed by histological analysis, an identical procedure was used with the following modifications: a solution of AF647-OVA (Thermo Fisher Scientific) dissolved in artificial CSF (Harvard Apparatus) at a concentration of 5 mg/mL was infused at a constant rate of 0.1 μL/min for 60 minutes; the 2- to 3-month-old wild-type mice were sacrificed at the end of the infusion.

RESOURCE AND TECHNICAL ADVANCE

For decalcification, intracardiac perfusion with PBS and 4% paraformaldehyde (PFA) was performed. Afterward, the mice were decapitated followed by the removal of skin, muscles, incisors, and the lower jaw from the cranium. The cranium was then immersed in 4% PFA for overnight fixation before being placed in 14% EDTA for 7 days (refreshed daily) at 4°C. Decalcified tissue was then immersed in 30% sucrose for 3 days for cryoprotection before OCT embedding. Then, 20 μm thick coronal sections were cut from a cryostat (CryoStar NX50, Epredia) and stored at – 80°C. For immunofluorescence staining of LYVE-1, frozen tissues were first hydrated with PBS for 10 minutes, then permeabilized by 0.1% Triton X-100 for 10 minutes. For blocking, 10% goat serum was used for 1 hour at room temperature. Tissues were incubated with primary antibody (rabbit anti–LYVE-1, AngioBio, catalog 11-034, 1:600 dilution) for 3 hours at room temperature and then washed with PBS before incubating with secondary antibody (goat anti-rabbit Alexa Fluor 488, 1:500 dilution, catalog A27034, Invitrogen) for 2 hours at room tem- perature. Imaging of the nasal region was done under a Zeiss Axio Zoom.V16 microscope equipped with a Teledyne Photometrics Prime BSI Scientific CMOS camera combined with a CoolLED pE-4000 illumination system and ZEN 2 software (Zeiss). Higher magnification images were then acquired using a Zeiss LSM800 confocal microscope.

For processing of draining lymph nodes, cervical lymph nodes were postfixed in 4% PFA at 4°C over- night. Lymph nodes were further immersed in 30% sucrose for 2 days at 4°C before being snap-frozen in melting isopentane with liquid nitrogen. The frozen tissue was cut serially into 15 μm sections with a cryo- stat microtome (Leica Microsystems). Sections were incubated with an anti–LYVE-1 (eBioscience, clone ALY7, 1:200) primary antibody for 2 hours at room temperature before incubation with a donkey anti-rat (catalog A21208, Invitrogen, 1:1000) secondary antibody conjugated with Alexa Fluor 488 for 1 hour at room temperature. Sections were finally counterstained with DAPI. ROIs were acquired with a Zeiss LSM 880 Axio Observer.

Statistics. Statistical analyses were performed with GraphPad Prism 5. Graphs represent mean ± SEM. Means of 2 groups were compared using an unpaired 2-tailed Student's *t* test. Two-way ANOVAs were used for comparison, with time points being a within-subject factor and age being a between-subject factor, followed by Bonferroni's post hoc test. A *P* value less than 0.05 was considered statistically significant.

Study approval. All mouse experiments were approved by the Landesamt für Gesundheit und Ver- braucherschutz, Saarbrücken, Germany (license numbers 31/2018 and 45/2019).

Author contributions

YD and STP conceived and designed the study. YD performed the MRI experiments. YD, LX, and AS per- formed the histology experiments. JK, YD, and STP analyzed the data. AM and YD applied for approval of animal experiments. AM maintained the MRI facility. KF made substantial contributions to the concep- tion of the study. YD and STP drafted the manuscript. All authors have approved the final version of the manuscript and have agreed to be accountable for all aspects of the work.

Acknowledgments

Address correspondence to: Yann Decker, Department of Neurology, Saarland University Medical Center, 66421 Homburg/Saar, Germany. Phone: 49.6841.1624215; Email: yann.decker@uks.eu. Or to: Steven T. Proulx, Theodor Kocher Institute, University of Bern, CH-3012 Bern, Switzerland. Phone: 41.31.631.5390; Email: steven.proulx@tki.unibe.ch.

1. Weed LH. Studies on cerebro-spinal fluid. No. IV: the dual source of cerebro-spinal fluid. *J Med Res*. 1914;31(1):93–118.11. 2. Davson H, Segal MB, eds. *Physiology of the CSF and Blood-Brain Barriers*. CRC Press; 1996.
3. Bradbury MWB, Cserr HF. Drainage of cerebral interstitial fluid of cerebrospinal fluid into lymphatics. In: Johnston MG, ed.

Experimental Biology of the Lymphatic Circulation. Elsevier; 1985:355–394.
4. McComb JG. Recent research into the nature of cerebrospinal fluid formation and absorption. *J Neurosurg*. 1983;59(3):369–383.

RESOURCE AND TECHNICAL ADVANCE

5. Koh L, et al. Integration of the subarachnoid space and lymphatics: is it time to embrace a new concept of cerebrospinal fluid absorption? *Cerebrospinal Fluid Res*. 2005;2:6.

6. Proulx ST. Cerebrospinal fluid outflow: a review of the historical and contemporary evidence for arachnoid villi, perineural routes, and dural lymphatics. *Cell Mol Life Sci*. 2021;78(6):2429–2457.

7. Ma Q, et al. Outflow of cerebrospinal fluid is predominantly through lymphatic vessels and is reduced in aged mice. *Nat Com- mun*. 2017;8(1):1434.

8. Ma Q, et al. Rapid lymphatic efflux limits cerebrospinal fluid flow to the brain. *Acta Neuropathol*. 2019;137(1):151–165.

9. Louveau A, et al. Structural and functional features of central nervous system lymphatic vessels. *Nature*. 2015;523(7560):337–341. 10. Aspelund A, et al. A dural lymphatic vascular system that drains brain interstitial fluid and macromolecules. *J Exp Med*.

2015;212(7):991–999.
11. Ahn JH, et al. Meningeal lymphatic vessels at the skull base drain cerebrospinal fluid. *Nature*. 2019;572(7767):62–66.
12. Pizzo ME, et al. Intrathecal antibody distribution in the rat brain: surface diffusion, perivascular transport and osmotic enhance-

ment of delivery. *J Physiol*. 2018;596(3):445–475.
13. Ma Q, et al. Clearance of cerebrospinal fluid from the sacral spine through lymphatic vessels. *J Exp Med*. 2019;216(11):2492–2502. 14. Brady M, et al. Cerebrospinal fluid drainage kinetics across the cribriform plate are reduced with aging. *Fluids Barriers CNS*.

2020;17(1):71.

15. Stanton EH, et al. Mapping of CSF transport using high spatiotemporal resolution dynamic contrast-enhanced MRI in mice:

effect of anesthesia. *Magn Reson Med*. 2021;85(6):3326–3342.

16. Faber WM. The nasal mucosa and the subarachnoid space. *Am J Anat*. 1937;62(1):121148.

17. Erlich SS, et al. Ultrastructural morphology of the olfactory pathway for cerebrospinal fluid drainage in the rabbit. *J Neurosurg*.

1986;64(3):466–473.

18. Kida S, et al. CSF drains directly from the subarachnoid space into nasal lymphatics in the rat. Anatomy, histology and immu-

nological significance. *Neuropathol Appl Neurobiol*. 1993;19(6):480–488.

19. Norwood JN, et al. Anatomical basis and physiological role of cerebrospinal fluid transport through the murine cribriform

plate. *Elife*. 2019;8:e44278.

20. Hsu M, et al. Neuroinflammation-induced lymphangiogenesis near the cribriform plate contributes to drainage of CNS-derived

antigens and immune cells. *Nat Commun*. 2019;10(1):229.

21. Mortensen AO, Sullivan WE. The cerebrospinal fluid and the cervical lymph nodes. *Anat Rec*. 1933;56(4):359–363.

22. Pile-Spellman JM, et al. Experimental in vivo imaging of the cranial perineural lymphatic pathway. *AJNR Am J Neuroradiol*.

1984;5(5):539–545.

23. Kwon S, et al. Fluorescence imaging of lymphatic outflow of cerebrospinal fluid in mice. *J Immunol Methods*. 2017;449:37–43. 24. Yamada S, et al. MRI tracer study of the cerebrospinal fluid drainage pathway in normal and hydrocephalic guinea pig brain.

Tokai J Exp Clin Med. 2005;30(1):21–29.

25. Hladky SB, Barrand MA. Mechanisms of fluid movement into, through and out of the brain: evaluation of the evidence. *Fluids*

Barriers CNS. 2014;11(1):26.

26. Steffensen AB, et al. Cotransporter-mediated water transport underlying cerebrospinal fluid formation. *Nat Commun*.

2018;9(1):2167.

27. Liu G, et al. Direct measurement of cerebrospinal fluid production in mice. *Cell Rep*. 2020;33(12):108524.

28. Louveau A, et al. CNS lymphatic drainage and neuroinflammation are regulated by meningeal lymphatic vasculature. *Nat Neu-*

rosci. 2018;21(10):1380–1391.

29. Rustenhoven J, et al. Functional characterization of the dural sinuses as a neuroimmune interface. *Cell*. 2021;184(4):1000–1016. 30. Oliver G, et al. The lymphatic vasculature in the 21st century: novel functional roles in homeostasis and disease. *Cell*.

2020;182(2):270–296.

31. Iliff JJ, et al. Brain-wide pathway for waste clearance captured by contrast-enhanced MRI. *J Clin Invest*. 2013;123(3):1299–1309. 32. Lee H, et al. The effect of body posture on brain glymphatic transport. *J Neurosci*. 2015;35(31):11034–11044.

33. Gakuba C, et al. General anesthesia inhibits the activity of the "glymphatic system". *Theranostics*. 2018;8(3):710–722.

34. Gaberel T, et al. Impaired glymphatic perfusion after strokes revealed by contrast-enhanced MRI: a new target for fibrinolysis?

Stroke. 2014;45(10):3092–3096.

35. Ringstad G, et al. Brain-wide glymphatic enhancement and clearance in humans assessed with MRI. *JCI Insight*.

2018;3(13):121537.

36. Xue Y, et al. In vivo T1 mapping for quantifying glymphatic system transport and cervical lymph node drainage. *Sci Rep*.

2020;10(1):14592.

37. Ringstad G, Eide PK. Cerebrospinal fluid tracer efflux to parasagittal dura in humans. *Nat Commun*. 2020;11(1):354.

38. Ghersi-Egea JF, et al. Rapid distribution of intraventricularly administered sucrose into cerebrospinal fluid cisterns via subarach-

noid velae in rat. *Neuroscience*. 1996;75(4):1271–1288.

39. Mestre H, et al. Flow of cerebrospinal fluid is driven by arterial pulsations and is reduced in hypertension. *Nat Commun*.

2018;9(1):4878.

40. Bedussi B, et al. Paravascular spaces at the brain surface: Low resistance pathways for cerebrospinal fluid flow. *J Cereb Blood Flow*

Metab. 2018;38(4):719–726.

41. Nagra G, Johnston MG. Impact of ageing on lymphatic cerebrospinal fluid absorption in the rat. *Neuropathol Appl Neurobiol*.

2007;33(6):684–691.

42. Preston JE. Ageing choroid plexus-cerebrospinal fluid system. *Microsc Res Tech*. 2001;52(1):31–37.

43. Karaman S, et al. Decline of lymphatic vessel density and function in murine skin during aging. *Angiogenesis*. 2015;18(4):489–498. 44. Proulx ST, et al. Quantitative measurement of lymphatic function in mice by noninvasive near-infrared imaging of a peripheral

vein. *JCI Insight*. 2017;2(1):90861.

45. Zolla V, et al. Aging-related anatomical and biochemical changes in lymphatic collectors impair lymph transport, fluid homeo-

stasis, and pathogen clearance. *Aging Cell*. 2015;14(4):582–594.
46. Da Mesquita S, et al. Functional aspects of meningeal lymphatics in ageing and Alzheimer's disease. *Nature*.

RESOURCE AND TECHNICAL ADVANCE

2018;560(7717):185–191.
47. Schwalbe G. Die arachnoidalraum ein lymphraum und sein zusammenhang mit den perichorioidalraum. [The arachnoidal

space as a lymphatic space with connection to the perichoroidal compartment.]. *Zbl Med Wiss*. 1869;7:465–467.
48. Erlich SS, et al. Ultrastructure of the orbital pathway for cerebrospinal fluid drainage in rabbits. *J Neurosurg*. 1989;70(6):926–931. 49. Ludemann W, et al. Ultrastructure of the cerebrospinal fluid outflow along the optic nerve into the lymphatic system. *Childs

Nerv Syst*. 2005;21(2):96–103.
50. Brierley JB, Field EJ. The connexions of the spinal sub-arachnoid space with the lymphatic system. *J Anat*. 1948;82(3):153–166. 51. Marmarou A, et al. Compartmental analysis of compliance and outflow resistance of the cerebrospinal fluid system. *J Neurosurg*.

1975;43(5):523–534.
52. Bozanovic-Sosic R, et al. Spinal and cranial contributions to total cerebrospinal fluid transport. *Am J Physiol Regul Integr Comp

Physiol*. 2001;281(3):R909–R916.
53. Bradbury MW, Westrop RJ. Factors influencing exit of substances from cerebrospinal fluid into deep cervical lymph of the rab-

bit. *J Physiol*. 1983;339:519–534.
54. Johnston M, et al. Evidence of connections between cerebrospinal fluid and nasal lymphatic vessels in humans, non-human

primates and other mammalian species. *Cerebrospinal Fluid Res*. 2004;1(1):2.
55. Mollanji R, et al. Intracranial pressure accommodation is impaired by blocking pathways leading to extracranial lymphatics. *Am

J Physiol Regul Integr Comp Physiol*. 2001;280(5):R1573–R1581.
56. Hablitz LM, et al. Increased glymphatic influx is correlated with high EEG delta power and low heart rate in mice under anes-

thesia. *Sci Adv*. 2019;5(2):eaav5447.
57. Voelz K, et al. A ferritin tracer study of compensatory spinal CSF outflow pathways in kaolin-induced hydrocephalus. *Acta Neu-

ropathol*. 2007;113(5):569–575.
58. Ma Q, et al. Lymphatic outflow of cerebrospinal fluid is reduced in glioma. *Sci Rep*. 2019;9(1):14815.
59. Lowhagen P, et al. The nasal route of cerebrospinal fluid drainage in man. A light-microscope study. *Neuropathol Appl Neurobiol*.

1994;20(6):543–550.
60. De Leon MJ, et al. Cerebrospinal fluid clearance in Alzheimer disease measured with dynamic PET. *J Nucl Med*.

2017;58(9):1471–1476.
61. Melin E, et al. In vivo assessment of cerebrospinal fluid efflux to nasal mucosa in humans. *Sci Rep*. 2020;10(1):14974.
62. Muller A, et al. Magnetic resonance lymphography at 9.4 T using a gadolinium-based nanoparticle in rats: investigations in

healthy animals and in a hindlimb lymphedema model. *Invest Radiol*. 2017;52(12):725–733.

8. <u>Acknowledgments</u>

At this point, I want to express how grateful I am for the support of my supervisors, Prof. Dr. med. Klaus Faßbender and Dr. Yann Decker. Their immense knowledge and experience encouraged me over the whole process of the dissertation.

I especially appreciated the constructive discussions with my supervisor, Dr. Yann Decker. His invaluable advice and continuous support and guidance during the process had a strong input to my motivation and the completion of my dissertation. Moreover, I am extremely grateful for his technical support on my study. I want to express my sincere gratitude for the permanent feedback on my work and the time he spent helping me create this dissertation.

9. **Kolloquiumsvermerk**

Tag der Promotion: 17.10.2023
Dekan: Prof. Dr. M.D. Menger
Berichterstatter: Prof. K. Faßbender
Prof. W. Reith